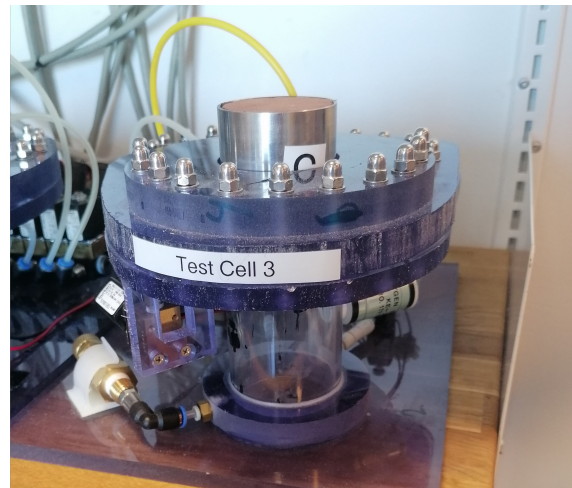


# Investigating the Correlation between Water Vapor Permeability and Pure Diffusion in Building Materials

- Master Thesis -



Patrick Hundevad and Tonje Luckenwald

Aalborg University  
Build Department





**AALBORG UNIVERSITY**  
STUDENT REPORT

**10th Semester**  
v/ **Build Department**  
Byggeri og Anlæg  
Thomas Manns Vej 23  
9220 Aalborg  
<https://www.build.aau.dk/>

**Title:**

Investigating the Correlation  
between Water Vapor Permeability  
and Pure Diffusion  
in Building Materials

**Project:**

Semesterproject

**Projectperiod:**

September 2022 - June 2023

**Students:**

Patrick Hundevad  
Tonje Luckenwald

**Supervisors:**

Rasmus Lund Jensen  
Kirstine Meyer Frandsen

**Number of pages: 121**

**Hand in June 9, 2023**

**Abstract:**

The water vapor transmission in building materials is mainly characterised by the wet/dry cup method, as described in the DS/EN ISO 12572. However, this method presents some challenges, such as the amount of time an experiment takes and Unstable boundary conditions. Therefore, another method, the Oxygen Diffusion Apparatus 2020 (ODA20), is investigated. This method uses oxygen as a tracer gas compared to the wet/dry cup method, which uses water vapour as a tracer gas. The ODA20 measures the pure diffusion and is compared with Water Vapor Permeability from the wet/dry cup method to see if there is any correlation. The results show that pure diffusion is less precise than the cup method. However, more samples can be investigated in a shorter amount of time, giving a quick overview of the material's diffusion rate. The cup method can take up to weeks, whereas the ODA20 only takes 2 hours. In conclusion, the choice between the ODA20 and the wet/dry cup method depends on the desired level of precision of the results.

*The content of the report is freely available, but publication (with source reference) may only take place in agreement with the authors.*



# Foreword

---

This report has been written by two master students of the BUILD department at Aalborg University with the specialty of Indoor Environmental and Energy Engineering.

## Reading Instructions

This Master Thesis contains a scientific article as it's main report and the more detailed description can be found in the appendix. The scientific paper is referred to in numbers, whereas letters are used for the appendixes. The scientific paper is about the comparison of the water vapor permeability and the pure diffusion, which is established on IMRAD-method of paper writing; Introduction, Methods, Results and Discussion. An additional conclusion has been inserted. The scientific paper part can be read alone, while the appendixes are referred in the parer for more detailed information.

References to sources will be written with the Vancouver numerical system, where references are numbered sequentially throughout the text. The numbers occur within square brackets ex. [2], and the reference list gives the references in numerical order.

Figures and tables are numerated to the belonging chapter and section, and have explaining text respectively below and above. For instance a figure in chapter A has the number A.1 and the following has A.2 and so on. If a figure taken from a source has been modified, a "\*" will appear next to the source from which the figure is derived in the figure text. For instance, this can look like [1]\*.

In this project thousand separators are given with commas, and when dividing the decimals, a dot is used.



# Contents

---

|   |           |
|---|-----------|
| Foreword  | v         |
| Investigating the Correlation between Water Vapor Permeability and Pure Diffusion in Building Materials | 1         |
| Bibliography  | 9         |
| <b>I Appendiks</b>  | <b>15</b> |
| <b>A Materials</b>  | <b>16</b> |
| A.1 Stone wool . . . . .  | 17        |
| A.2 Wood Fiber Insulation . . . . .   | 17        |
| A.3 Wood . . . . .  | 18        |
| A.4 Unfired Brick . . . . .   | 18        |
| A.5 Brick . . . . .   | 19        |
| A.6 Clay . . . . .  | 19        |
| <b>B Pore Structure and Hygrothermal Processes</b>  | <b>20</b> |
| B.1 Hygrothermal processes in organic materials . . . . .   | 20        |
| B.1.1 Hydrophilic Surfaces . . . . .  | 20        |
| B.1.2 Surface Tension and Capillary Rise . . . . .  | 22        |
| B.1.3 Movement of Water Molecules . . . . .   | 25        |
| B.2 Pore Structure . . . . .  | 26        |
| B.2.1 Types of Pores . . . . .  | 26        |
| B.2.2 The Pore Structure for Insulation Materials . . . . .   | 27        |
| B.2.3 Clay Based Materials Pore Structure . . . . .   | 28        |
| B.2.4 Wood's Pore Structure . . . . .   | 28        |
| <b>C Water vapor Permeability by the Wet/Dry Cup Method</b>   | <b>31</b> |
| C.1 Methodology for the Wet/Dry Cup Method . . . . .  | 31        |
| C.1.1 Data analysis . . . . .   | 32        |
| C.2 Detailed Measurement Plan . . . . .   | 34        |
| C.2.1 The Setup used in the Dry Cup Experiments . . . . .   | 35        |
| C.2.2 Method used step by step . . . . .  | 36        |
| C.3 Results and discussion from the Dry Cup Experiments . . . . .                                       | 37        |
| <b>D Oxygen Diffusion Coefficient by the Oxygen Diffusion Apparatus</b>                                 | <b>42</b> |
| D.1 Methodology of the ODA20 . . . . .  | 43        |
| D.2 Equipment . . . . .   | 44        |
| D.3 Setup . . . . .   | 45        |
| D.3.1 Method used Step by Step . . . . .  | 45        |

|          |   |           |
|----------|---|-----------|
| D.4      | Results of the ODA20 . . . . .  | 45        |
| D.4.1    | Selection of Samples for the Wet/Dry Cup Method . . . . .                               | 48        |
| <b>E</b> | <b>Sample Preparation for ODA20 and Wet/Dry Cup Method</b>                              | <b>50</b> |
| E.1      | Process of Cutting the Material . . . . .   | 50        |
| E.2      | Sealant . . . . .   | 51        |
| E.2.1    | Equipment . . . . .   | 54        |
| E.2.2    | Setup . . . . .   | 54        |
| E.2.3    | Method used Step by Step . . . . .  | 55        |
| E.2.4    | Results . . . . .   | 55        |
| E.3      | Sealing the Material . . . . .  | 55        |
| E.3.1    | RWI and WFI . . . . .   | 55        |
| E.3.2    | BR, UBR and Wood . . . . .  | 56        |
| E.3.3    | Clay . . . . .  | 57        |
| E.4      | Density of the Samples . . . . .  | 58        |
| <b>F</b> | <b>Study of Salt Solutions Stability Over Time</b>                                      | <b>59</b> |
| F.1      | Detailed Measurement Plan . . . . .   | 60        |
| F.1.1    | Setup used in the Investigation of Salt Solutions Stability over Time                   | 61        |
| F.1.2    | Method used step by step . . . . .  | 62        |
| F.2      | Observations . . . . .  | 62        |
| F.3      | Results from the Investigation of Salt Solutions Stability over Time . . . . .          | 63        |
| F.4      | Conclusion and Discussion . . . . .   | 64        |
| <b>G</b> | <b>Equipment</b>  | <b>65</b> |
| G.1      | Sartorius Entris 2202-1S Balance . . . . .  | 65        |
| G.2      | Metal Cylinder . . . . .  | 67        |
| G.3      | 3D-Printed Pressing device . . . . .  | 67        |
| G.4      | The VCL 7010 Climate Chamber . . . . .  | 69        |
| G.5      | The IC-meter Mobile (GSM) . . . . .   | 70        |
| G.6      | The Mensor 2104 Digital Pressure Gauge . . . . .  | 71        |
| G.7      | The Memmert UF110 Heating Oven . . . . .  | 72        |
| G.8      | The Honeywell humidity Sensor . . . . .   | 73        |
| G.9      | The F200 Precision Thermometer . . . . .  | 74        |
| G.10     | The Novasina Hygrodat 100 Precision Humidity Sensor . . . . .                           | 75        |
| G.11     | The Kimo VT110 Anemometer . . . . .   | 76        |
| G.12     | Oxygen Sensor . . . . .   | 77        |
| <b>H</b> | <b>The Design Process for The Test Cup</b>  | <b>79</b> |
| <b>I</b> | <b>Sample Validation for Wet/Dry Cup Method</b>   | <b>86</b> |
| <b>J</b> | <b>Projection of the Test Samples Stable Permeability</b>                               | <b>91</b> |
| <b>K</b> | <b>Graphs for Comparison of Pure Diffusion Coefficient and Water Vapor Permeability</b> | <b>93</b> |
| <b>L</b> | <b>Calibration of RH sensors</b>  | <b>95</b> |

---

|          |   |            |
|----------|---|------------|
| L.1      | The Matlab Code used to process the data . . . . .              | 96         |
| <b>M</b> | <b>Calibration of IC meter</b>                                  | <b>98</b>  |
| M.1      | Calibration of the RH sensor in the IC meter . . . . .          | 98         |
| M.2      | Calibration of the temperature sensor in the IC meter . . . . . | 99         |
| M.3      | The Matlab Code used to process the data . . . . .              | 101        |
| <b>N</b> | <b>Calibration of ODA20</b>                                     | <b>104</b> |
| N.1      | Equipment . . . . .   | 104        |
| N.2      | How the ODA is Calibrated . . . . .                             | 104        |
| N.3      | Results . . . . .   | 105        |
| <b>O</b> | <b>Calibration graphs of the ODA20</b>                          | <b>107</b> |
| O.1      | Week 14 . . . . .   | 107        |
| O.2      | Week 18 . . . . .   | 111        |
| <b>P</b> | <b>Example data of each Material</b>                            | <b>115</b> |



# Investigating the Correlation between Water Vapor Permeability and Pure Diffusion in Building Materials

Patrick Andersen Hundevad<sup>1</sup>, Tonje Luckenwald<sup>1</sup>

<sup>1</sup>Department of the Built Environment, Aalborg University, 9220 Aalborg, Denmark

**Abstract.** The water vapor transmission in building materials is mainly characterised by the wet/dry cup method, as described in the DS/EN ISO 12572. However, this method presents some challenges, such as the amount of time an experiment takes and Unstable boundary conditions. Therefore, another method, the Oxygen Diffusion Apparatus 2020 (ODA20), is investigated. This method uses oxygen as a tracer gas compared to the wet/dry cup method, which uses water vapour as a tracer gas. The ODA20 measures the pure diffusion and is compared with Water Vapor Permeability from the wet/dry cup method to see if there is any correlation. The results show that pure diffusion is less precise than the cup method. However, more samples can be investigated in a shorter amount of time, giving a quick overview of the material's diffusion rate. The cup method can take up to weeks, whereas the ODA20 only takes 2 hours. In conclusion, the choice between the ODA20 and the wet/dry cup method depends on the desired level of precision of the results.

## 1. Introduction

The diffusion in building materials play a significant role in the indoor environment. Water vapor transmission in building materials is predominantly experimentally characterized by the wet/dry cup method, as described in DS/EN ISO 12572 [1]. The method employs water vapor as the transport medium by creating gradients in the vapor pressure across material samples. As such, the water vapor transmission rate is not only determined by water molecules diffusing through open pore spaces; it is further impacted by physical interactions between water molecules and pore surfaces, for example, sorption, surface diffusion, and capillary effects. The physical interactions mean that it can take a long time to complete an experiment using this method, which can require many resources. Therefore, a new method developed from soil physics and based on a single chamber will be investigated. The new Oxygen Diffusion Apparatus 2020 (ODA20) method characterizes a material's diffusivity by employing oxygen as a tracer gas instead of the water vapor used in the wet/dry cup method. As oxygen is physically, biologically and chemically non-reactive, the method neglects moisture mechanisms such as evaporation, condensation and liquid transfer at water-air interfaces and water-filled pore spaces, enabling the method to determine the pure diffusion through the material. The lack of physical reactions and the fact that oxygen particles are much smaller than water particles will drastically reduce the resources and time required to find the water vapor transmission through a material.

Initial studies have indicated a significant difference between pure diffusivity measured by ODA20 and effective water vapor permeability measured by wet/dry cup found in the literature. A study from 2020 [2] estimated the factor between pure and effective diffusivity to express the additional moisture mechanisms that influence and delay water vapor transmission.

There is an uncertainty as to whether ODA can be used to find the permeability of building materials. This uncertainty leads to the question of how big of an influence it will have and whether it will impact the results when doing building simulations. In general, it becomes more and more expensive the more accurate the number gets, so it is interesting to investigate whether ODA20 has sufficient accuracy, meaning that there will be no need to use the extra resources to determine it through the cup method. In practice it may be more advantageous to find ten pure diffusion in a shorter time rather than making one wet/dry cup method measurement. In reality, would it be better to utilize the shorter determined time to find ten pure diffusion values through the material to consider other uncertainties, such as the material's homogeneity over only being able to make one wet/dry cup method measurement? Meanwhile, another study from 2022 [3] has found significant uncertainty in the wet/dry cup method's internal conditions, giving the results a relative error between 5% to 450% between the estimated water vapor permeability found by simulation and the measured water vapor permeability.

This study comprises measurements of water vapor permeability in building materials using the dry cup method and pure diffusion using the ODA20 method. The hypothesis is that the uncertainties from ODA20 can be minimized by using the shorter determination time to reduce other uncertainties, such as material homogeneity and improvement of the sample. The hypothesis will be investigated by comparing ten measurements of pure diffusion and comparing with a measurement of effective diffusion to see which experiment gives the most knowledge about the material. Isolating pure diffusion from effective diffusion can also improve understanding of the physical phenomena occurring during water vapor transmission.

## 2. Materials and Methods

### 2.1 Materials

Six materials have been chosen in this study; stone wool (RWI), wood fibre insulation (WFI), wood, unfired brick (UBR), brick (BR), and clay. These materials have been chosen to understand different pore structure and their diffusivity. Clay is the raw material of BR and UBR and has a less denser structure. A sample of each material can be seen in figure 0.1



**Figure 0.1** A sample of each material used in this project. From left to right: Rockwool Insulation, Wood Fibre Insulation, Wood, Brick, Unfired Brick and Clay

The insulation materials have very open pore structure, and have low density indicating that the diffusivity should be high. RWI is also water repellent meaning water vapor will not be absorbed by the material.[4] BR and UBR however are more dense and are expected to have one of the lowest diffusivity, but also wood as this is a material with potential narrow pores even though it's density is higher than BR and UBR. For further reading see appendix A. The density is used to compare the pure diffusion with the porosity. An overview of the materials and their properties can be seen in table 0.1.

**Table 0.1** Six materials have been chosen for this study. The insulation materials: stone wool (RWI), and wood fibre insulation (WFI), the traditional; wood, brick (BR) , and unfired brick (UBR), the soil; clay. Some of the properties can be seen in this table. [4], [5], [6], [7], [8], [9], [10], [11] [12]

| <b>Material</b> | Bulk Density<br>[kg/m <sup>3</sup> ] | Thermal conductivity<br>[W/m · K] | Particle density<br>[kg/m <sup>3</sup> ] | Dry density<br>[kg/m <sup>3</sup> ] |
|-----------------|--------------------------------------|-----------------------------------|--|-------------------------------------|
| RWI             | 46.4                                 | 0.033-0.045                       | 2.65                                     | 462                                 |
| WFI             | 40-58                                | 0.036-0.038                       | 154                                      | 48                                  |
| Wood            | 400-700                              | 0.072-0.097                       | 154                                      | 356                                 |
| UBR             | 1,700                                | 0.91                              | 27                                       | 1,802                               |
| BR              | 1,800                                | 0.5-1.0                           | 27                                       | 1,768                               |
| Clay            | 746-1515                             | 2.8                               | 27                                       | 1,107                               |

## 2.2 Methods

### 2.2.1 Water Vapor Permeability by the Wet/Dry Cup Method

The wet/dry cup method uses water vapor pressure to measure the water vapor permeability by keeping track of the mass change in a material. The differences in pressure in the cup and the surrounding forces water vapor to diffuse through the material. The water vapor permeability is then later converted to water vapor diffusion by using the equation (1).

$$\delta = W \cdot d = \frac{G}{A \cdot \Delta p} \cdot d \quad (1)$$

Where  $\delta$  is the water vapor permeability [kg/(m · s · Pa)],  $W$  is the water vapor permeance [kg/(m<sup>2</sup>·s · Pa)],  $d$  is the thickness of the sample [m],  $G$  is the water vapor flow through the sample [kg/s],  $A$  is the exposed area [m<sup>2</sup>], and  $\Delta p$  is the gradient of the partial pressures of water vapor [Pa]

The setup was designed to follow the DS/EN ISO 12572 [1] as closely as possible, and can be seen on figure 0.2. The samples that best represented the materials have been chosen to be used in this study. The best represented samples have been found in the ODA20 method, see section . A metal cup have been designed according to the DS/EN Standard ISO 12572[1]. The design process can be found in appendix H. It has been decided to do a dry cup method using silica gel as as the drying agent. An investigation of the drying agent can be found in appendix F. The setup follows the method best suitable for self supporting materials, which can be further investigated in DS/EN ISO 12572 [1], with some exceptions. It is desired to use the test samples from the ODA20 method, therefore

the recommendation that the diameter of the sample must be at least twice the sample's thickness, have been ignored.

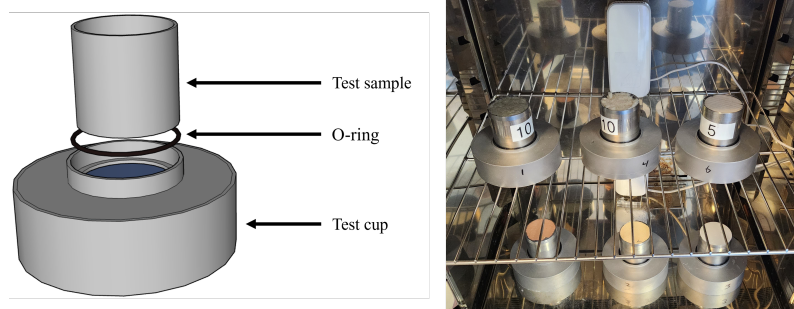


**Figure 0.2** The setup of the dry cup method and a picture of the cups with the test samples in the climate chamber. On the upper shelf from left to right: RWI, WFI, and Wood and on the lower shelf from left to right: UBR, BR, and Clay.

### 2.2.2 Pure Diffusion by the Oxygen Diffusion Apparatus 2020

The Oxygen Diffusion Apparatus 2020 (ODA20) is based on Ficks law and the one single chamber method. Ficks law states that particles will diffuse from areas of high concentration to areas of low concentration and over time the concentration will be equal in the system. [13] Ficks first law describes the gas volume pr. unit time through the sample, and can be expressed by equation 2.

$$\frac{dq}{dt} = -D_p A \frac{\Delta C}{h_s} \quad (2)$$

Where  $\frac{dq}{dt}$  is the volume of gas pr. unit time [ $\text{cm}^3/\text{s}$ ],  $t$  is the time [s],  $D_p$  is the diffusion coefficient [ $\text{cm}^2/\text{s}$ ],  $A$  is the cross section area of the sample.

The ODA20 uses oxygen as a tracer gas, unlike the dry/wet cup method, which uses water vapor. The oxygen is non-reactive both physically and chemically, neglecting effects such as evaporation, condensation, liquid transfer at water-air interfaces, and water-filled pores spaces. Water will react physically with the existing water in the material, making it difficult to find its pure diffusivity. Oxygen, however, will not react; therefore, the pure diffusion can be found in this method. In figure 0.3, a sketch of the ODA20 is illustrated, and in figure 0.4, the setup in the laboratory can be seen.

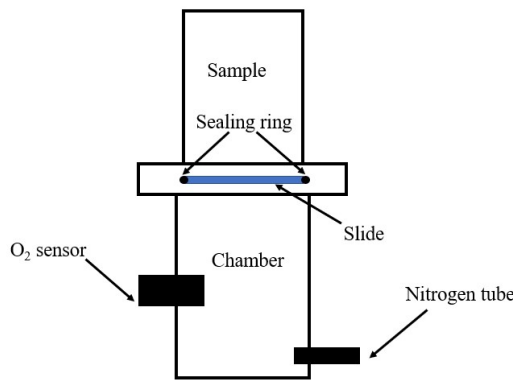


**Figure 0.3** Figure sketch of the ODA20.



**Figure 0.4** The ODA20 and a test sample.

The setup consists of a chamber, a slide, O-rings to seal the test sample, a test sample, a tube to the nitrogen source and an oxygen sensor. When the chamber is flushed with nitrogen, the slide closes the chamber so that no nitrogen can escape. The test sample is placed on the slide and sealed with an inflated O-ring to ensure maximum sealant. An oxygen sensor placed in the chamber measures the  $O_2$ -concentration, ensuring the concentration is close to zero. When the  $O_2$ -concentration reached its minimum, the chamber is opened so that the oxygen can diffuse through the sample. For further reading, see appendix D.

The material sample is packed in a cylinder with MR as a sealant to ensure the oxygen only diffuses from top to bottom. Preparing the sample can be further studied in appendix E. Ten samples of each material have been made to find the mean value so that the sample closest to the mean is used for the dry cup method.

### 3. Results and discussion

#### 3.1 The Water Vapor Permeability

Figure 0.5 illustrates the water vapor permeability of each test sample. As expected, the insulation material's permeability is higher than the other materials, with wood having the lowest permeability. The low permeability is due to the narrow and long pores in wood, making it difficult for the water vapor to diffuse as described in section B.2.4.

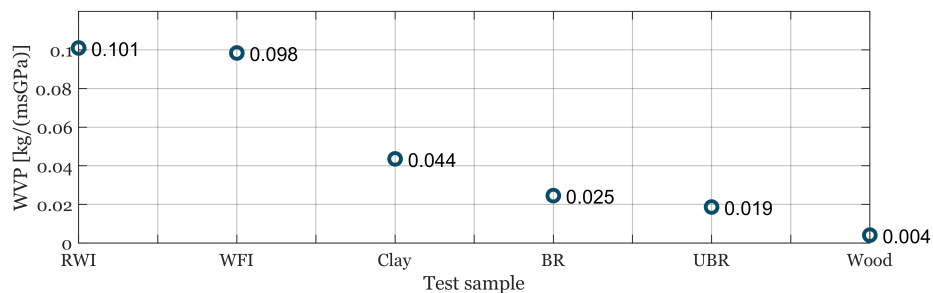


**Figure 0.5** The measured water vapor permeability for the dry cup experiments performed with silica gel.

As the materials have different porosity, they reach stability on different days. RWI and WFI reached stability on day 18 and 19, respectively, but the other materials have not reached stability yet.

### 3.2 The Pure Diffusion

Figure 0.6 illustrates the  $D_p$  for the six building materials. The results indicates that the lower the density, the higher the  $D_p$ -value, except for wood. Wood has a low density compared to BR and UBR, but also the  $D_p$ -value is the lowest. This could be due to the complex pore structure of wood, as the wood has tracheids in it's structure meaning the pores are long and narrow, making it difficult for the gas to diffuse. UBR and BR have a low  $D_p$ -value as they have small pores and more dense compared to the other materials. Clay is a little more porous than BR and UBR indicating the higher  $D_p$ -value. A further discussion of the results can be found in section D.4.

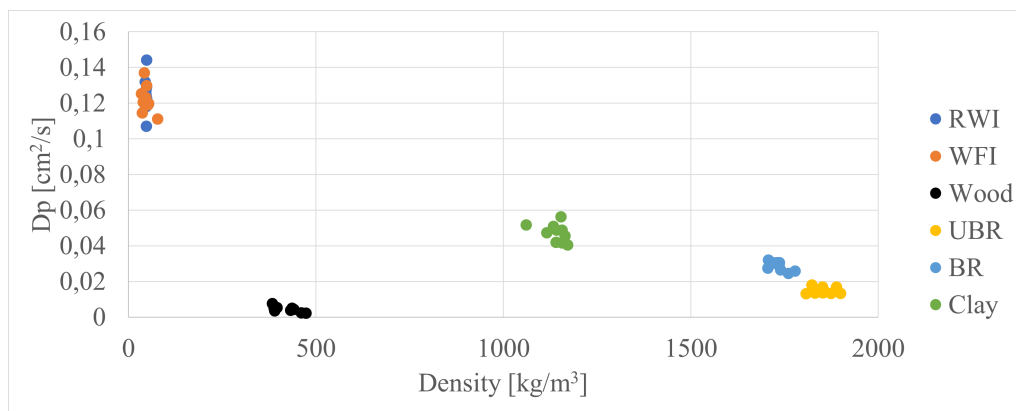


**Figure 0.6** The diffusion coefficients of each material compared to the material's density.

A correlation between the material's diffusion and porosity has been made to better understand the material's tortuosity, which can be found in section D.4. The mean  $D_p$ -value has been taken to find the test sample that is used for the dry CUP Method. The mean  $D_p$ -value, and it's density and  $D_p$ -value can be seen in table 0.2. The study of selecting the sample can be found in section D.4.1.

**Table 0.2** The mean  $D_p$ -value and the chosen sample for the dry cup method's  $D_p$ -value and density for each material.

| Material | Mean $D_p$ [cm <sup>2</sup> s <sup>-1</sup> ] | $D_p$ of the Sample [cm <sup>2</sup> s <sup>-1</sup> ] | Density [kg/m <sup>3</sup> ] |
|----------|---|--|------------------------------|
| RWI      | 0.125   | 0.124  | 47                           |
| WFI      | 0.120   | 0.120  | 39                           |
| Wood     | 0.004   | 0.004  | 441                          |
| UBR      | 0.014   | 0.014  | 1858                         |
| BR       | 0.029   | 0.029  | 1735                         |
| Clay     | 0.047   | 0,047  | 1116                         |

### 3.3 Comparison of Water Vapor Permeability and Pure Diffusion

The main objective of this study is to compare pure diffusion with water vapor permeability. For this, the  $D_p$ -value of the six chosen samples is plotted with the water permeability, see figure 0.7, revealing a correlation between them. A linear tendency of the results can be observed with a correlation factor of 0,99.

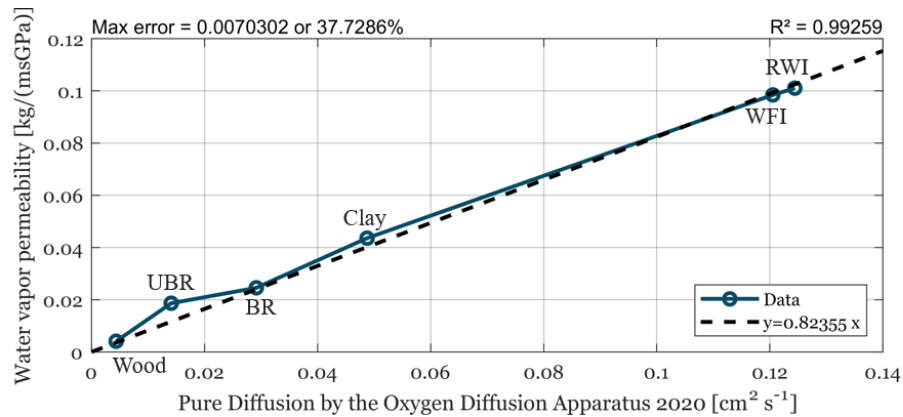


**Figure 0.7** Plot of the water permeability and the pure diffusion. A tendency linear function with a correlation factor of 0.99.

Even though the  $D_p$ -value does not exhibit the same precision as desired, they still show a close relationship. UBR experiences the highest error; however, it should be noted that wood, UBR, BR, and clay have not reached stable conditions yet. As clay, BR, UBR, and wood have not reached stable conditions yet, a prediction model has been made.

As described in the section C.3, a prediction of the results when all materials have reached stable conditions. It is shown that the linear tendency fits the materials better, except for wood. As shown in section D.4.1, the wood's uncertainty between sample still has a high relative error, which could be of how unpredictable wood and its pore structure is.

### 3.4 Discussion

When executing the dry cup method, several parameters need to be considered, including the amount of test sample, the RH layer in the air layer of the cup, the thickness of the samples, and the sample preparation. For the ODA20 method, sample preparation also plays a significant role in the results. As mentioned in section E.4, the calculated density of the RWI samples was significantly higher than the manufacturer's density, which could potentially influence the results. However, as this does not play a significant role when comparing the two methods, this can be negligible.

Another factor to consider is the number of samples used in the cup method. Unlike the ODA20, which had a total of 10 samples for each material, in the cup method, only one sample per material is used due to production costs. The cup method can yield different results despite using multiple samples from the same material. DS/EN ISO 12572 [1] also recommends using 3-5 samples to draw reliable conclusions. Therefore, using a larger number of samples could have been beneficial in investigating the comparability of the ODA20 and cup method.

In addition the sample thickness should also be taken into account. The chosen thickness allows the same sample to be used in the ODA20 and dry cup methods. However, these samples, with a thickness of 51 mm, may take more than five weeks to stabilize, depending on the material and its pore structure. Therefore, considering a thinner sample could be more appropriate. Furthermore, when conducting the dry cup method, the samples should have been conditioned in the climate chamber for more than a week, as described in section C. The samples do not have an even distribution of RH throughout the material, resulting in the material attempting to reach steady-state conditions before the pressure flow is evenly distributed. This affects the time required to achieve a stable condition. Whether the salt solution is stable throughout the dry cup method is also unsure. In appendix F, the stability of the silica gel is investigated, and it shows that the RH is not stable in more open conditions. However, during the dry cup method, the RH in the air layer in the cup could not be measured, so it is unsure if the salt solution was stable during the measurement.

The use of pure diffusion also has its limitations. The results indicate that the diffusion coefficient could be more precise when plotting water vapor permeability against pure diffusion. However, the difference is minor, and considering the time and cost involved in conducting the experiments, the ODA20 method is more advantageous when quick and cost-effective material properties are needed. Additionally, the increased number of samples that can be used in the ODA20 method provides a better overview of the material. In this project, it can be observed that the material yields varied results (see appendix I) when using the ODA20 method. However, since the CUP method uses only one sample, concluding anything from those results is challenging. The choice of method depends on the desired result. When an overview suffices, the ODA20 method is beneficial as it is fast and relatively precise. If a more accurate result is required, the CUP method is recommended.

## 4. Conclusion

A comparison has been made between the Dry CUP Method and the ODA20. The diffusion coefficient for pure diffusion revealed that the insulation materials had the highest  $D_p$ -value, while wood had the lowest. Both methods showed that porosity and tortuosity play a significant role in diffusion. It was evident that even though wood had the 3rd highest porosity, the material's tortuosity greatly impacted the  $D_p$ -value, resulting in the corresponding  $D_p$ -value. The ODA20 yielded results consistent with the dry cup method. When comparing the two, it can be seen that the  $D_p$ -value obtained from the ODA20 was less precise than the water vapor permeability of the dry cup method. One advantage of the ODA20 method over the cup method is that more experiments can be done in a shorter time frame. This is advantageous when a larger amount of results is desired. The ODA20 method is also faster, with a sample taking two hours, whereas the cup method can take several weeks depending on the material's porosity and thickness.

In conclusion, the choice between the ODA20 and cup methods depends on the desired level of precision. If a quick overview with multiple samples is required, the ODA20 method is advantageous. However, the cup method may be preferred for more precise results, even though this experiment takes longer.

# Bibliography

---

- [1] Dansk Standard 2016 *Byggematerialers og -produkters hygroteermiske ydeevne- Bestemmelse af vanddamptransmissionsegenskaber- Kopmetoden.*
- [2] Frandsen K M, Antonov Y I, Johra H, Møldrup P and Jensen R L 2020 Experimental investigation of water vapor diffusivity in bio-based building materials by a novel measurement method URL <https://orca.cardiff.ac.uk/id/eprint/145287/1/RM4L2020%20Conference%20Proceedings%20-%20Online%20Version.pdf>
- [3] Colinart T and Glouannec P 2022 *Building and Environment* 217 109038 ISSN 0360-1323 URL <https://www.sciencedirect.com/science/article/pii/S0360132322002797>
- [4] Rockwool 2023 *A-Batts* accessed: 19-05-2023 URL <https://www.rockwool.com/dk/produkter-og-konstruktioner/produktoversigt/bygningsisolering/a-batts/#Tekniskeegenskaber&sortiment>
- [5] Hayes J and Haan C Tand Barfield B J 1994 *Design Hydrology and Sedimentology for Small Catchments* (Elsevier Inc.) ISBN 978-0-12-312340-4 URL <https://www.sciencedirect.com/book/9780123123404/design-hydrology-and-sedimentology-for-small-catchments#book-description>
- [6] Veitmans K and Grinfelds U 2016 *Wood Fiber Insulation Material* (Researcher For Rural Development 2016)
- [7] Redding T E, Hannam K D, Quideau S A and Devito K J 2005 Particle density of aspen, spruce, and pine forest floors in alberta, canada accessed June 07, 2023 URL [https://www.researchgate.net/publication/242206691\\_Particle\\_Density\\_of\\_Aspen\\_Spruce\\_and\\_Pine\\_Forest\\_Floors\\_in\\_Alberta\\_Canada](https://www.researchgate.net/publication/242206691_Particle_Density_of_Aspen_Spruce_and_Pine_Forest_Floors_in_Alberta_Canada)
- [8] Mitchell J 2018 *Density of wood in kg/m<sup>3</sup>, g/cm<sup>3</sup>, lb/ft<sup>3</sup> – the ultimate guide* URL <https://www.engineeringclicks.com/density-of-wood/>
- [9] Schjønning P, McBride R A, Keller T and Obour P B 2017 Predicting soil particle density from clay and soil organic matter contents accessed June 08, 2023 URL <https://www.sciencedirect.com/science/article/pii/S001670611630636X>
- [10] Tegl R 2021 *Datasheet of RT215 Classica gelb geflammt wasserstrich* (Rander Tegl)
- [11] Oti J, Kinuthia J and Bai J 2009 *Design thermal values for unfired clay bricks* URL <https://www.sciencedirect.com/science/article/pii/S0261306909003471>
- [12] M A N H, T B D and A B 2008 Thermal conductivity evolution of saturated clay under consolidation process accessed: May 31, 2022 URL <https://ascelibrary.org/doi/10.1061/%28ASCE%291532-3641%282008%298%3A2%28114%29>

- [13] Goforth C 2022 Fick's first law equation & examples accessed: June 2, 2022 URL <https://study.com/learn/lesson/ficks-first-law-equation-examples.html>
- [14] AKaramanosa, SHadiarakoub and AMPapadopoulos 2008 *The impact of temperature and moisture on the thermal performance of stone wool* accessed: 19-05-2023 URL <https://www.sciencedirect.com/science/article/pii/S0378778808000078>
- [15] AMPapadopoulos 2005 *State of the art in thermal insulation materials and aims for future developments* accessed: 19-05-2023 URL <https://www.sciencedirect.com/science/article/pii/S0378778804001641>
- [16] I E H E nd *Wood Fibre Insulation - Should I Use it?* accessed: 08-06-2023 URL <https://www.eco-home-essentials.co.uk/wood-fibre-insulation.html>
- [17] Geving S, Lunde E and Holme J 2015 *Laboratory Investigations of Moisture Conditions in Wood Frame Walls with Wood Fiber Insulation* URL <https://www.sciencedirect.com/science/article/pii/S1876610215019025>
- [18] greenspec 2023 *Wood fibre insulation: Introduction* accessed: 19-05-2023 URL <https://www.greenspec.co.uk/building-design/woodfibre-insulation-intro/>
- [19] Thermocell 2023 *Thermocell Teknisk data* accessed: 19-05-2023 URL <https://woodfibre.dk/loesuld/teknisk-data/>
- [20] Rasmussen T V, Thybring E E, Munch-Andersen J, Nord-Larsen T, Jørgensen U, Gottlieb S C, Bruhn A, Rasmussen B, Beim A, Thomsen M R, Munch-Petersen P, Primdahl M B, Bentsen N S, Frederiksen N, Koch M, Beck S A, Bretner M L and Wittchen A 2022 *BIOGENE MATERIALERS ANVENDELSE I BYGGERIET* (SBI)
- [21] Božiková M, Kotoulek P, Bilčík M, Ľubomír Kubík, Hlaváčová Z and Hlaváč P 2021 *Thermal properties of wood and wood composites made from wood waste* (International Agrophysics)
- [22] Koronthalyova O and Matiasovsky P 2007 *Porestructure and thermal conductivity of brunt clay bricks* (Vydavateľstvo STU)
- [23] Sørensen I 2019 *Ingeniørgeologi* (Praxis- Nyt Teknisk Forlag)
- [24] Torraca G 2005 *Porous Building Materials: materials science for architectural conservation* (ICCROM)
- [25] Ahmad D, van den Boogaert I, Miller J, Presswell R and Jouhara H 2018 *Energy Sources, Part A: Recovery, Utilization, and Environmental Effects* 40 2686–2725 URL <https://doi.org/10.1080/15567036.2018.1511642>
- [26] Antonov Y I, Jensen R L, Møldrup P and Pomianowski M 2017 *Energy Procedia* 132 189–194 ISSN 1876-6102 11th Nordic Symposium on Building Physics, NSB2017, 11-14 June 2017, Trondheim, Norway URL <https://www.sciencedirect.com/science/article/pii/S1876610217349044>

- [27] Zumdahl S S and DeCoste D J 2017 *Chemical Principles* 8th ed (Cengage Learning) ISBN 978-1-305-58198-2
- [28] Academy K 2021 Hydrogen bonding in water accessed: June, 2023 URL <https://www.khanacademy.org/science/ap-biology/chemistry-of-life/structure-of-water-and-hydrogen-bonding/a/hydrogen-bonding-in-water>
- [29] Chertkov V 2000 *Geoderma* 95 215–246 ISSN 0016-7061 URL <https://www.sciencedirect.com/science/article/pii/S0016706199000877>
- [30] Thommes M, Kaneko K, Neimark A V, Olivier J P, Rodriguez-Reinoso F, Rouquerol J and Sing K S 2014 Physisorption of gases, with special reference to the evaluation of surface area and pore size distribution (iupac technical report) URL <https://www.degruyter.com/document/doi/10.1515/pac-2014-1117/html>
- [31] Thermocell 2023 *Thermocell Fugt og diffusion* accessed: 08-06-2023 URL <https://woodfibre.dk/bygningsfysik/fugt-og-diffusion/>
- [32] Colinart T, Glouannec P, Bendouma M and Chauvelon P 2017 *Energy and Buildings* 152 42–51 ISSN 0378-7788 URL <https://www.sciencedirect.com/science/article/pii/S0378778817314445>
- [33] Collet F and Pretot S 2014 *Building and Environment* 82 459–466 ISSN 0360-1323 URL <https://www.sciencedirect.com/science/article/pii/S0360132314003102>
- [34] Collet F, Chamoin J, Pretot S and Lanos C 2013 *Energy and Buildings* 62 294–303 ISSN 0378-7788 URL <https://www.sciencedirect.com/science/article/pii/S0378778813001783>
- [35] Casnedi L, Cappai M, Cincotti A, Delogu F and Pia G 2020 *Journal of Building Engineering* 27 100987 ISSN 2352-7102 URL <https://www.sciencedirect.com/science/article/pii/S2352710219309908>
- [36] Kirstine M Frandsen 2023 *Hygrotermisk bygningsfysik og bygningers energiforbrug, HYGBYG6 - Glasers metode*
- [37] Civan F 2007 Petrographical characteristics of petroleum-bearing formations URL <https://www.sciencedirect.com/topics/earth-and-planetary-sciences/tortuosity>
- [38] Rockwool production accessed June 08, 2023 URL <https://production.rockwool.dk/>
- [39] Frandsen K M, Antonov Y I, Møldrup P and Jensen R L 2020 *NSB 2020* 12th URL [https://vbn.aau.dk/ws/portalfiles/portal/409829015/e3sconf\\_nsb2020\\_17005.pdf](https://vbn.aau.dk/ws/portalfiles/portal/409829015/e3sconf_nsb2020_17005.pdf)
- [40] Power N N/A Stone wool – material table – applications – price last accessed 26 October 2022 URL <https://material-properties.org/stone-wool-properties-application-price/>

- [41] greenspec nd *Wood fibre insulation: Manufacturing processes* accessed: 08-06-2023 URL  
<https://www.greenspec.co.uk/building-design/woodfibre-manufact-process/>
- [42] Burning of bricks accessed June 08, 2023 URL  
[https://www.brainkart.com/article/Burning-of-Bricks\\_3594/](https://www.brainkart.com/article/Burning-of-Bricks_3594/)
- [43] greenspec nd Bricks: Fired, unfired clay, reclaimed and calcium silicate accessed June 08, 2023 URL <https://www.greenspec.co.uk/building-design/bricks/>
- [44] Heath A nd Unfired clay bricks accessed June 08, 2023 URL  
<https://www.greenspec.co.uk/building-design/unfired-clay-bricks/>
- [45] Gao Q F, Jrad M, Hattab M, Fleureau J M and Ameer L I 2020 *International Journal of Geomechanics* 20 04020057 URL  
<https://ascelibrary.org/doi/abs/10.1061/%28ASCE%29GM.1943-5622.0001682>
- [46] Institut T 2023 Kemiske sammensætning af træ URL  
<https://www.trae.dk/leksikon/kemiske-sammensaetning-af-trae/>
- [47] Boisselet A 2017 Functional optimization of tracheids and vessels in wood URL  
<https://blogionik.org/blog/2017/03/16/tracheids-vessels/>
- [48] dupont 2020 Understanding vapor permeability URL  
<https://www.dupont.com/knowledge/truth-about-vapor-permeability.html>
- [49] Mustapha R, Zoughaib A, Ghaddar N and Ghali K 2020 *Energy* 195 117057 ISSN 0360-5442 URL  
<https://www.sciencedirect.com/science/article/pii/S036054422030164X>
- [50] Frandsen, Kirstine M and Antonov, YI and Johra, H and Møldrup, P and Jenen, R L 2021 *Experimental investigation of water vapor diffusivity in bio-based building materials by a novel measurement method*
- [51] Rolson D and Moldrup P 2002 Gas diffusivity
- [52] Iversen B V, Koppelgaard M, Christensen B B, Pérez M P, de Jonge L W and Arthur E 2016 *Laboratory Exercises Merging Measurement and Modelling of Soil Physics* 10–14
- [53] King F 1904 URL <https://www.jstor.org/stable/1631970>
- [54] Richter J and Stank K 2021 *Journal of Physics: Conference Series* 9
- [55] Fugemasse I B nd *Raytech, Støbemasse, Mængde: 500 g, Gummi, Emballage: Sæt* accessed: 08-06-2023 URL  
<https://www.stark.dk/icopal-butyl-fugemasse-310-ml?id=9240-5821620>
- [56] RS nd *Raytech, Støbemasse, Mængde: 500 g, Gummi, Emballage: Sæt* accessed: 08-06-2023 URL <https://dk.rs-online.com/web/p/indstobningsmasser/7031228>

- [57] Holysz L 1998 *Colloids and Surfaces A: Physicochemical and Engineering Aspects* 134 321–329 ISSN 0927-7757 URL <https://www.sciencedirect.com/science/article/pii/S0927775797001672>
- [58] VERTIZ O R, BRINDISI M A and MEROS E J 1967 *United States Patent Office* 3,313,739 1–3
- [59] Bry-Air nd What is silica gel and what are the advantages of it as a desiccant? Bry-Air Website URL <https://www.bryair.com/news-and-events/articles/what-is-silica-gel-and-what-are-the-advantages-of-it-as-a-desiccant/>
- [60] Sartorius N/A Sartorius entris 2202-1s balance 2200 x 0.01 g URL <https://www.scalesgalore.com/product/Sartorius-Entris-22021S-Balance-2200-x-001-g-px36703.cfm>
- [61] Vötsch 2009 *VTL and VCL for Temperature and Climatic Tests* URL [https://www.citrotek.dk/images/2009\\_laborhelfer\\_E\\_06.pdf](https://www.citrotek.dk/images/2009_laborhelfer_E_06.pdf)
- [62] Memmert 2021 Memmert uf110 universal oven accessed: 20-05-2023 URL <https://www.memmert.com/products/heating-drying-ovens/universal-oven/UF110/>
- [63] Honeywell 2008 HIH-4000 Series Humidity Sensors URL <https://www.tme.eu/Document/e6db3bab38139fc9aad882160ef7c62e/HIH-4000.pdf>
- [64] ASL nd *New F200 SERIES* URL [http://www.isotechna.com/v/vspfiles/pdf\\_datasheets/asl/F200.pdf](http://www.isotechna.com/v/vspfiles/pdf_datasheets/asl/F200.pdf)
- [65] AG N 2018 Novasina hygrodat 100 datasheet URL <https://d3pcsg2wj9izr.cloudfront.net/files/444/download/439608/1NovasinaHygrodat100datasheet.pdf>
- [66] kimoinstruments nd Vt 110 / vt 115 hotwire thermo-anemometer accessed: 22-05-2023 URL <https://www.kimoinstruments.com/detail/vt-110-vt-115-hotwire-thermo-anemometer>
- [67] Figaro 2014 *Data sheet of the Figaro GS Oxygen Sensor KE-Series*
- [68] RS 2023 Rs pro o-ring, nitrilgummi, id: 48.9mm, tykkelse: 2.62mm URL <https://dk.rs-online.com/web/p/pakninger-og-o-ringe/1964784>
- [69] Writer S 2020 What is a non-porous material? URL <https://www.reference.com/world-view/non-porous-material-a49974d247ab202e>
- [70] Sartorius 2015 *Sartorius Entris User Manual* URL <https://www.dataweigh.com/media/14445/sartorius-entris-user-manual.pdf>
- [71] thyssenkrupp materialscouk 2023 Density of aluminium accessed: 17/05/2023 URL <https://www.thyssenkrupp-materials.co.uk/density-of-aluminium.html>
- [72] thyssenkrupp materialscouk 2023 Density of stainless steel accessed: 17/05/2023 URL <https://www.thyssenkrupp-materials.co.uk/density-of-stainless-steel>

- [73] Alloys U 2021 Stainless steel vs. aluminum accessed: August 22, 2021 URL  
<https://www.unifiedalloys.com/blog/stainless-steel-vs-aluminum/>
- [74] xometry nd Selective laser sintering (sls) 3d printing technology overview accessed:  
18-05-2023 URL  
<https://www.thyssenkrupp-materials.co.uk/density-of-aluminium.html>
- [75] RS 2023 Rs pro o-ring, nitrilgummi, id: 110mm, tykkelse: 1.5mm URL  
<https://docs.rs-online.com/f20f/A700000006699145.pdf>

Part I

Appendiks

# Materials A

---

In this appendix, the different materials that are chosen for this project are described. This project has chosen to use materials such as stone wool, brick, unfired brick but also organic materials such as wood and wood fibre insulation. Stone wool has been chosen because of its open structure and its widely use as insulation in the building industry. To compare stone wool with a more environmental friendly product, wood fibre insulation has been chosen in order to compare these materials and their performances in diffusion. Bricks are more traditional materials and they have a denser structure compared to the insulation materials. To compare the traditional fired brick, unfired brick is also used in this project as this has different properties than brick. Another material that has been considered is clay, as this is the raw material of brick and has another pore structure than brick and unfired brick. The diffusion of clay is an interesting aspect to look at as the density of clay is different to bricks and therefore it is worth to look at this material.



**Figure A.1** A sample of each material used in this project. From left to right: RWI, WFI, Wood, Brick, UBR and Clay.

On figure A.1 a sample of each material can be seen. The clay is already packed in a cylinder as this could not keep its form outside of the cylinder.

**Table A.1** Six materials that have been chosen for this study. The insulation materials: stone wool (RWI), and wood fibre insulation (WFI), the traditional; wood, brick (BR) , and unfired brick (UBR), the soil; clay. Some of the properties can be seen in this table. [4], [5], [6], [7], [8], [9], [10], [11] [12]

| <b>Material</b> | Bulk Density<br>[kg/m <sup>3</sup> ] | Thermal conductivity<br>[W/m · K] | Particle density<br>[kg/m <sup>3</sup> ] | Dry density<br>[kg/m <sup>3</sup> ] |
|-----------------|--------------------------------------|-----------------------------------|--|-------------------------------------|
| RWI             | 46.4                                 | 0.033-0.045                       | 2.65                                     | 46.2                                |
| WFI             | 40-58                                | 0.036-0.038                       | 1.54                                     | 48                                  |
| Wood            | 400-700                              | 0.072-0.097                       | 1.54                                     | 356                                 |
| UBR             | 1,700                                | 0.91                              | 2.7                                      | 1,802                               |
| BR              | 1,800                                | 0.5-1.0                           | 2.7                                      | 1,768                               |
| Clay            | 746-1,515                            | 2.8                               | 2.7                                      | 1,107                               |

## A.1 Stone wool

Like most other insulation materials, stone wool insulation has a low thermal conductivity because air is embodied in the material's mass. Air when not moving and in small quantity, has the lowest thermal conductivity typically 0.024 W/(m · K). [14] The advantage of using stone wool is that it can be used in very high temperatures giving it a high fire resistance. However, it is affected by wetness and it is important to look at the performance of stone wool when moisture occurs. [14] Stone wool's structure consists of fibres with a circular cross-section and a small diameter, usually  $d < 15\mu m$  and can be oriented perpendicularly or parallel, where the first is an improvement in mechanical strength and sound absorption and the latter is an improvement in thermal insulation properties. Additional materials are used to increase the products resistance to biological impact, such as temperature change or moisture build up. [14]. Research [14] shows that when stone wool has undergone a waterproofing process, it can almost recover to its full potential, in thermal conductivity, when getting wet. This is due to the open structure that ensures when water penetrates the material it displaces the air and does not effect the material's fibres. However when stone wool is not waterproofed, study shows, that the thermal conductivity is significantly affected due to vapour condensing between fibres. The material allows for water absorption and therefore the thermal conductivity increases.

The thermal properties for stone wool insulation can vary in its thermal properties depending on its usage. The density can vary between 25-200 kg/m<sup>3</sup> with respectively varying thermal conductivity from 0.033-0.045 W/(m · K). [15]

This project chose Rockwool (RWI) as stone wool insulation as this was in stock at the time. RWI has also gone through waterproofing process, indicating that it can recover to its full potential when getting wet. The specific product that has been chosen is an A-Batt with the dimensions 965x560x95mm. [4] The density of this product is 29 kg/m<sup>3</sup>, the thermal conductivity is 0.037 W/(m · K). [4]

## A.2 Wood Fiber Insulation

Wood fibre insulation (WFI) was first introduced about 20 years ago when engineers tried to reuse timber waste from the wood processing industry. Since WFI has better

environmental properties regarding  $CO_2$ -emission, which could lead to higher demand, it is interesting to investigate this option. WFI has a higher moisture capacity than RWI and could affect the moisture condition experiences. [16] A study [17] that has done a hygrothermal simulation for a wood frame construction in Nordic climate found that WFI performs similarly to glass wool, performing slightly worse or similar during winter and slightly better or similar during summer.

Another study [6] has investigated in thermal properties of WFI, and the results show that Birch WFI can be used to obtain high-quality thermal insulation material. In addition, the study also found that the thermal conductivity quotient of WFI is characteristic of organic insulation and similar to the commonly used insulation materials such as stone wool and glass wool. The WFI demonstrates high water absorption capacity meaning more pores in the material. [6]

WFI has densities between  $30\text{-}60\text{ kg/m}^3$  and can be used in all building parts as insulation material. The thermal conductivity ranges between  $0.036\text{-}0.043\text{ W}/(\text{m} \cdot \text{K})$ . [18]. The density of this material is between  $40\text{-}58\text{ kg/m}^3$  and the thermal conductivity is  $0.036\text{-}0.038\text{ W}/(\text{m} \cdot \text{K})$ . [19]

### A.3 Wood

Wood is one the most significant types of biogenic material that is used in the building industry worldwide. It is a complex, porous material comprised of different types of cells given the material different types of pores. The characteristics of pores in wood, such as their size, shape, and distribution, play a crucial role in the material's water vapor permeability, and research and knowledge on the pore structure of wood are therefore essential. [20] There are different types of wood that is used and the density varies and is dependent on the moisture content in the material and can range in between  $100\text{-}1.000\text{ kg/m}^3$ . [8]

The wood used in this project is spruce and has the density  $400\text{-}700\text{ kg/m}^3$ . As wood has different cell structure the thermal conductivity ranges between  $0.072\text{-}0.097\text{ W}/\text{m} \cdot \text{K}$  for spruce [21]

### A.4 Unfired Brick

Unfired bricks (UBR) are air dried to reduce shrinkage and improving strength compared to conventional bricks. A study [11] shows that UBR full fill requirements for thermal transmittance as the thermal conductivity was  $0.24\text{-}0.28\text{ W}/(\text{m} \cdot \text{K})$ , which is lower than fired brick. The thermal conductivity increase with the increase of moisture, as moisture leads to heat transfer by conduction, hence the increase. In addition the water vapor diffusion coefficient  $\mu$ , is similar to the one for fired brick. [11] The ability for moisture to move through the UBR is higher, which creates better indoor environment and also prevents mold growth. [11] The study also shows that the thermal conductivity increases with the increase of density.[11] The UBR that is used for this project is a brick with the density  $0.800\text{ kg/m}^3$  and the thermal conductivity is  $0.91\text{ W}/\text{mK}$ .

## A.5 Brick

Bricks (BR) are one of the most used building materials worldwide. Different types of BRs have been developed over the years to either reduce economic costs or increase thermal properties. BRs are porous in nature and mainly have interconnected pores. The microstructure depends on many factors, such as particle size distribution and the type of burning additives. [22] A study [22] shows that the thermal conductivity of dry clay BRs can be similar to plasters and insulation boards. In addition, the study shows that the thermal conductivity/porosity dependence can be expressed by empirical relation. The average thermal conductivity is  $0.5\text{-}1.0\text{ W}/(\text{m}\cdot\text{K})$ , indicating a fairly low thermal conductivity. This contributes to effective insulation in buildings making it interesting to investigate diffusion through the material but also because of its pore structure.

This project uses the RT215, a classica yellow BR with the dimensions  $245\times 120\times 65\text{mm}$ . The density is  $1.700\text{ kg}/\text{m}^3$  and a specific thermal conductivity is not provided, so the average thermal conductivity is taken.[10]

## A.6 Clay

Clay is the main composition of fired and unfired bricks, which changes the different properties. Clay as just a raw material has a low permeability but high capillarity which means that the pore space always will be filled with water unless it is dried. [23] Clay contains different minerals; smectite, illite, chlorite, kaolin and amectit. The quantity of those minerals in the clay determine the properties of the clay. For example a clay with high amounts of smectite results in high plasticity which expands or contracts depending on the water content.

The clay used in this project is dry kaolinite clay, which later will be re hydrated as described in E. The density of kaolinite clay is  $746\text{-}1.515\text{ kg}/\text{m}^3$ . [12]

# Pore Structure and Hygrothermal Processes

---

# B

The building material's pore structure and hygrothermal processes are two fundamental properties used when modelling moisture transportation in buildings. Understanding these factors is essential to ensure the long-term functionality and the overall efficiency, durability, and comfort of a building. A building's pore structure is generally characterized by the material's porosity, pore size distribution, and connectivity, which directly impacts fluid and vapor transport through building materials. A material's pore structure can affect properties such as thermal conductivity, water vapor permeability, and capillary action. These properties are vital when modelling energy efficiency and moisture transportation within a building envelope. [20] [24]

Hygrothermal processes involve the heat and moisture transfer phenomena occurring within building materials. These processes can cause temperature and humidity variations throughout building components, affecting their properties such as thermal conductivity and water vapor permeability. Understanding hygrothermal processes is essential for managing moisture-related issues, such as condensation, mould growth, and material degradation, which can compromise the health and well-being of building occupants and the longevity of the building structure itself. [20] [24] [25]

## B.1 Hygrothermal processes in organic materials

Hygrothermal processes are most commonly used to refer to how water or moisture interacts with building materials, typically resulting in heat and vapor transfer. Here, hydrophilic surfaces play a crucial role these processes by impacting water absorption and release rates, as well as the surface energy of building materials. Hygrothermal processes are particularly significant in organic materials, which are inherently more susceptible to moisture damage than non-organic materials. [24] [25] [26]

### B.1.1 Hydrophilic Surfaces

To understand what a hydrophilic surface is, knowing the difference between a hydrophilic and a hydrophobic molecule is essential. Hydrophilic (from ancient Greek, water-loving) molecules can attract to water. Hydrophilic molecules are polar due to an asymmetrical distribution of electrons around the molecule. The asymmetrical distribution of electrons means they have regions of partial positive and negative charges. On the other hand, hydrophobic molecules are non-polar because they have a symmetrical distribution of electrons. This symmetrical distribution of electrons makes the hydrophobic molecule

repel water, meaning the molecule does not easily dissolve or mix with water. An example of a hydrophilic and a hydrophobic molecule is shown in figure B.1. [27] [24]

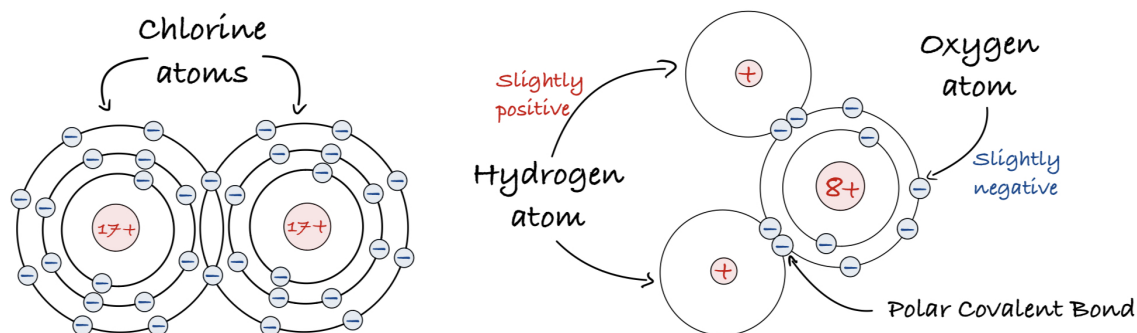


**Figure B.1** An sketch of a hydrophilic and a hydrophobic molecule in the form of a water molecule on the right and a chlorine molecule on the left.

On the left of figure B.1 is a sketch of a chlorine molecule, and on the right is a water molecule. Here, the chlorine molecule on the left comprises two chlorine atoms that bond by sharing their electrons. This kind of bond is what is called a polar covalent bond. Chlorine molecules are electrically neutral because they have an equal number of positively charged protons and negatively charged electrons. On the other hand, water molecules are an example of a polar molecule. Polar molecules have permanent poles of electrical charge like a magnet due to an asymmetrical distribution of electrons around the molecule. On the right is a sketch of a water molecule which consists of two hydrogen atoms and one oxygen atom. However, this means there is an uneven number of positively charged protons and negatively charged electrons around the molecule, making it slightly positive charge on one of the sides and slightly negative charge on the other. [24] [27]

When polar molecules are near each other, a force of attraction known as the Van der Waals Force will occur between the molecules because of their oppositely charged poles. When the slightly positive charge hydrogen atoms come close to a nitrogen, oxygen or fluorine atom, a strong type of Van der Waals force known as a hydrogen bond will occur. A hydrogen bond between water molecules is sketched in figure B.2. [24] [27]

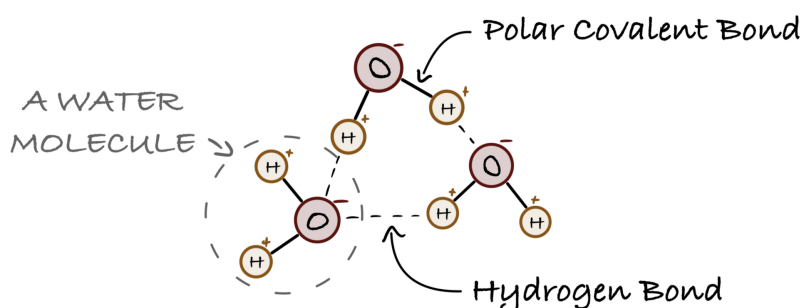


**Figure B.2** A sketch of three water molecules, consisting of two hydrogen atoms and one oxygen atom, that are bonded together by a polar covalent bond. It can be seen that a force of attraction known as a hydrogen bond occurs between the molecules. [24] [28]

Bricks and other stones are composed of carbonate crystals, silicates, aluminates or oxides. The surfaces of these crystals, or glasses, are rich in oxygen atoms which carry negative

electrical charges. It is also believed that the surface oxygen is frequently bound on one of the sides of a hydrogen atom, forming a hydroxyl group, which is sketched in figure B.3. [24] [29]

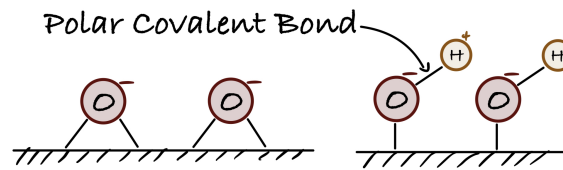


**Figure B.3** On the left, a surface of oxygen is sketched. The oxygen atoms are bound to the surface by a polar covalent bond. On the right, a hydroxyl group is sketched, which occurs when a surface oxygen bounds on one of the sides of a hydrogen atom. [24] [28]

Water molecules can be attracted to a surface if it comes close enough to the oxygen on the surface. This attachment will happen because the positively charged hydrogen atom will bond to the negatively charged oxygen atom on the surface by creating a hydrogen bond. In the case of surface hydroxyl groups, the water molecules can attach to both the positive hydrogen and the negatively charged oxygen. As water molecules can attach to both types of surfaces, the surface is categorised as a hydrophilic surface. Both types of surfaces are sketched in figure B.4. [24] [27]

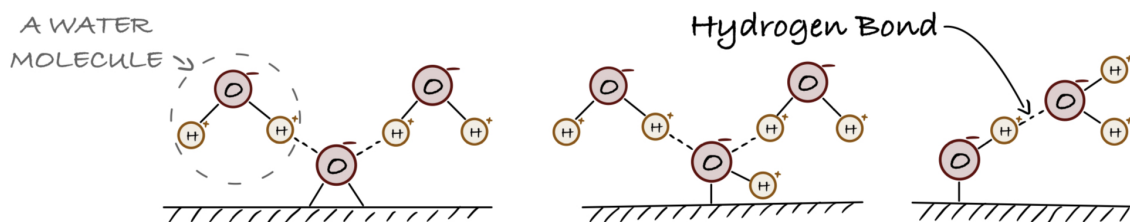


**Figure B.4** On the left, a hydrogen bond between a surface of oxygen and a water molecule is sketched. In the middle and on the right, a hydroxyl group surface is sketched, where the water molecules can attach to either the positive hydrogen atom or the negatively charged oxygen atom. [24] [28]

Usually, every oxygen atom forms two hydrogen bonds besides the two polar covalent bonds it constantly forms. In contrast, a hydrogen atom only can form one hydrogen bond in the opposite direction from its polar covalent bond. The hydrogen bond is ten times weaker than a typical polar covalent bond but is still strong enough to require a significant amount of energy before it will break. Because the bond is so strong, a layer of water can form on the surface, creating waterfilm, potentially leading to water-filled pores. [24]

### B.1.2 Surface Tension and Capillary Rise

The water molecules at the surface of a water droplet will experience a downward force. This force is because the molecules are attracted to the molecules to the left and right and the molecules below it. Since no water molecules are above it, the water molecule will not experience an upward force. The missing molecule means that the force acting on a water droplet will be directed towards the interior of the water droplet, given the water droplet its spherical shape, as sketched in figure B.5. This force is also known as surface tension. [24]

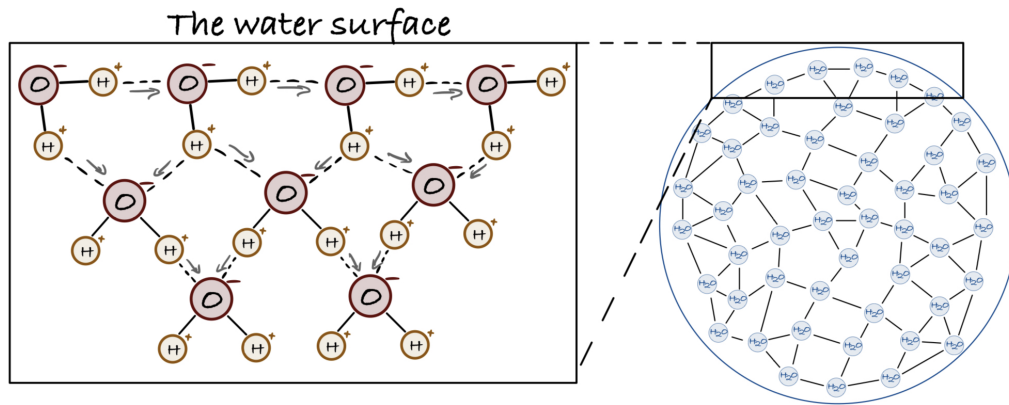


**Figure B.5** On the right is a water droplet sketched, where it is possible to see the individual water molecules. If zoomed in on the surface of the water drop, it can be seen that the water molecules at the surface of a water droplet will experience a downward force since no water molecules are above it. This downward force creates what is known as surface tension. Water droplets have a spherical shape because surface tension wants to minimise the surface area of water. [24] [28]

When a water droplet comes in contact with a hydrophilic surface, the shape of the droplet is determined by the force of attraction of water molecules at the droplet's surface to the hydrophilic surface. Here, the contact angle between the water molecule and the hydrophilic surface is an easy way to measure the force of attraction. A large contact angle in polar liquids like water shows that the force of attraction is weak. In contrast, a small contact angle indicates that the force of attraction is strong. Therefore, the contact angle will depend on whether the internal hydrogen bond or the external attraction between the solid and the water is the dominant attraction force. The contact angle is sketched in figure B.6. [24]

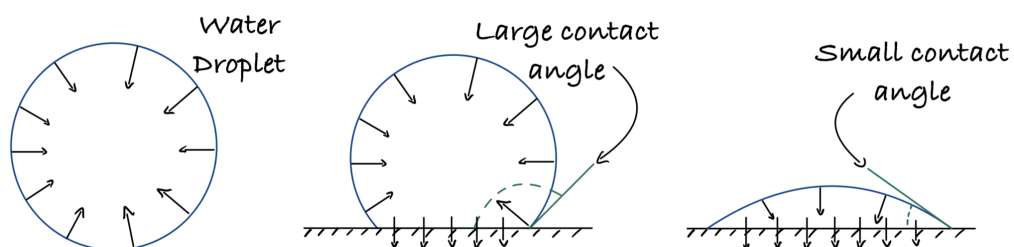


**Figure B.6** On the left is a sketch of a water droplet, where the force created by surface tension can be seen as arrows. A water droplet and a solid are shown in the middle, with a low attraction between the two objects. Lastly, on the right is a water droplet and a solid is shown with a high attraction between the two objects. [24]

In tiny pores, the water molecules will be attracted toward both walls of the pores, meaning that the water droplet will form a meniscus shape due to the water surface being drawn inward by the hydrogen bonds. This attraction can lead to water-filled pores, which will be blocked, which is sketched in figure B.7. [24]

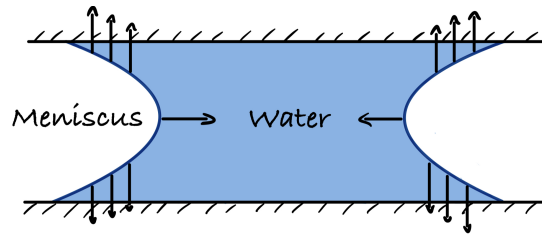


**Figure B.7** A sketch of a tiny water-filled pore where the meniscus shape is shown. The shape is caused by the water surface being drawn inward by the hydrogen bond. [24]

In minuscule pores, water will be drawn into the pores if the attraction to the surfaces of the pores is stronger than the water's internal attraction. The suction force's size will depend on the pore surface's hydrophilicity and the pore's diameter. The smaller the pore's diameter, the stronger the suction force. The suction force, also called the capillary force, is frequently large enough to offset the force of gravity and make the water rise inside pores. This phenomenon is also known as capillary rise. [24]

### Water Distribution in Porous Materials Under Various Moisture Levels

Absorption and adsorption are two fundamental processes that affect water vapor transport through these materials. However, it is common to switch between the two terms. Adsorption involves the water molecule adhesion of molecules to the material's external or internal surface. The adhesion can be a physical or chemical process. For example, silica gel is known for its ability to adsorb water from the air. On the other hand, absorption refers to the process by which a material draws water molecules into the bulk of the material. For example, water is absorbed by a sponge when it is soaked up. It is sometimes difficult or impossible to distinguish between adsorption and absorption. Therefore, it is sometimes beneficial to use the wider term sorption, as it contains both absorption and adsorption. Absorption and adsorption is sketch in figure B.8. [30]

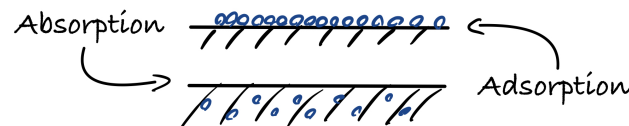


**Figure B.8** A sketch which shows the difference between absorption and adsorption.

While sorption takes water vapor from its environment, desorption is when a material releases water vapor back into the environment. To accurately predict and control water vapor transmission, it is common to use a sorption isotherm to understand the absorption and desorption behaviour of building materials. A sorption isotherm is a graph or equation that shows the relationship between the amount of moisture that can be absorbed and the relative humidity in the surrounding environment. An example of a sorption isotherm is shown in figure B.9. [30]

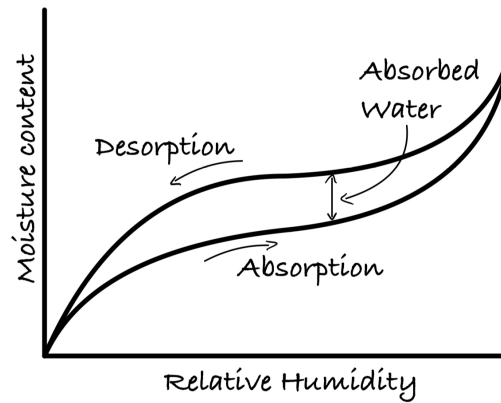


Figure B.9 A sketch of a sorption isotherm [30]\*

The two curves that can be seen represent two extremes, i.e. how a material will react if it is completely dry and how it will react if the material pore is entirely wet. In daily use, a material will lie somewhere between the two curves. The difference between the two curves is that the material absorbs some moisture, which will remain in the material for longer. However, the moisture can also be adsorbed. If a dehydrated material, meaning all pores are empty, gets exposed to moisture, only the smallest pores (capillaries) will be filled in the start due to the Van der Waals Force, as the moisture will be attracted to the nearby surfaces. After some time, all the capillaries will eventually be filled up, and the surfaces of the large pores will have a film of water. If enough moisture appears, both capillaries and large pores are full. If desorption occurs, the moisture will leave the large pores, but due to the chemical bond through the Van der Waals Force, the moisture will remain in the capillaries. Because it is necessary to destroy the bond before the moisture disappears, it will also be seen that the material will have adsorbed some moisture in a sorption isotherm. This process is sketch in figure B.10. [24] [30]

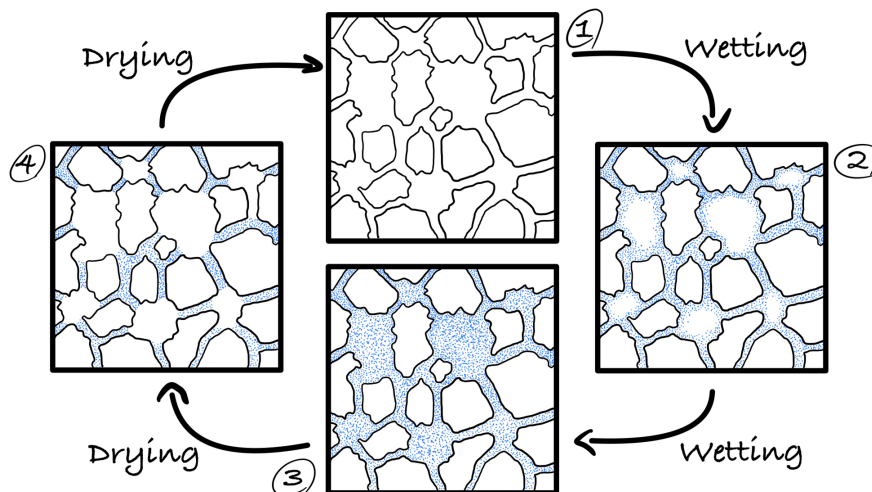


Figure B.10 A sketch of water distribution in a porous material. [24]\*

### B.1.3 Movement of Water Molecules

Several types of forces can cause the movement of liquid water inside a porous material. Water can move through suction forces as the force that creates capillary rise. Water can

also move through diffusion if the material has a high water content above (2) in figure B.10. If the water content is high enough, water will also move from warmer regions to colder ones. Although these forces are not immediately expected to affect the movement of water vapour, the forces can affect the previously described water film, which may appear on the material surface. However, as building material's water content hardly ever gets high enough for these forces to impact the water vapor transmission significantly, will the forces not be investigated further. Therefore, the focus will instead be on the forces that create movement in water vapour. [24] [31]

One force expected to impact water vapour's movement significantly is the force created by vapor diffusion. The force is created by a water vapor pressure differential across a material. The higher differential pressure will increase the permeability of a material, as the water vapor will be transferred from regions with a higher number of water molecules in the air to regions with fewer water molecules. Condensation is also something to consider, as when warm, moist air comes into contact with a cold surface, water droplets can form on the surface of the material. [32] [33] [34] [24]

## B.2 Pore Structure

The materials in this project consist of different pore structures. the insulation materials consist of very open pore structure whereas wood is more complicated. The clay based materials have a pore structure with smaller pores but still slightly porous.

### B.2.1 Types of Pores

In order to understand how the pore structure affects the permeability of a material, it is essential to be aware of the composition of the material. The composition of the material, including its chemical structure, porosity, and surface area, affects the material's ability to allow water vapor to pass through it. The pore structure of a building material can significantly influence its permeability. The size and distribution of the pores can also play a significant role in the material's permeability. For example, a material with smaller pore sizes will typically have less permeability, as there is less space for fluids to flow through. The type of pores within a material can vary, including open, closed, and interconnected pores. These types of pores are sketched in figure B.11. [35] [36]

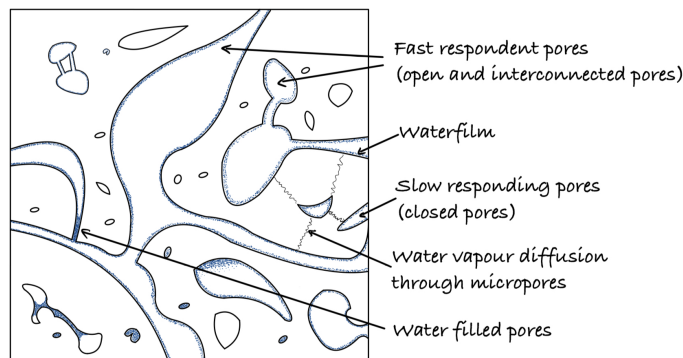


**Figure B.11** A sketch of the type of pores found within a material. [36]\*

The tortuosity of a material's pore structure is also essential in its permeability. Tortuosity measures the degree to which the flow path through the pore structure differs from a straight line. A material with high tortuosity will have a more convoluted or winding flow path, which can increase the resistance to flow and reduce permeability. A sketch that visualizes tortuosity is shown in figure B.12. [37]

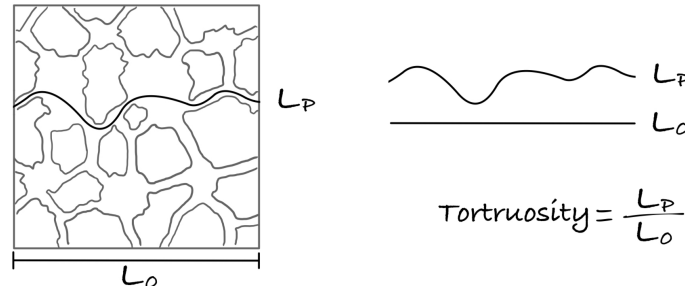


**Figure B.12** A sketch to visualize tortuosity. [24]\* [37]

### B.2.2 The Pore Structure for Insulation Materials

In this project, two types of insulation materials will be investigated. The first type is RWI. The material is made from natural rocks that are heated and spun into thin, smooth fibres. These fibres are then bound with a binder to create a dense, non-combustible insulation material. [38] A Scanning Electron Microscopy (SEM) image is shown in figure B.13 and B.14. [39]

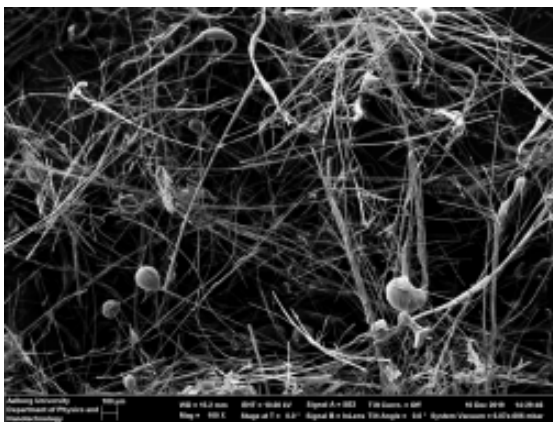


**Figure B.13** An SEM image of RWI with a low magnification of 100x. [39]

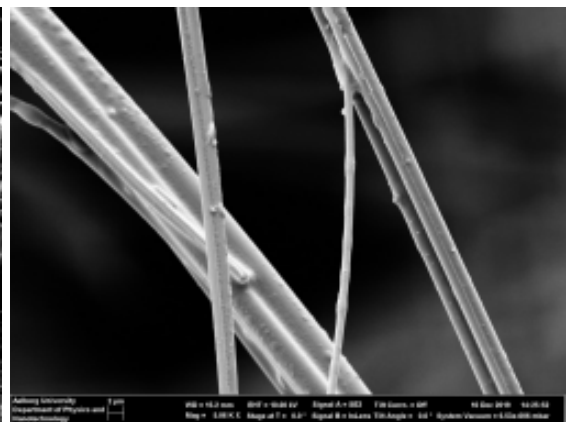


**Figure B.14** An SEM image of RWI with a high magnification of 500x. [39]

The fibres in figure B.13 and B.14 appear to have a thickness of approximately 2-10  $\mu\text{m}$  in diameter. The unique pore structure in RWI works to provide superior thermal, acoustic, and fire-resistant properties. The fine fibres in RWI create a non-directional, irregular network, allowing the material to maintain its shape without settling over time. The gaps between the fibres create open pores, also known as air pockets, which are interconnected. The combination of an irregular fibre network and the open pores trap air within its structure. This trapped air forms a barrier against heat and sound transfer as the fibres slow down the movement of the air molecules. As shown in figure B.13, RWI has a mix of small and large pores, resulting in a broad range of pore sizes. The smaller pores provide

effective sound absorption, while the larger pores contribute to reducing convective heat flow and airflow. [40] [14]

On the other hand, wood fiber insulation (WFI) is made from wood chips or sawdust, mixed with a binder and compressed into a batt. The difference between the two materials is found primarily in their fibres. WFI has much larger fibres than RWI. The fibres in WFI also have a high cellulose content, which gives them excellent hygroscopic properties. This property means the fibres can absorb and release moisture. [31] [41]

### **B.2.3 Clay Based Materials Pore Structure**

BR and UBR are typically made from clay, but even though both are based on the same material, can their pore structure vary significantly due to their manufacturing processes. BR are made by moulding clay, after which the clay is dried and burnt at high temperatures of 900 or higher. This manufacturing process results in several changes in the material's pore structure. The high temperatures cause the clay to partially vitrify, meaning a small quantity of glass-like material forms. The vitrification reduces porosity by melting clay particles which will fill some pores. The melted clay particles make the bricks more dense and less permeable. The process can also shrink the clay, causing pores to be smaller. [42] [43]

UBR are made from clay and water moulded and then allowed to dry in the sun. The lack of firing in their manufacturing process leads to different pore structures and properties. Because unfired bricks do not undergo any vitrification or shrinkage during production, the material usually has larger pores and, therefore, a higher porosity than the fired bricks. [44]

Unmoulded clay minerals have a layered structure, with water molecules and other ions often occupying spaces between the layers, which can significantly impact the overall pore structure of the clay. The particle size of clay can vary greatly, with smaller particles resulting in a more densely packed structure and a higher specific surface area, leading to a more substantial volume of pores. The presence of water in clay also affects its pore structure, as it creates a waterfilm over the surface, making the pore smaller and creating water-filled pores, thereby blocking the pores. [29] [45]

### **B.2.4 Wood's Pore Structure**

Wood has a slightly more complicated pore structure than the other materials described. Wood is made up of small hollow vessel pores that are significantly longer along the length than across. Typically cells are about 1–3 mm long and about 10–100 times smaller across. Therefore, these cells act as long straws that can transport water across the wood. On a nanometer scale, wood is a chemical composed mainly of cellulose, hemicellulose, and lignin, along with small amounts of other organic and inorganic compounds. The chemical composition of wood can vary depending on the species, age, and growth conditions of the tree, as well as the part of the tree from which the wood is obtained. [20]

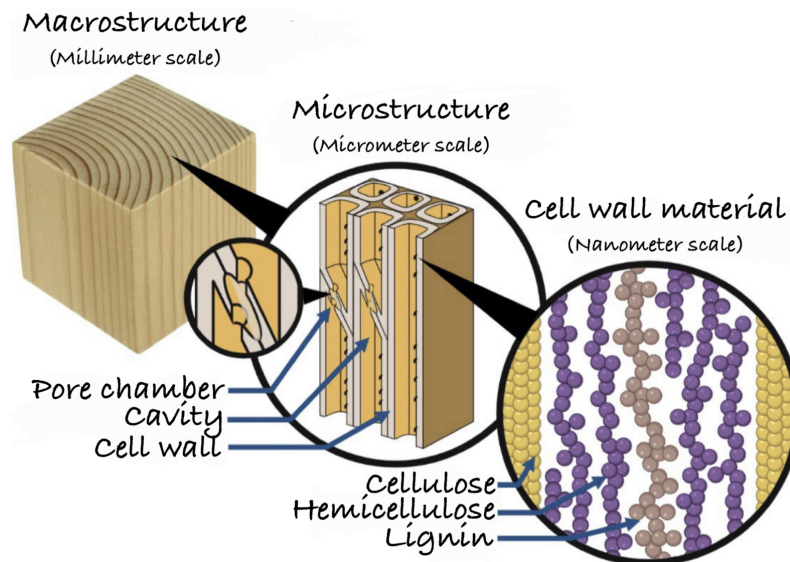


**Figure B.15** Picture of the pore structure of wood. [20]\*

Cellulose is the most abundant organic compound in wood, accounting for about 40-50% of its dry weight. It is a complex carbohydrate made up of long chains of glucose molecules, arranged in a crystalline structure. This is also shown in figure B.15. Cellulose provides strength and rigidity to wood making it tightly packed, which limits the movement of water vapor through the wood structure. [46] [20]

Hemicellulose is another type of carbohydrate that makes up about 20-30% of the dry weight of wood. It is composed of shorter chains of various sugars, such as xylose, mannose, and galactose. Hemicellulose acts as a cementing material that binds cellulose fibers together and contributes to the overall structure of wood. As hemicellulose is less crystalline than cellulose in its structure, hemicellulose also has a higher water vapor permeability compared to cellulose. [46] [20]

Lignin is a complex polymer that makes up about 20-30% of the dry weight of wood. It provides rigidity and strength to wood and acts as a natural adhesive that binds cellulose and hemicellulose together. Lignin is hydrophobic and can reduce the water vapor permeability of wood. Water vapor diffuses through the cell walls, meaning the presence of lignin in the cell walls makes it difficult for water molecules to pass through. The hydrophobic nature of lignin creates a barrier against water vapor diffusion, reducing the rate of moisture transfer through the wood. [46] [20]

Wood may also contain various organic and inorganic compounds. These compounds are also known as extractives, and are not content as part of the main structural components of wood. Extractives may include compounds such as resins, oils, tannins, waxes, and pigments. Extractives can also influence the water vapor permeability of wood by blocking some of the pores. The compounds may also have hydrophobic or hydrophilic properties, depending on their chemical nature. [46] [20]

On a micrometer scale, wood pores are categorized into two types: vessel elements and tracheids. These pores are interconnected channels that allow for the movement of water vapor, air, and other substances within the wood. Vessel elements are normally found

in hardwood and are shorter, wider cells that are arranged end-to-end to form vessels. Tracheids on the other hand are longer, narrower cells that are found in both hardwoods and softwoods. This section will focus on tracheids, as this is the type of pores found in the wood that will be examined. Tracheids have smaller openings called bordered pits on their cell walls, which allow for lateral water movement between adjacent cells. An illustration of the pore structure on a micrometer scale can be seen in figure B.15, where the small openings can be seen as small black dots. [20] [47]

However, the size, shape, and distribution of pores in wood are not homogeneous throughout the material. Due to changes in temperature over the different seasons, the size of the newly formed pores will vary. This can be seen on most types of wood as small rings through wood samples. There can be a significant difference in the size, shape, and distribution of the pores in these rings, which can greatly impact water vapor permeability. The types of wood that have these rings are also known as ring-porous woods. Other woods, such as maple and pine, have smaller, less distinct pores and are referred to as diffuse-porous woods. [20]

# Water vapor Permeability by the Wet/Dry Cup Method



---

The transmission of water vapor is essential to modelling moisture transportation in buildings [48]. Water vapor transmission is most commonly expressed as water vapor permeability, and various specialized test apparatuses exist to measure water vapor permeability in materials. However, the wet/dry cup method published by The European Standard (DS/EN) and defined in DS/EN ISO 12572 [1] is the most commonly expressed. The method is based on Ficks law of diffusion and determines water vapor permeability by generating vapour pressure gradients across material samples [49]. The gradient is specified in the DS/EN ISO 12572 [1] and tries to simulate the boundary conditions observed across building elements under real-world conditions. The wet/dry cup method keeps track of the mass change rate by weighing the sample periodically, which is the foundation for finding the water vapor permeability. However, using water vapor as the tracer gas is found to cause issues as water vapor is generally hard to control. Additional moisture mechanisms, such as water vapor sorption, surface diffusion, capillary effects, and Van der Waals forces, can impact the physical interactions in the water-air and air-pore surface interface. Such moisture mechanisms are, for example, observed in the new bio-based building materials, requiring reliable methods to characterize their strange hygrothermal behaviour.

Appendix D will introduce a new method that isolates pure diffusion through a material to better understand how moisture affects water vapor transmission. The method that will be used is developed from soil physics and is based on a single-chamber set-up: in this case, the Oxygen Diffusion Apparatus 2020 (ODA20). The apparatus characterises a material's diffusivity by employing oxygen as a tracer gas instead of the water vapor used in the wet/dry cup method.

## C.1 Methodology for the Wet/Dry Cup Method

Water vapor permeability was measured using the wet/dry cup method, and the setup was designed to follow the recommendation of DS/EN ISO 12572 [1] as closely as possible. Six different materials were selected for the measurement as described in appendix A. The materials are prepared by getting cut into a circular shape with a diameter of 49 mm and a height of 51 mm, giving the sample a volume of 100 cm<sup>3</sup>. The sample side edges are sealed with magic rubber and put into a metal cylinder to prevent water vapor from passing through the edges. Before testing, the samples were conditioned at a temperature of 23 ±

1.0 °C and an RH at  $50 \pm 5\%$  in the VCL 7010 climate chamber. When the test samples are conditioned, the test cup will be filled with 15 mm salt solution measured from the bottom, which gives the air layer between the test sample and desiccant a thickness of 15 mm. Using an O-ring, the test sample will be sealed to the open side of a test cup. This assembly is shown as a 3D model in figure C.1, and a deeper description of the test cup can be found in appendix H.

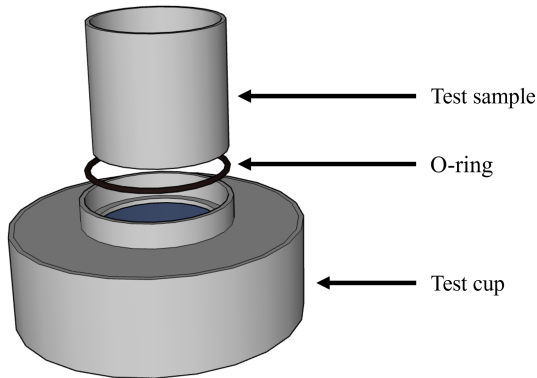


**Figure C.1** 3D model of the test assembly showing the cylinder, O-ring, and test cup. **Figure C.2** A picture of a example of a test test assembly used in the experiments.

After the test assembly is put together, it is weight and then placed back into the VCL 7010 climate chamber. The difference in the vapour pressure between the cup and the chamber will cause a vapour flow through the permeable test sample. The test assembly will then be periodically weight to determine the mass change rate, which will be used to find water vapor permeability. When the test assembly is weighed, it will be removed from the climate chamber and placed on the ENTRIS 2202-1S balance. This process is outlined in figure C.3, and the entire method is outlined in the measurement plan, which can be found in section C.2.

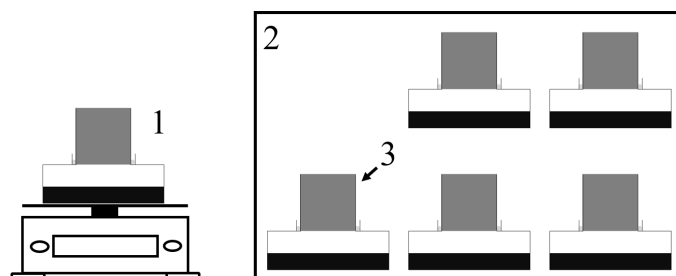


**Figure C.3** 1: Balance, 2: Controlled environment/Climate chamber, 3: Test assembly.

### C.1.1 Data analysis

Before finding the water vapor permeability, it is necessary to find the mass change rate, which can be used to find the water vapor permeance, which multiplied by the thickness of the test sample, gives the water vapor permeability.

#### Mass Change Rate

To find the water vapor pressure gradient over the sample, measuring how much water vapor enters the sample is first necessary. The method that will be used in this report is

to measure the mass change rate. The change in mass can be used to estimate the amount of water vapor that crosses the sample for some time. The mass change rate,  $\Delta m_{12}$ , is calculated for each set of weighing the specimens by using equation C.1:

$$\Delta m_{12} = \frac{m_2 - m_1}{t_2 - t_1} \quad (\text{C.1})$$

Where

|                 |   |        |
|-----------------|---|--------|
| $\Delta m_{12}$ | is the change of mass per time for a single determination | [kg/s] |
| $m_1$           | is the mass of the test assembly at time $t_1$            | [kg]   |
| $m_2$           | is the mass of the test assembly at time $t_2$            | [kg]   |
| $t_1$ and $t_2$ | are the successive times of weighings                     | [s]    |

Then the water vapor flow rate through specimen (also known as  $G$ ) can be found from the mean of five successive determinations of  $\Delta m_{12}$  for each test sample can be calculate. When each of the last five  $\Delta m_{12}$  is within  $\pm 5\%$  of  $G$ , the final water vapor flow rate through specimen value,  $G$ , is obtained.

### The water vapor permeance

To find the water vapor permeability, the water vapor permeance,  $W$ , must first be found, which is given by equation C.2:

$$W = \frac{G}{A \cdot \Delta p} \quad (\text{C.2})$$

Where

|            |   |                                |
|------------|---|--------------------------------|
| $W$        | is the water vapor permeance                        | [kg/(m <sup>2</sup> · s · Pa)] |
| $G$        | is the water vapor flow rate through sample         | [kg/s]                         |
| $A$        | is the exposed area                                 | [m <sup>2</sup> ]              |
| $\Delta p$ | is the gradient of partial pressures of water vapor | [Pa]                           |

When following the methods suitable for self-supporting materials described in DS/EN ISO 12572 [1], the exposed area is the mean exposed area of the samples upper and lower exposed area:  $A = (A_1 + A_2)/2$ . In the case of the sample used in this test,  $A = A_1 = A_2$  as it is a uniform cylinder and the opening in the cup has the same diameter as the test sample inner diameter. For test condition A, which is chosen for these measurements,  $\Delta p$  will be 1404 Pa.

### The water vapor permeability

Now, the the water vapor permeability,  $\delta$ , can be found as a product of the water vapor permeance and the thickness of a homogeneous specimen as given in equation C.3.

$$\delta = W \cdot d \quad (\text{C.3})$$

Where

$$\delta \left| \begin{array}{l} \text{is the water vapor permeability} \\ \text{is the thickness of the sample} \end{array} \right. \begin{array}{l} [kg/(m \cdot s \cdot Pa)] \\ [m] \end{array}$$

It has been chosen to focus on making a dry cup method measurement using silica gel as the salt solution. Silica gel is chosen as a salt solution, which is also recommended in the DS/EN ISO 12572. [1] However, the silica gel is found to have some challenges, such as not staying at 0% RH. This could be due to several reasons. The study [3] lacks details about the silica gel used, including particle size, concentration, or if the silica gel has been prepared by being dried. Therefore an investigation of the silica gel can be found in appendix F. Based on this investigation found in appendix F, it has been seen that silica gel can keep the relative humidity within the recommendations made in DS/EN ISO 12572 [1], and it has therefore been chosen to use silica gel for the measurements that can be found in this appendix.

## C.2 Detailed Measurement Plan

This measurement plan investigates how the dry cup method is used in the project, including the equipment used, how the test assembly is build, and the measurements' results. The project uses the cup method to investigate how a building material's pore structure and hygrothermal processes affect water vapor transmission. The hygrothermal processes will be analysed by comparing the dry cup method data to the ODA20's oxygen diffusion. The water vapor permeability will be measured on six samples of various materials. The chosen materials and justification for choosing the materials can be found in chapter A. Details about the equipment used in the dry cup method can be found in table C.1 below.

**Table C.1** List of equipment used in the setup used to find water vapor permeability by the dry cup method.

| Brand     | Model                 | Description               | Serial Number  |
|-----------|-----------------------|---------------------------|----------------|
| Microsoft | Surface Book 2        | Computer                  | 000872474957   |
| MathWorks | Matlab R2020b         | Software                  | -              |
| Vötsch    | VCL 7010              | 100L Climate chamber      | 56546008970010 |
| Sartorius | ENTRIS-2202-1S        | Balance                   | 0037102819     |
| Mensor    | 2104                  | Digital pressure gauge    | 53099          |
| IC-Meter  | IC-Meter Mobile (GSM) | Sensor                    | 872d5688       |
| ASL       | F200                  | Precision Thermometer     | 000031/74      |
| Novasina  | Hygrodat 100          | Precision Humidity Sensor | 0901002        |
| Kimo      | VT110                 | Anemometer                | 1p15087710     |
| RS PRO    | Nitrile rubber 48.9   | O-ring                    | 196-4784       |
| -         | The test cup          | Measuring Method          | -              |
| -         | Silica gel            | Desiccants                | -              |
| -         | Test sample           | The Investigated Material | -              |

### C.2.1 The Setup used in the Dry Cup Experiments

The wet/dry cup method is a well-known method for determining water vapor permeability by generating vapour pressure gradients across material samples. The gradients specified by the standard DS/EN ISO 12572 [1] have been designed to simulate the boundary conditions observed across building elements under actual conditions. The method is described in detail in DS/EN ISO 12572 [1] and a schematic sketch of how the setup in this experiment will look like can be seen in figure C.3.

The method used in this experiment is based on the DS/EN ISO 12572 [1] standard but with a few modifications. It is desired to use the same sample as examined in the ODA20 tests, see appendix D, and it has therefore been chosen to ignore the requirement that the diameter of the sample must be at least twice the sample's thickness. The test cups used in the experiment are based on the method suitable for self-supporting materials described in DS/EN ISO 12572 [1]. The test cup is described in detail in section H. The test cup and the cylinder are held together by an o-ring with an inner diameter of 48.9 mm and a thickness of 2.62 mm.

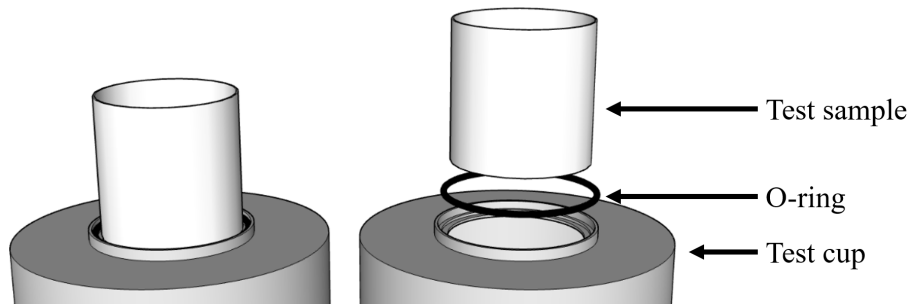


**Figure C.4** 3D model of the test assembly showing the cylinder, O-ring, and test cup.

To create the boundary conditions described in DS/EN ISO 12572 [1], the air layer in the test cup needs to have an RH at  $0 \pm 5\%$ . Orange silica gel has been used as the drying agent to adsorb moisture from the air in the test cup. An investigation of the drying agent can be found in appendix F, where more specific details of how the moisture physics in silica gel works can be found.

To achieve the boundary conditions described in DS/EN ISO 12572 [1] around the test assembly, the test assembly will be placed in the VCL 7010 climate chamber by Vötsch with a RH of  $50 \pm 5\%$  and a temperature of  $23 \pm 1.0^\circ\text{C}$  until the assembly has gained more than 1.5 g per 25 ml of desiccant in the cup. In order to ensure uniform conditions throughout the chamber, the air will be mixed so as to obtain velocities between 0.02 m/s and 0.3 m/s by a fan in the bag of the chamber. To check that the VCL 7010 complies with the air velocity, a Kimo VT110 anemometer has been used to measure the air velocity in the climate chamber. Here, the speed was measured to be between 0.15 m/s and 0.25 m/s, within the recommendations described in DS/EN ISO 12572 [1]. Before the climate chamber is used, a quality control of the temperature and relative humidity inside the climate chamber is carried out using precision equipment such as the F200 precision thermometer and the Novasina Hygrodat 100 precision humidity sensor.



**Figure C.5** The picture showcases the interior of a climate chamber, where the six test assemblies can be seen.

As an additional control in the climate chamber, two IC-meter will be used to keep a constant eye on the temperature and the RH. To find the water vapor permeability of air, the barometric pressure is also needed. The barometer will be connected to the climate chamber using a tube. To be able to measure the mass change rate of the test sample, it is necessary to have a balance that has specifications capable of weighing the test assembly with the repeatability needed for the required accuracy. As described in section H, a balance resolution of 0.01 g is considered sufficient, and the ENTRIS 2202 1S is therefore chosen. A more in-depth description of all the equipment can be found in chapter G.

### C.2.2 Method used step by step

1. Place the IC-meter inside the climate chamber and check that the climate chamber is filled with distilled water.
2. Switch on the climate chamber for a minimum of one hour before testing or until it reaches a stable temperature of  $23 \pm 1.0^\circ\text{C}$  and a RH of  $50 \pm 5\%$ .
3. Set up the barometer and pull a tube from the barometer into the climate chamber.
4. When the climate chamber is stabilized, make a quality control of the air velocity, temperature and relative humidity inside the climate chamber by using precision equipment.
5. Place the test sample in the climate chamber at a temperature of  $23 \pm 1.0^\circ\text{C}$  and a RH of  $50 \pm 5\%$  until the weight of the sample stabilizes.
6. When the test sample weight stabilizes, fill the test cup to 15 mm from the bid with silica gel (equivalent to approximately 110 g).
7. Assemble the test setup by assembling the test cup with the test sample using an o-ring, see figure C.4.
8. Measure the weight of the assembly and place the assembly in the climate chamber. The weight of the cup should be measured at regular intervals during the test to determine the rate of water vapor transmission through the sample (approximately once a day).
9. This is repeated until the assembly has gained more than 1.5 g per 25 ml of desiccant in the cup. The test cup used in this experiment has 150 ml, the experiment is until the assembly has gained 9 g.

It is expected that this experiment will take three to four weeks, or until the mass change rate is stable.

### C.3 Results and discussion from the Dry Cup Experiments

For dry cup experiments, six test samples have been tested according to the recommendation of DS/EN ISO 12572 [1]. There has only been tested one samples for each building material. The number of test samples is due to the main objective of this report is to compare data from the dry cup method to the pure diffusion found by the ODA20, which has been found in appendix D. The test assembly has been weighted periodically, as shown in figure C.6. Before the experiment started, the six materials were kept in the climate chamber under a stable temperature of  $23 \pm 1.0^\circ\text{C}$  and an RH of  $50 \pm 5\%$  for a week to stabilize the samples. In figure C.6, it can be seen that the clay sample started three days later than the rest of the test samples. The later start was because the clay was very fragile, and the selected test sample was damaged while being stabilized inside the climate chamber. Therefore, clay sample No. 4 was used instead of No. 2, found in appendix D.

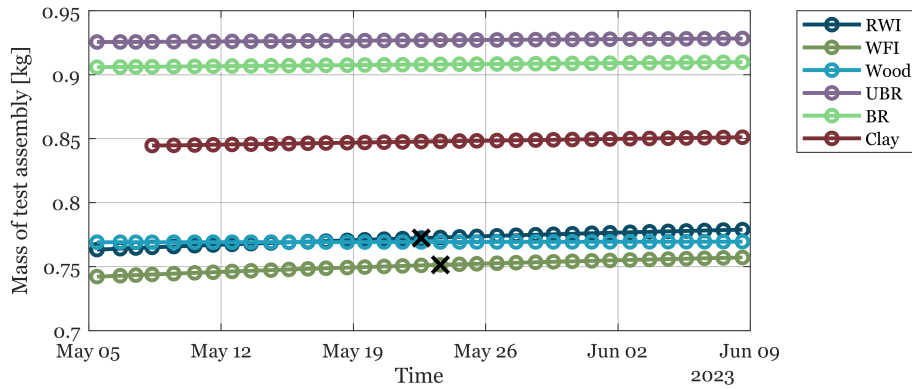


**Figure C.6** Measurement of the test assemblies weighted during dry cup experiments performed with silica gel. In the figure, two crosses can be seen on RWI and WFI, respectively. The crosses maker when samples have achieved a weight increase of 9 g, which means that they are stable according to the DS/EN ISO 12572 [1].

In figure C.6, the mass of the test assembly is shown over the time the measurement has run. On RWI and WFI, it is marked when the test assemblies achieved a weight increase of 9 g, which is one of the criteria for the test being stable according to the DS/EN ISO 12572 [1]. Figure C.6 shows that the first sample that becomes stable according to this recommendation is RWI, which becomes stable after 18 days. After that, it is WFI that achieves stability after 19 days. DS/EN ISO 12572 [1] also recommends that the water vapor flow rate through the sample ( $G$ ) used for the calculations should be within  $\pm 5\%$  of each of the last five determination of the mass change per time ( $\Delta m_{12}$ ). To investigate if  $G$  meets this criterion, the density of the water vapor flow rate, defined as  $g$  in DS/EN ISO 12572 [1], is calculated after each weighing of the sample, as shown in figure C.7.  $g$  is  $G$  divided by the exposed area, as is chosen to be shown as it is used in other papers [3], and it will therefore be easier to compare.

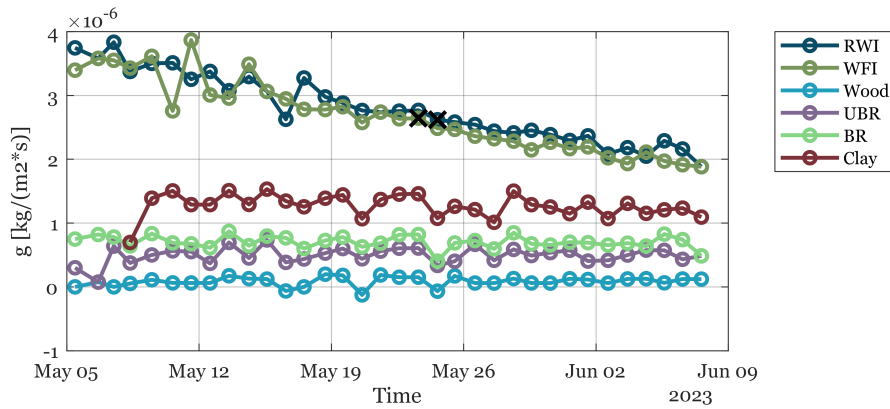


**Figure C.7** Measurement of the density of the water vapor flow rate ( $g$ ) during dry cup experiments performed with silica gel. In the figure, two crosses can be seen on WFI and RWI, respectively. The crosses mark when each of the last five  $\Delta m_{12}$  is within  $\pm 5\%$  of  $G$ , which gives the final  $G$  value according to the DS/EN ISO 12572 [1].

Figure C.7 shows how the density of the water vapor flow rate,  $g$ , decreases over time. The decrease is due to the test sample being air-dry when the experiment starts and therefore has the same humidity throughout the sample. Therefore, when the sample boundary conditions change from 50% at the bottom to 0% at the start of the experiment, the moisture in the bottom of the sample will easily penetrate into the cup. Then the moisture in the centre of the sample will have to penetrate the sample, which needs to penetrate more material. This will slowly create a moisture gradient through the sample, as shown in figure C.8.

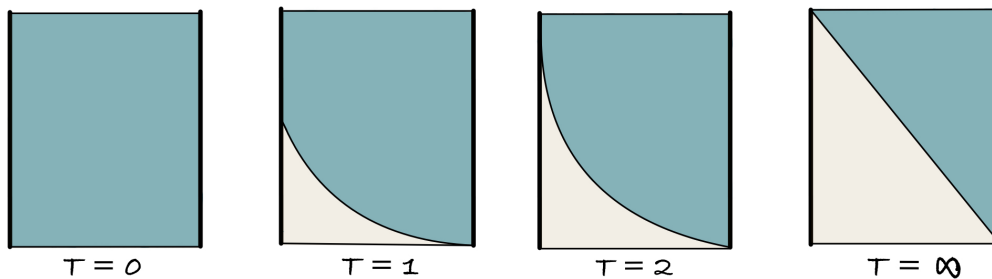


**Figure C.8** A sketch of the change in moisture throughout the sample over time. Here it can be seen that the amount of moisture is stable throughout the sample before the test starts. At the start of the experiment, the boundary condition at the bottom is changed to 0% RH, which means that a moisture gradient will slowly be created through the sample.

In figure C.7, it is marked when  $G$  is within the criterion recommended by DS/EN ISO 12572 [1]. Compared to figure C.6, it can be seen that WFI again achieves the criterion on day 19, whereas RWI only achieves it on day 20, two days later than when it achieves the first criterion shown in figure C.6. Based on the study done on silica gel in appendix F, it is estimated that silica gel will maintain an RH of less than 5% for up to 21 days. Since DS/EN ISO 12572 [1] recommends that the experiment is stable at  $\pm 5\%$  RH, it has been decided to use the data from day 20 to find the permeability for RWI since it is expected that the sample still complies with the recommendation of less than 5%. Day 19 will be used to find the permeability for WFI, as this is the day when both criteria are achieved. Since none of the other test assemblies has achieved a weight increase of 9 g, it has been

chosen to use the latest data for these samples. Figure C.9 shows the permeability for the six samples.

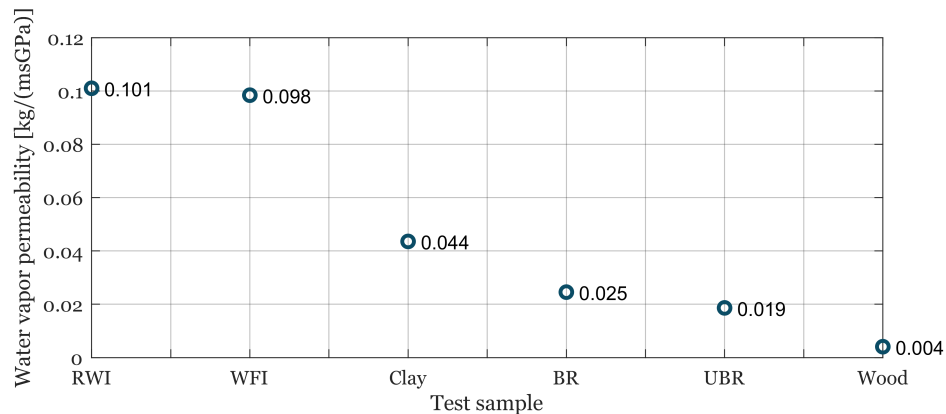


**Figure C.9** The measured water vapor permeability for the dry cup experiments performed with silica gel.

Since only two of the six materials have achieved the two criteria for becoming stable according to DS/EN ISO 12572 [1], it has been chosen to try to predict the permeability when the four other test assembly achieves the requirement for a weight increase of 9 grams out of the current data. The prediction will be made using two methods. The first projection method (PM1) will use data from the two stable test assemblies. Here it has been found that the last determination of  $G$ , in both cases, had decreased by 22.9% compared to the first determination of  $G$ . Therefore, PM1 will find that the permeability based on the final  $G$  is 22.9% less than the mean of the first determination of  $G$ . The two determinations of  $G$  are shown in figure C.10 and C.11.

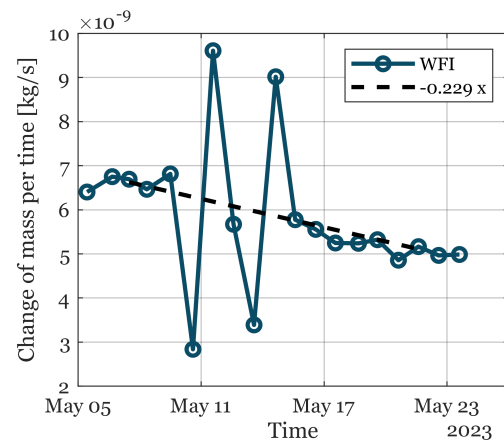
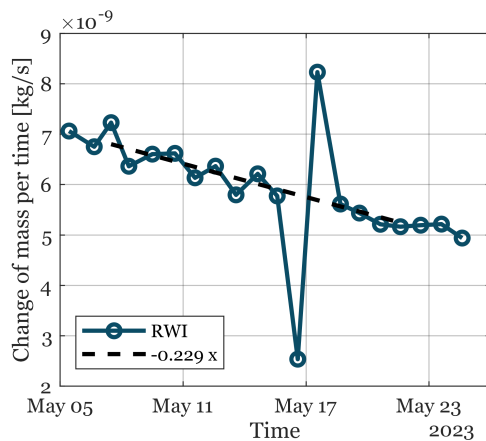


**Figure C.10** Here, the mass change per time,  $\Delta m_{12}$ , for RWI is shown. A black line indicates the slope between the first and last determination of  $G$ . **Figure C.11** Here, the mass change per time,  $\Delta m_{12}$ , for WFI is shown. A black line indicates the slope between the first and last determination of  $G$ .

However, this method is problematic because the two samples that have become stable have a completely different pore structure compared to the other four materials. The different pore structure means the change over time can differ from what is experienced by the two stable test assemblies. Therefore, the second projection method (PM2) will use a

tendency from the unstable samples measured mass change rates to find the water vapor flow rate density,  $G$ , for when the test assembly achieved the desired weight increase. The projection is made by finding the trend between the mass change rate and the weight gain. Based on this trend, it can then be predicted what the mass change rate will be when the test assembly has increased by 9 g. All the trend lines used in PM2 are shown in appendix J. The measured permeability for all six materials and the predicted permeability for the four unstable materials is shown in figure C.12.

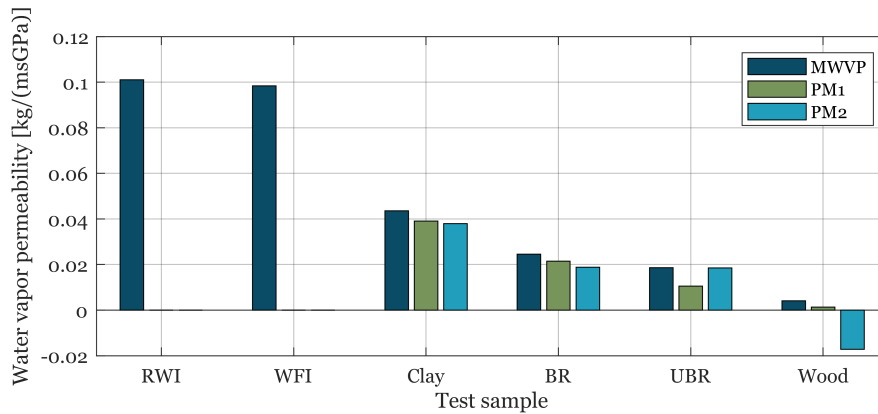


**Figure C.12** The measured and predicted water vapor permeability for the dry cup experiments performed with silica gel.

Figure C.12 shows that both PM1 and PM2 have shown similar results on clay, BR and UBR. However, it must be considered that all three materials have a hydrophilic surface and smaller pores. The hydrophilic surface can cause the materials to attract water droplets to their surface over time. This means that there can be a waterfilm over the surfaces, reducing pore size over time, while the already smaller pores mean it will be harder for the water molecules to penetrate the materials. In tiny pores, the water film can also cause the pores to be blocked due to capillary rise leading to a different tortuosity.

On the other hand, the predicted vapor permeability for wood is very different between PM1 and PM2. The difference comes from the mass change rate of wood increasing over time while it decreases for all the other materials. This increase may be because the wood's pore structure differs significantly from the other materials, as the water vapor in the wood primarily penetrates via capillary forces through the small tracheids. However, it must be considered that although many measurements have been taken, the test assembly with wood has only had a weight increase of less than half a gram, so many changes can happen before it becomes stable. Another thing to consider is that the correlation coefficient,  $R^2$ , for the four trend lines is very low in PM2. As the correlation coefficient is close to 0, the trend line may not represent the data well, so using it to make meaningful predictions is difficult. The projection method will still be used as the trend line represents the mean of the mass change rate quite well.

The chosen balance could be a limitation. As described in appendix H have it been chosen to use a balance with a resolution of 0.01 g over the 0.001 g recommended by DS/EN ISO 12572 [1]. Due to the lower resolution, the mass change rate has been rounded, which may be one of the reasons why large spikes are seen in the data shown in figure C.7. However,

this is not seen as a problem since it has been possible to find a final  $G$  that complies with the recommendation in DS/EN ISO 12572 [1]. The spikes shown in C.7 can also be because it has been forgotten to use the tare function on the balance to reset the balance to zero. However, the spikes can also be seen in the data from other studies[3].

On figure C.7, it can be seen that WFI and Clay increased the density of the water vapor flow rate ( $g$ ) on the first day instead of a decrease as experienced for the rest of the measurement. This increase can be due to the samples not having an even distribution of moisture levels throughout the material.

Although a study has been done on silica gel in this report, see appendix F, it is still uncertain what the exact RH is in the air layer in the cup. Therefore, conducting further studies of the silica gel would be beneficial using a small humidity sensor that could lie in the air layer.

# Oxygen Diffusion Coefficient by the Oxygen Diffusion Apparatus

The wet/dry cup method is a long-term approach, and the results can vary with each measurement. Considering the amount of time this method takes, an alternative method is being investigated to compare its results with the wet/dry cup method and determine its potential for replacement. The method used in this project is the Oxygen Diffusion Apparatus (ODA20). The ODA20 is an experimental single-chamber setup based on Fick's Law of diffusion. Unlike the wet/dry cup method described in EN 12572, which uses water vapor, the ODA20 makes use of oxygen as a tracer gas to determine the oxygen diffusion coefficient. The oxygen diffusion coefficient can be advantageous, as the method neglects effects such as evaporation, condensation, and liquid transfer at water-air interfaces and water-filled pore spaces. As water molecules react with the surface and the existing water molecules in the material, oxygen does not physically react with it, making it possible to only focus on the diffusion, as seen on figure D.1

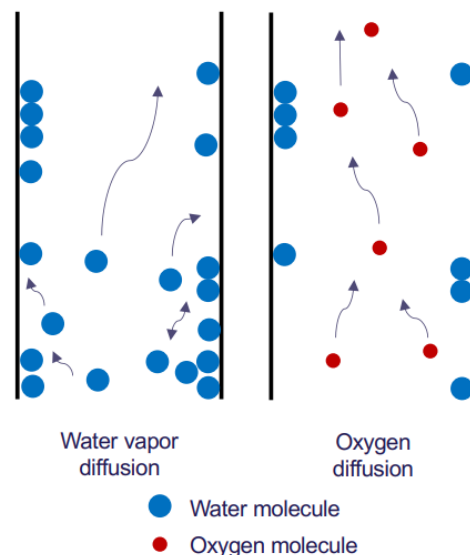


**Figure D.1** Illustration of water vapor diffusion and Oxygen diffusion. The water vapor reacts with the existing water in the material, while Oxygen does not react in any way with the water. [50]

A sketch of the ODA20 set up can be seen in figure D.2. The chamber in the sketch has an

oxygen sensor measuring the  $O_2$ -concentration and a tube connected to a nitrogen flask. A sample is placed above the chamber, and an O-ring is inflated, sealing the sample so that the nitrogen is forced through the sample. A slide separates the sample from the chamber. When the test is started, the chamber is closed with the help of the slide. The chamber is then flushed with nitrogen. The slide will then open to let the nitrogen diffuse through the sample. As nitrogen is lighter than air, the chamber will be filled with air, and the oxygen sensor will measure the concentration of  $O_2$  in the chamber over time.

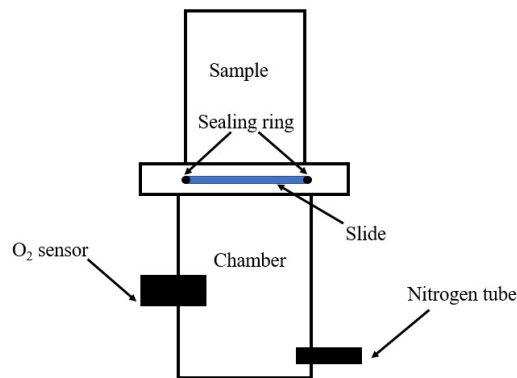


**Figure D.2** Figure sketch of the ODA20.

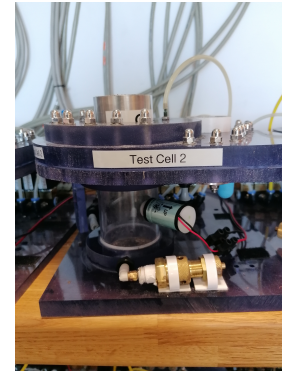


**Figure D.3** The ODA20 and a test sample.

The ODA20 is used to compare the diffusion value with the water vapor diffusion coefficient. However due to the lack of resources, the ODA20 is also used to find a mean diffusion value, out of multiple samples, and use the sample that is closest to the mean, to do the wet/dry cup method. In the following, the theory, the experimental setup, and the results will be described in order to compare this method with the wet/dry cup method.

## D.1 Methodology of the ODA20

The ODA20 is based on Fick's law and can be solved analytically according to [51]. When the initial values and the boundary conditions are known, Fick's first law can be solved analytically. The boundary and initial conditions are as followed: The concentration of the gas, that the chamber is surrounded in, will stay constant, and the concentration of the chamber is zero, meaning no oxygen is in the chamber. In addition, the air content in soil is also assumed constant in space and time. With this information, the gas volume per unit time through the sample, can be described by Fick's first law, see equation D.1. [51]

$$\frac{dq}{dt} = -D_p A \frac{\Delta C}{h_s} \quad (D.1)$$

Where

|                 |                                       |
|-----------------|---------------------------------------|
| q               | Volume of gas [ $m^3$ ]               |
| t               | time [s]                              |
| $\frac{dq}{dt}$ | Volume gas pr. unit time              |
| $D_p$           | Diffusion coefficient [ $cm^2$ pr. s] |
| A               | Area of the sample [ $cm^2$ ]         |
| $h_s$           | Height of sample [mm]                 |

The gas volume pr. unit time can also be described as equation D.2

$$\frac{dq}{dt} = \frac{d(\Delta C_t)}{dt} h_c A \quad (D.2)$$

Where  $h_c$  is the height of the chamber. [51] By combining equation D.1 and D.2 equation D.3

$$D_p dt = -h_s h_c \frac{d\Delta C_t}{\Delta C_t} \quad (D.3)$$

[51]

By integrating equation D.3 using the boundary conditions, equation D.4 is given:

$$\ln\left(\frac{\Delta C_t}{\Delta C_0}\right) = -\frac{D_p}{h_s h_c} t \quad \Leftrightarrow \quad \ln\left(\frac{\Delta C_t}{\Delta C_0}\right) = K \cdot t \quad (D.4)$$

[51]

Thus equation D.4 expresses a linear relation between the gas concentration difference and the time. [52] Here  $K$  is the slope of the linear relation and therefore the diffusion coefficient can be calculated as:

$$D_p = -h_s h_c K \quad (D.5)$$

[51]

## D.2 Equipment

Details about the equipment used for the ODA20 can be found in table D.1.

**Table D.1** List of equipment for the ODA20.

| Brand     | Model                                   | Description            | Serial Number |
|-----------|---|------------------------|---------------|
| Microsoft | Surface Book 2                          | Computer               | 000872474957  |
| MathWorks | Matlab R2020b                           | Software               | -             |
| NI        | LabVIEW 2020SP1                         | Software               | -             |
| -         | Oxygen Diffusion Apparatus 2020 (ODA20) | single-Chamber Methods | -             |
| Sartorius | ENTRIS 2202-1S                          | Balance                | 0033906127    |
| -         | -                                       | Test sample            | -             |

## D.3 Setup

For the setup the sample is prepared by putting it in the metal cylinder. The cylinder is used in order to force the tracer gas through the upper and lower opening. More about the metal cylinder can be read in appendix G. The preparing of the sample is further described in the appendix E.

### D.3.1 Method used Step by Step

Part 2: Manual measurement procedure

1. Open and run the VI script.
2. Open ‘Manual Control’ for the test cell you are going to use.
3. Create a new file.
4. Start logging the data.
5. Make sure the oxygen levels are of stable (ambient) conditions.
6. Close the hatch (Valve 4).
7. Insert the sample into aforementioned test cell.
8. Seal the sample (Valve 1).
9. Turn on the safety valve (Valve 7).
10. Turn on flushing of nitrogen (Valve 6) and open the nitrogen gas cylinder.
11. Let the nitrogen flush for approximately 5 – 10 seconds and then turn off flushing of nitrogen (Valve 6).
12. Turn the safety valve off (Valve 7).
13. Wait until minimum levels for the oxygen have been reached in the chamber.
14. Turn on ‘Open hatch’ (Valve 3).
15. Turn on ‘Seal chamber’ (Valve 2).

The expected time for each test will take between 1-3 hours per sample.

## D.4 Results of the ODA20

The  $D_p$ -value in relation to the density can be seen in figure D.4. A total of ten samples for each materials have been measured in order to find the  $D_p$ -value.

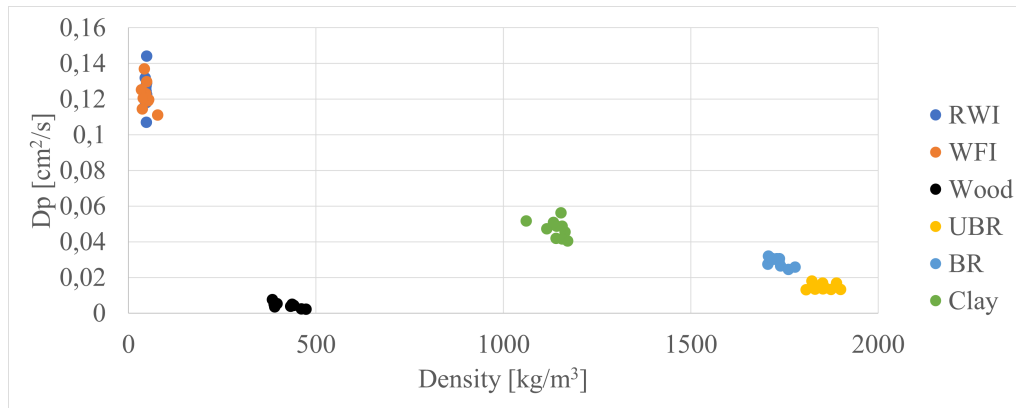


**Figure D.4** The diffusion coefficients of each material in relation to density. The Insulation materials have a higher  $D_p$ -value compared to the other materials. Wood having the lowest, indicating that the pore structure can be narrow and difficult for the oxygen to pass through. Clay having the highest  $D_p$ -value in comparison with BR and UBR which is expected as BR and UBR are denser.

A variation of the  $D_p$ -value can be seen in the insulation materials, compared to the other materials. This could be due to the sample preparations, where they could have been compressed in different variation. However the  $D_p$ -value is higher than the rest of the materials, as expected, since these materials have high porosity. Furthermore, based on figure D.4, it can be observed that when the density increases, the  $D_p$ -value decreases. Except for wood; as this type of wood is a soft wood tracheids are found in the structure meaning pores are longer and narrower, indicating a higher resistance diffusing through the material, see section B.2.4. BR and UBR have similar densities and follow the theorem by having low  $D_p$ -values, but BR having slightly higher values. BR is a fired brick which decreases the water content in the brick making the pores more open. UBR are air dried and absorb more moisture than fired brick, which can increase the water content, making it more resistance for gas or water vapor to diffuse through the material.

The diffusion also depends on the porosity of the material. Figure D.5 shows the  $D_p/D_o$  in terms of the air filled porosity that is compared with the Buckingham model [53]. The air filled porosity is found by finding the correlation of the dry density and the particle density. The figure shows that the observed diffusion values of the materials are above the predicted Buckingham model, indicating a higher diffusion rate than expected by the porosity alone.

Wood, however, exhibits a different behaviour; with its high porosity, its diffusion values are below the Buckingham model, indicating a lower diffusion rate to its porosity. This discrepancy can be associated with the pore structure of wood, which slows down the diffusion.

Both BR and UBR have  $D_p$ -values that align with the Buckingham model. This means that the  $D_p$ -value corresponds well with their porosity, suggesting a correlation between diffusion and porosity.

Clay is close to the Buckingham model line. Its  $D_p$ -value matches well with its porosity, indicating a predicted diffusion behaviour that corresponds well with the Buckingham model.

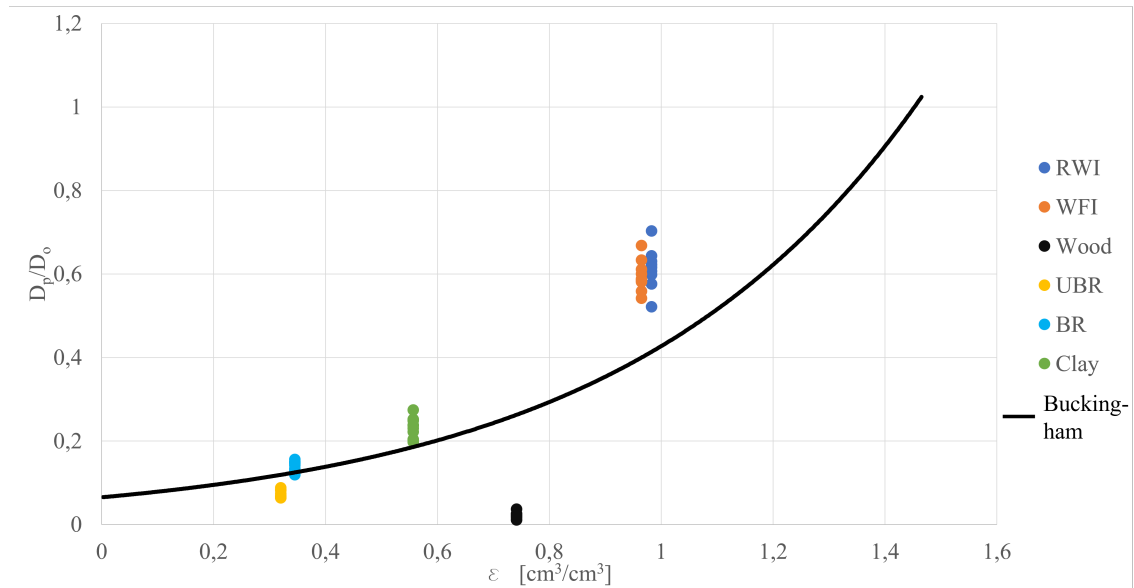


**Figure D.5** The  $D_p$ -value in terms of the air-filled porosity. A Buckingham model has been made.

On figure D.6 the tortuosity of the 6 materials can be seen. The insulation materials have the lowest tortuosity and wood having the highest. RW and WFI demonstrate a near-unobstructed pathway for gas penetration due to the tortuosity being almost one. Wood has a large amount of air-filled pores, compared to UBR, BR and clay, but due to its tortuosity the gas struggles to diffuse through the material. The tortuosity of wood can get up to 8 meaning it takes 8 times the thickness of the wood, for the gas to pass through it.

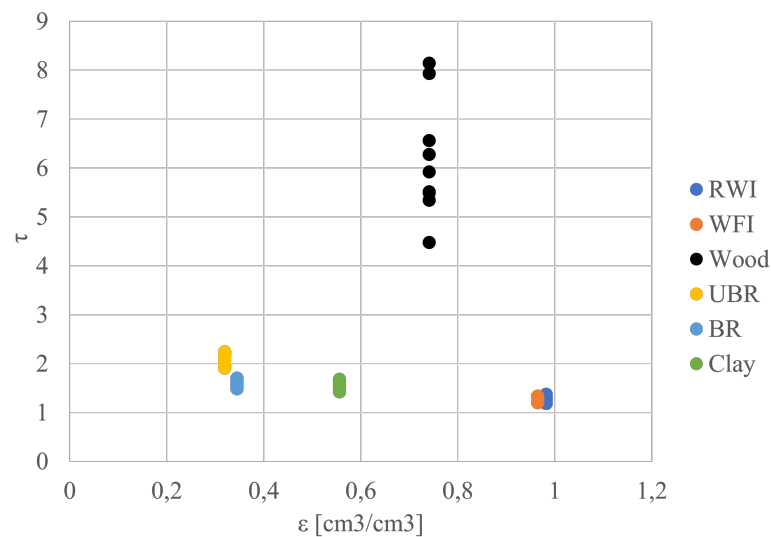


**Figure D.6** The tortuosity of the materials in terms of the air-filled porosity.

UBR, BR and clay range between 1.5 and 2 which is close to the insulation materials. However the diffusion coefficient is significant lower than the insulation materials, because of their porosity. Figure D.6 indicates that the diffusion coefficient is low because of the porosity and that the tortuosity only has a small effect on the gas penetration through

the material, compared to wood. UBR has the highest tortuosity of those three materials which could be the reason why the  $D_p$ -value is slightly higher than BR's.

#### D.4.1 Selection of Samples for the Wet/Dry Cup Method

As previously mentioned, ten samples of every material have been made to find a mean diffusion coefficient. The samples closest to the mean, will be used for the wet/dry cup method, because of limited resources only one sample can be used, which is the closest to the mean.

An overview of the relative error for each material can be seen in figure D.7. Here sample 9 of wood is not taking into account, since its results were out of the scope compared to the rest of the samples. The box plot shows the min and max value but also the 1<sup>st</sup> and 3<sup>rd</sup> quadrant as well as the mean and median. The mean value is indicated with a "x".

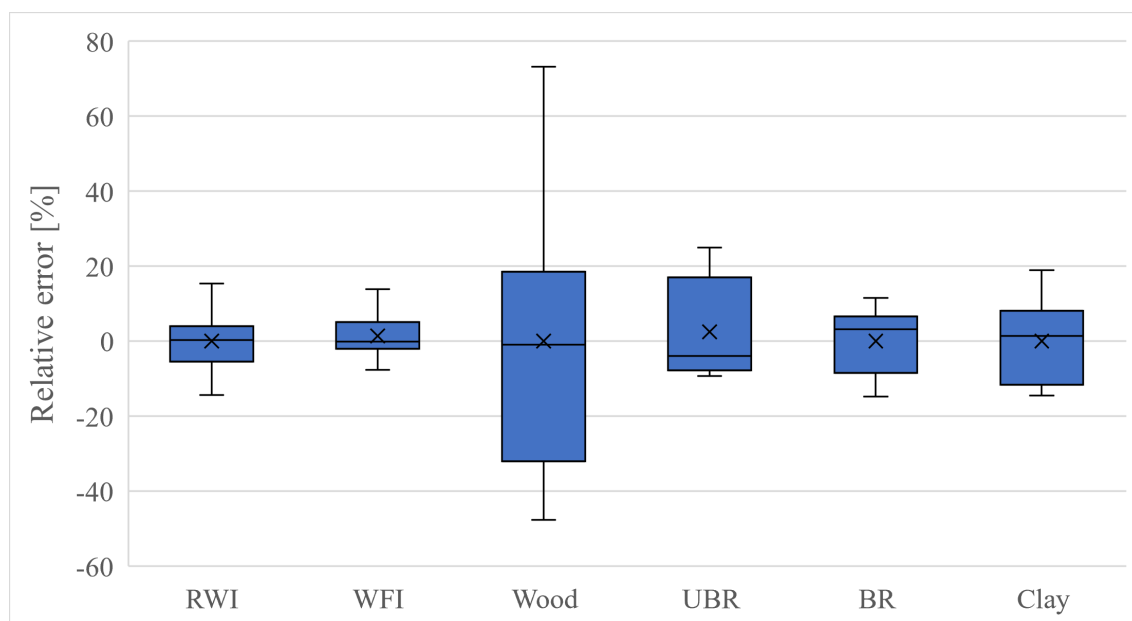


**Figure D.7** Relative error of each material. This box plot shows the min and max errors as well as the median and the mean value. The mean value is marked with an "x".

The box plot shows the variation of the relative errors, especially wood has a large deviation. Even with excluding sample 9 the maximum relative error is significantly high. It can also be seen that the relative errors above the mean for wood are not as spread as the relative errors underneath the median. However the relative errors above the 3<sup>rd</sup> quadrant, are widely spread. RWI and WFI have the smallest variation whereas BR and clay have similar variations. Both materials show that the relative errors above the median are more compacted whereas below the median the relative error is widely spread. The box plot for UBR shows that the median is close to the 1<sup>st</sup> quadrant, indicating that the relative errors below the medians are compact and not as spread than the relative errors above the median.

**Table D.2** The mean density of each material and the chosen sample, that will be used for the dry/wet CUP-method.

| Material | Mean $D_p$ cm <sup>2</sup> /s | Chosen sample | $D_p$ -value of<br>chosen sample m <sup>3</sup> /m · s |
|----------|-------------------------------|---------------|--|
| RWI      | 0.1249                        | 7             | 0.1244   |
| WFI      | 0.1203                        | 10            | 0.1205   |
| Wood     | 0.0043                        | 5             | 0.0043   |
| UBR      | 0.0144                        | 7             | 0.0141   |
| BR       | 0.0287                        | 9             | 0.0291   |
| Clay     | 0.0473                        | 2             | 0.0472   |

The mean value for every material has been calculated and based on these calculations, a sample has been chosen that will be used for the wet/dry cup method. The mean value and chosen sample, can be seen in table D.2. However as described in section C.3 the clay sample is very fragile and was damaged during the dry cup method. Therefore the next best sample has been taken.

# Sample Preparation for ODA20 and Wet/Dry Cup Method **E**

---

For both ODA 20 and wet/dry cup method experiments, the samples need to be prepared. The samples are placed in a metal cylinder with or without sealing, depending on the material. Some factors such as different densities and textures are considered when preparing the materials, which can make the process of putting the material into the cylinder challenging. RWI, for example, has a very soft texture, and when pressed into the cylinder, the pore structure can be changed, and the results are affected. To avoid this, the casting technique has been studied, and two different sealants have been investigated. In addition, the cutting of the insulation materials has been studied.

## E.1 Process of Cutting the Material

In order to fit the materials in the cylinder, some cutouts have to be made as most materials are too big for the metal cylinder. RWI and WFI for example are supplied in sheets, which are too big and therefore a sample is taken out of one sheet. A square with the dimensions 95x95mm is cut out and then the square is put into a frame made out of wood. This is used for stability when using a drill stand to cut out the sample in the right size. A sharp metal cylinder that has a diameter of 48 mm is pressed down onto the square cutting out a sample that can fit into the metal cylinder used in the experiments. The drill and wood frame can be seen on figure E.1.



**Figure E.1** On the left: Wood frame with the inner dimensions of 95x95mm. On the right: The drill that cuts out the RWI sample with the wood frame placed under it.

However, when trying to cut out a WFI sample, the drill was not sharp enough, and the WFI was getting too compressed. It is therefore decided only to use the drill for the RWI samples. For WFI, the sample was cut out with an insulation knife making them as round as possible. Except for clay, the other samples were already cut out before they were received. Clay is the only material that is directly packed in the metal cylinder and does not need any sealant.

## E.2 Sealant

For the sealant it is important that it cannot react to water or water vapor as this will influence the wet/dry cup method. Different studies have investigated different types have been used or studied. [54] One of the types is butylene. The results show it is water vapor resistant and has no influence on the experiment and it is therefore chosen to investigate this type of sealant. On figure E.2 the chosen product can be seen. The butylene is viscous and can be smeared on the inner walls of the metal cylinder.

Another sealant that has been investigated is a product called "Magic Rubber" from Ray tech (MR) see figure E.3. This is a liquid isolation that turns into rubber ones it dries at room temperature. It has a low viscosity right after mixing the two components together, making it challenging to smear it on the inner walls of the metal cylinder.



**Figure E.2** Sealant type, Butylene. [55]\*



**Figure E.3** Sealant type, Magic Rubber. [56]\*

Both products have difficulty when applying it and therefore different casting techniques will be investigated. For this study plastic cylinders have been provided that will represent a sample. The idea is that since the plastic cylinder is fully closed, the results should be identical with the closed test dummy that is used when calibrating the ODA20. There are two different types of cylinder: one with rough sides and one with smooth sides, see figure E.4 and E.5 respectively. The reason for the different types is to test if the sealants will have the same results as the sample with the smooth sides. This is to represent test samples that do not have smooth sides. Both samples will be inserted into a metal cylinder.



**Figure E.4** Plastic cylinder with rough sides.



**Figure E.5** Plastic cylinder with smooth sides.

The butylene has a drying period of 5 hrs and the samples with the butylene were left to dry for more than a week. When lifting the metal cylinder with the sealant and the plastic dummy, the plastic dummy slipped through, because the butylene was too viscous.

Another sample has been tested, and when this sample was put onto the ODA20, after 5 min. the plastic dummy slipped through. This is demonstrated on figure E.6. Therefore it is decided not to do further investigations with butylene.



**Figure E.6** The chamber of a ODA20 with a plastic cylinder coated with Butyl.

Two samples for MR have been made to investigate if the MR is air tight and does not affect the measurement. Since MR is fluid it also investigated if the MR will be penetrating the samples. This was done by smearing some MR directly on a RWI sample, and waiting for it to dry. On figure E.7 the RWI sample with the MR can be seen, and it shows that the MR does not penetrate the RWI. As this is one of the porous materials, it is assumed that it will not penetrate the other materials, and therefore it will be used for further investigations. In addition the drying period for MR is 10 min, which is quite faster than the butylene.



**Figure E.7** Cross-section of a RWI sample with MR on the sides. The MR does not penetrate the RWI.

It was observed that the layer of MR over the sample was very thin and uneven, which resulted in some of the surface not being covered. Therefore, it was investigated whether it would be beneficial to let MR stand and dry before pouring it over the sample. Based on trial and error, it was found that it would be beneficial to let the MR dry for 5 minutes after stirring before it is poured over the sample. Figures E.8 and E.9 show the difference in the surface if MR is poured over the sample immediately after stirring compared to if it is allowed to dry for 5 minutes.

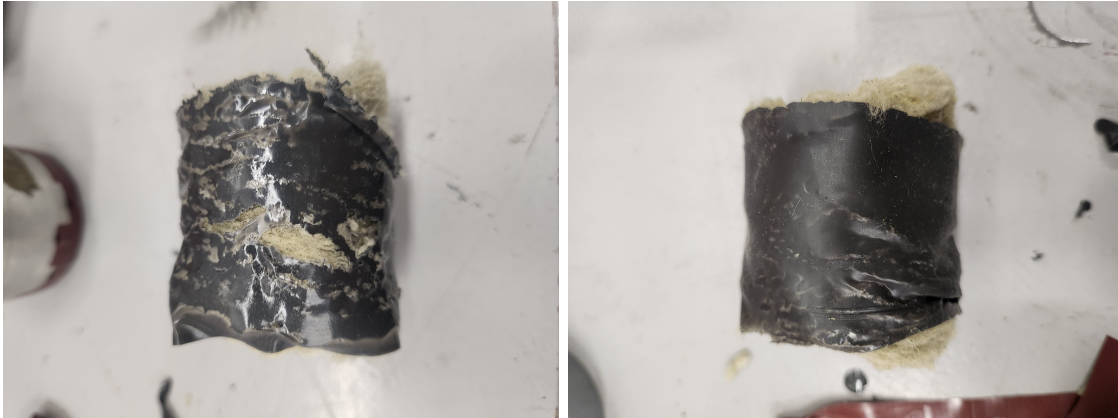


**Figure E.8** The outer surface of an RWI sample surface after application of MR. Here is the surface after application of MR. Here is the MR poured over the sample immediately after stirring.

**Figure E.9** The outer surface of an RWI sample surface after application of MR. Here is the surface after application of MR. Here is the MR poured over the sample after a drying period of 5 minutes.

### E.2.1 Equipment

Details about the equipment used can be found in Table E.1 below.

**Table E.1** List of equipment.

| Brand     | Model                                   | Description                     | Serial Number |
|-----------|---|---------------------------------|---------------|
| Microsoft | Surface Book 2                          | Computer                        | 000872474957  |
| MathWorks | Matlab R2020b                           | Software                        | -             |
| -         | Plastic Cylinder Ø48mm                  | Plastic Cylinder smooth surface | -             |
| -         | Plastic Cylinder Ø48mm                  | Plastic Cylinder rough surface  | -             |
| -         | Oxygen Diffusion Apparatus 2020 (ODA20) | Single-Chamber methods          | -             |
| -         | Metal Cylinder Ø53mm                    | Cylinder for Test sample        | -             |
| Icopal    | Butyl Fugemassee                        | Sealant                         | -             |
| Ray tech  | Magic rubber                            | Sealant                         | -             |

### E.2.2 Setup

The general setup is described in appendix D as the method is the same.

### E.2.3 Method used Step by Step

1. Make two test dummies for each sealant. One with rough sides and one with smooth.
2. A thin layer of sealant is smeared on the inner sides of the metal cylinder.
3. Then the plastic cylinder will be pushed into it.
4. Use the ODA20 to get the oxygen diffusion coefficient for the test samples and compare them. A description of how to use the ODA20 can be found in Appendix D.

### E.2.4 Results

The results of the plastic dummy can be seen on figure E.10 and E.11.

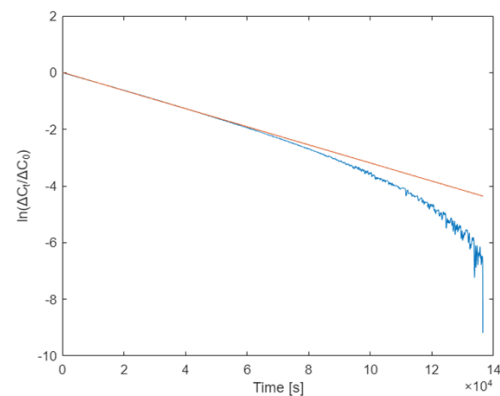
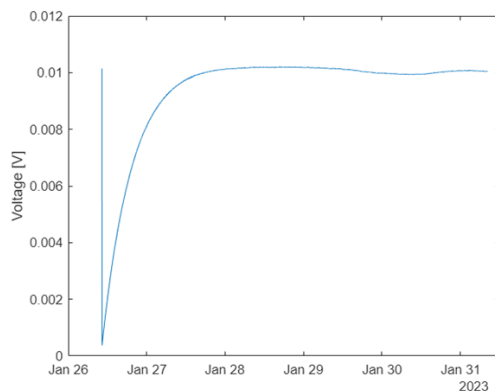


**Figure E.10** The raw data of the first MR sample. **Figure E.11** The logarithm data of the first MR sample.

In order to see if there is any leakage, the diffusion coefficient will be calculated as described in chapter N. The diffusion coefficient is  $D_{MR1} = 0.00782 \text{ m}^3 \text{ sample/m} \cdot \text{s}$ . It is expected that the diffusion coefficient is equal to the diffusion coefficient of the test dummy used in the calibration. The diffusion coefficient for this calibration is  $D_{td} = 0.00790 \text{ m}^3 \text{ sample/m} \cdot \text{s}$  meaning there is a 1.05% difference. This error is low, meaning it can be neglected and the MR is tight enough and will be used for further investigations.

## E.3 Sealing the Material

There are different methods when sealing the samples and different factors need to be considered. The more softer materials like RWI and WFI have a high risk of being too compressed which requires extra attention as this can influence the pore structure and the pore sizes. For both dense and soft materials, it is important to avoid sealing at the top and bottom part of the material as this will influence the diffusion through the material.

### E.3.1 RWI and WFI

The casting technique used for RWI and WFI is identical. To ensure that the samples are not compressed, a pressing device was made that will push the RWI sample into the

cylinder. The device can be seen in figure G.4 in chapter G. The inner side of the cylinder is covered with MR and the device is filled with a RWI or WFI sample.

The device is then positioned onto the cylinder and the top part is then pushed downward making the sample being pushed into the cylinder. The device ensures that the pressure, when pushing down, is not too high so that the sample is not being compressed. This, however, causes the lower part of the sample to be coated with MR. To avoid this, the sample is cut a little longer than the cylinder so that the sample can be cut into the same height as the cylinder when the sealing is hardened, see figure E.12.



**Figure E.12** On the left: A RWI sample cut a little longer than the cylinder. On the right: A RWI sample that is placed into the cylinder. Underneath another cylinder to capture the rest of the MR.

When coating the inner part of the cylinder, some of the MR will be pushed down. An additional cylinder is taped under the main cylinder because the RWI sample is a little longer, the extra cylinder will help preventing the RWI sample to get compressed. An example of how it looks can be seen on figure E.12. The samples are weighed to ensure that the densities are the same before and after the preparing. The weighing is done with the Sartorius Entris 2202 1S that is further described in section G.1.

### E.3.2 BR, UBR and Wood

The more denser materials, BR, UBR and wood, are pre-cut into the right size so that it fits the cylinder. Compared to the insulation materials, these materials do not have a part that can be cut of, when the MR is dry, making it challenging to avoid getting sealing on the top and bottom part of the sample, which requires another method than the one used for the soft materials. A technique where the bottom and top of the material are taped so that no MR will touch the sample. The tape that is used is masking tape, because it leaves no residue on the material. This method makes it easier to remove the MR by cutting along the edge of the cylinder separating the two layers. A thin layer of MR is smeared on the inner wall of the cylinder, and the material is pushed into it and the MR is left to dry. The tape is then taken off, showing the top and bottom with no residue of MR, ensuring no influence on the diffusion. An example can be seen on figure E.13 where a wood sample has been prepared.

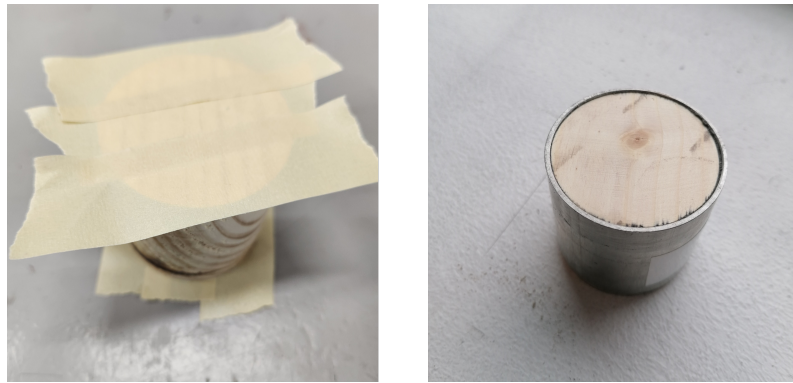


**Figure E.13** On the left: Wood that has taped top and bottom. On the right: Wood in the cylinder after the preparing and the tape taking of.

### E.3.3 Clay

Compared to the other materials, clay is a powder and can therefore be packed in the cylinder meaning no sealing is needed. To ensure that the powder can be packed, the clay needs at least to have a water content of 3%. When the clay was received, it had a water content of 0.75%, making it difficult to pack, as the moisture content is too low to hold the material together. To make it easier, the clay was moistened so that the water content was approximately 3%. The clay powder was weighted for this, and an amount of water equivalent to 3% of the weight was added. The water content of the clay was measured to be 3.35% on the day it was mixed with the water and then left for 24 hours to ensure the water was mixed well with the clay. The water content was measured again to 3.16%, indicating that the water was mixed well and the process of packing could be continued.

The packing process involves using a stamper to compact the clay into three layers, ensuring it remains intact, homogenous and does not slip through. The cylinder is filled with clay, and 1/3 of its volume is stamped and packed. This procedure is repeated for the remaining 2/3 of the cylinder. Figure E.14 shows the stamper used for the packing and figure E.15 shows a packed cylinder.



**Figure E.14** Stamper for stamping the clay into the cylinder.



**Figure E.15** A clay sample packed in a metal cylinder.

## E.4 Density of the Samples

The density of all materials has been calculated to ensure that there has been no changes when preparing the samples. The mean density of each material, as well as the manufactures density, can be seen in table E.2. Since all materials have been cut out with a device or have been pre cut, the volume of all materials except for clay, is calculated to be  $9.2 \cdot 10^{-5} m^3$ . Since clay does not need any sealing it will fill the entire cylinder and therefore the volume is  $1 \cdot 10^{-5} m^3$ .

**Table E.2** Mean density of the samples from each material. Ten samples have been made and while preparing the samples, the density has been calculated to ensure that the material was not compressed. The mean density is then compared with the manufactures density.

| Material | Mean $\rho$<br>[kg/m <sup>3</sup> ] | Manufacturers $\rho$<br>[kg/m <sup>3</sup> ] | Absolute error | Relative error [%] |
|----------|-------------------------------------|--|----------------|--------------------|
| RWI      | 47                                  | 29   | 18             | 63                 |
| WFI      | 44                                  | 40-58  | -              | -                  |
| Wood     | 426                                 | 400-700                                      | -              | -                  |
| BR       | 1,732                               | 1,700  | 33             | 2                  |
| UBR      | 1,854                               | 1,800  | 54             | 3                  |
| Clay     | 1,140                               | 746-1,515                                    | -              | -                  |

When looking at table E.2 the densities generally lay in range of the manufactures except for RWI. RWI is almost double it's manufacturers density, as seen on the relative error, indicating that it has been compressed when preparing the samples. The relative error is 63% which can result in uncertainty in the measurement for the diffusion coefficient, as the outcome can be much higher than expected. In addition, when preparing the WFI sample, the weight of the sample, that has been cut, was not measured and therefore the actual density is assumed. One sample has been taken out of the cylinder and the MR was removed and the sample was weight. This weight has then been subtracted from the weight of the prepared cylinder. However the mean lies in the range of the manufacturers stated density and therefore it is assumed that the rest of the samples have the same outcome. Wood shows similar results than WFI. Its density lies within the range resulting in a absolute and relative error of 0.

The relative error of BR and UBR are negligible and can be disregarded, as it is assumed it will not have an influence on the results.

# Study of Salt Solutions Stability Over Time

# F

This appendix describes the preparation of the selected silica gel for the CUP method. Silica gel is a desiccant made from silicon dioxide and is used to absorb moisture and therefore commonly used to prevent the growth of mold, mildew, and corrosion in various products and environments. Silica gel works by adsorbing moisture from its surroundings using adsorption, which is the process where molecules adhere to the surface of a solid or liquid. Silica gel is made up of tiny, porous particles that have a high surface area relative to their size. These pores trap moisture molecules that come into contact with the silica gel through van der Waals forces. [24] [57]

The wet/dry cup method is challenging because it depends on the boundary conditions created by the RH under and over the test sample, defined in DS/EN ISO 12572 [1]. The study from 2022 [3] examined the internal conditions during wet/dry cup method experiments, as there are no requirements for sensors inside the cup. The focus was on the RH and temperature created by the desiccants or saturated salt solutions used to control the conditions inside the cup. The study [3] has found that the salt solution recommended for the method by DS/EN ISO 12572 [1] does not consistently deliver the expected RH. As shown in figure F.1, none of the tested desiccants achieves the recommended RH of 0% in the study [3]. The deviation in RH resulted in a relative error between 5% to 450% between the estimated water vapor permeability found by simulation and the measured water vapor permeability. [3]

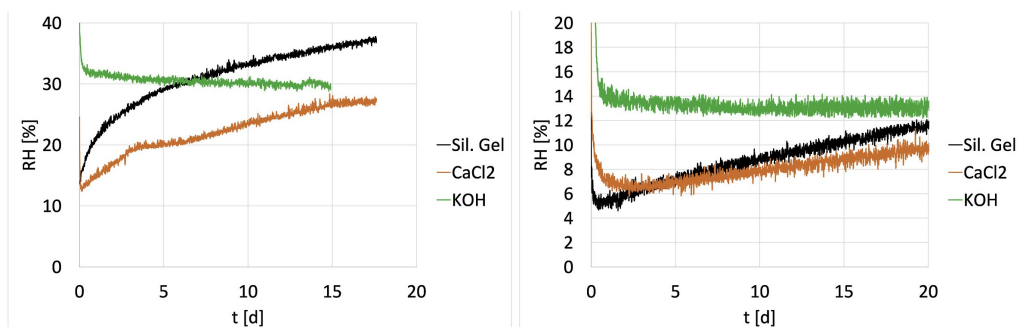


**Figure F.1** Measured variations in RH in the air layer with different desiccants for gypsum board (highly permeable material) on the left and for hollow concrete blocks (less permeable material) on the right. [3]

However, there are areas for improvement in the study, as details about the salt solutions used, including particle size, concentration, and if the salt solution has been dried, have not been described in detail. These details are essential to make a salt solution work optimally.

[58] Six silica gel samples have been under observation for four weeks to better understand the desiccant's stability. Silica gel is a choice on the background of the previously described study [3], as it is the desiccant with the lowest observed RH, see figure F.1. The silica gel has been put in an oven of 105 °C to remove all water that can create water-filled pore spaces.

Silica gel is also relatively inexpensive, non-toxic, non-flammable material that is widely available and is recommended by standard DS/EN ISO 12572 [1]. Silica gel can also easily be regenerated by heating, making it reusable and cost-effective. Silica gel has a very high adsorption capacity due to a high surface area relative to their size, making it an effective drying agent. As the silica gel adsorbs moisture, its colour change, indicating that it has reached its maximum capacity, as shown in Figure F.2. [59]



**Figure F.2** A picture of orange silica gel. As the silica gel adsorbs moisture, its color change from orange color to green, indicating that it has reached its maximum capacity for moisture adsorption.

## F.1 Detailed Measurement Plan

The objective of this measurement plan is to outline the steps and procedures for preparing silica gel for use in the wet/dry cup method experiment, as described in standard DS/EN ISO 12572. Details about the equipment used can be found in Table F.1 below.

**Table F.1** List of equipment used in the setup for the in the investigation of salt solutions stability over time.

| Brand     | Model            | Description               | Serial Number |
|-----------|------------------|---------------------------|---------------|
| Intel     | Nuc              | Computer                  |               |
| Arduino   | Uno              | Microcontroller           |               |
| Honeywell | Hum-1            | Humidity Sensor           |               |
| Memmert   | UF110            | Heating oven              |               |
| -         | Silica gel [0 %] | Desiccants                |               |
| -         | 500 ml           | Conical Flask             |               |
| -         | RWI              | Rock Wool Insulation      | 240394001     |
| -         | Plug             | Plug with hole for sensor |               |

### F.1.1 Setup used in the Investigation of Salt Solutions Stability over Time

To test the long-term stability of silica gel, a simple experiment will be done over four weeks. The experiment is illustrated in figure F.3, where the placement of the sensor relative to the silica gel can be seen.

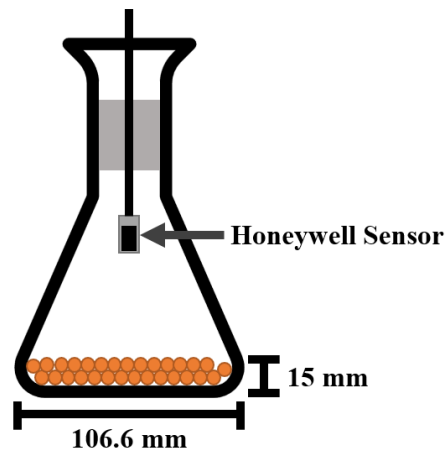


**Figure F.3** An illustration of the setup for the long-term stability test. Here, the silica gel can be seen as orange circles in the bottom of the conical flask. Above the Honeywell sensor, a grey area can be seen. This is where either a sample of RWI or a plug will be placed.

The gray area above the Honeywell sensor shown in figure F.3 marks where a RWI sample or a plug will be placed. This is done to see how stable the silica gel will be in different cases during the wet/dry cup method. RWI is chosen to give a picture of how the silica gel will be in more open conditions and a plug is chosen to see it in more closed conditions. Here it should be noted that the plug is not completely closed, and there will therefore be a small air change rate. In order to try to achieve the same conditions as under the wet/dry cup method, it has been chosen to use a 500 ml conical flask for the test. This is chosen as it has an inner diameter of 106.6 mm, which is close to the 113.0 mm that will be used under the cup method. For the same reason, 15.0 mm silica gel will be filled up in the bottom of each conical flask as shown in figure F.3.

To ensure that there are no water molecules in the silica gel, the conical flasks will be placed in an oven set to 105 °C for a minimum of 24 hours before use. This has been chosen on the basis that a higher temperature is desired than the evaporation temperature of the water, which is 100 °C. After a minimum of 24 hours, the conical flasks must be placed in a place with stable conditions. This is done to ensure that the boundary conditions to which the silica gel is exposed are stable. This is repeated in three different conical flasks to give a more homogeneous result. In addition, it is also repeated over two times, where one must simulate the wet/dry cup method with very permeable materials and the other must simulate more closed materials. Figure F.4 shows an example of two conical flasks, one with a RWI sample and one with a plug.



**Figure F.4** An example of two conical flasks, one with a RWI sample and one with a plug, to show the two different setups.

A test has been designed to better understand the silica gel used for the dry cup method. The test is designed to investigate how the silica gel will affect the RH in the air layer in the cup method. The test will be done for two scenarios, a scenario simulating a dry cup method with low permeability material and a scenario simulating a dry cup method with high permeability material.

### F.1.2 Method used step by step

1. Measure silica gel using the conical flasks and filling it up 15 mm from the bottom.
2. Place the conical flasks with silica gel in the oven and let them dry at 105°C for 24 hours.
3. Take the silica gel out of the oven and place the Honeywell sensor in the conical flasks. Close the conical flasks using either a RWI or a plug.
4. Let the measurements run for four weeks.

## F.2 Observations

- The yield of silica gel before drying was approximately 90 g.
- There is no visible difference between the silica gel before and after the drying process.
- The Honeywell sensor is very affected by noise.
- The silica gel will change to a green color if left out in the open.

As the Honeywell sensor is affected by noise, it has been set to log data every second to reduce the noise's effect on the data. Due to the high sample rate, it is considered that the noise will not be a problem for the results.

## F.3 Results from the Investigation of Salt Solutions Stability over Time

In this section, it will be possible to see the data of the six measurements made with silica gel. The six measurements are divided into two different categories. The first category consisting of the first three tests is the low permeability test, simulating a dry cup method using a material with low permeability. The second category consisting of the last three tests is the high permeability test, simulating a dry cup method using a material with high permeability. All the data will be displayed through plots, where the x-axis will show the time after the start of the experiment, and the y-axis will show the RH. The graphs on the left show the test from the first category, whereas the figures on the right show the test from the first category.

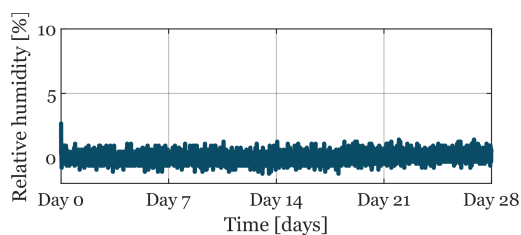


Figure F.5 The results from test nr. 1.

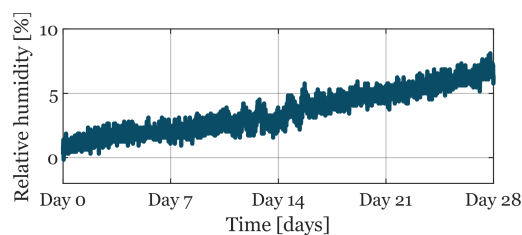


Figure F.6 The results from test nr. 4.

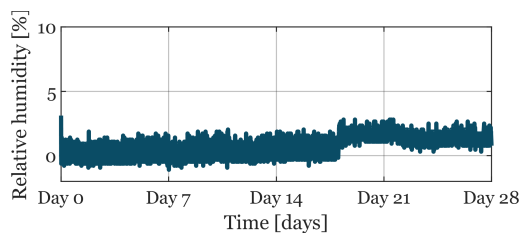


Figure F.7 The results from test nr. 2.

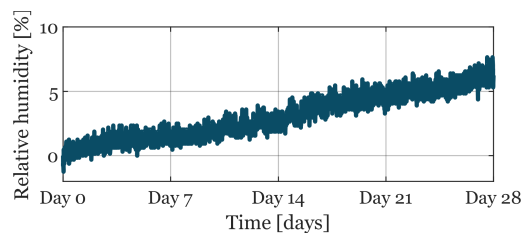


Figure F.8 The results from test nr. 5.

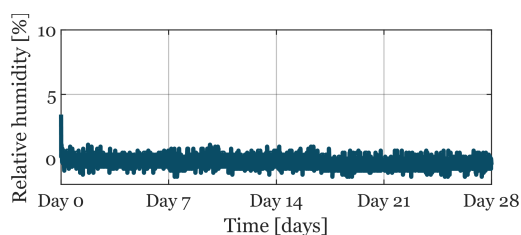


Figure F.9 The results from the test nr. 3.

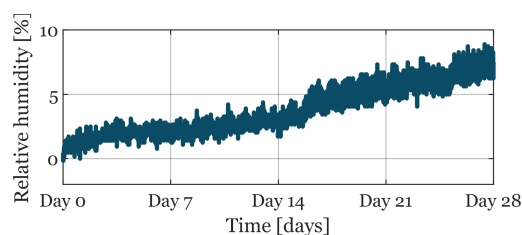


Figure F.10 The results from test nr. 6.

As shown in figure F.5, F.7, and F.9, the silica gel is very stable under more closed conditions and remains at 0% RH during the four weeks the test has taken place. However, there is the exception for figure F.7, where a slight increase in RH can be seen. The increase is because the entire setup was moved due to an electrician, which affected one of the conical flasks for some unknown reason. However, the story changes when more open materials are looked at, as shown in figure F.6, F.8, and F.10, where the silica gel under the more open conditions is not kept stable during the four weeks.

By comparing the data from the observation to the data from the previously mentioned study [3], it can be seen that there is a big difference in the performance of the silica gel. In the data from the study [3] shown in figure F.1, it can be seen that the silica gel starts with an RH of 7-13%, which is higher than the 0% experienced by the observation shown in figure F.5, F.6, F.7, F.8, F.9, and F.10. Nonetheless, it can be seen in both cases that the RH increases with time, depending on the permeability of the material used for the experiment. Therefore, it can be assumed that the boundary conditions in the dry cup method change over time, and the experiment will be dependent on time. These constant changes in boundary conditions must be considered when assessing whether the cup method has become stable. DS/EN ISO 12572 [1] recommends that the air layer's RH stays is within  $\pm 5\%$ , meaning that it will take approximately three weeks before the air layer boundary conditions can be seen as unstable a material with high permeability is used.

## F.4 Conclusion and Discussion

It can be concluded that it is essential to prepare the silica gel, as it can be seen that the RH achieved in the air layer is highly dependent on how dry the silica gel is. However, there is variation between the results shown in section F.3 and what would happen in a dry cup method. The variation is because the test cups were unavailable when this test was done, which meant that the conical flask was used instead. The conical flask means that the internal dimensions change, resulting in a change in the air layer's volume. In addition, the conical flask has made it impossible to use the same test sample used in the dry cup method. Therefore, the permeability will not be the same. Additionally, this test had not occurred in a climate chamber, which means a change in air velocity over the opening, affecting whether the air above the sample is mixed correctly. However, it needs to be taken into account that the purpose of the experiment was to gain a better understanding of the silica gel and not know the precise RH in the cup air layer.

As an opportunity for further work, it could be beneficial to investigate whether the amount of silica gel affects the RH's stability in the air layer under open conditions.

# Equipment G

---

This chapter aims to provide a detailed overview of the equipment utilized throughout the various experiments conducted during this project. The primary objective of this chapter is to introduce the tools used to ensure a complete understanding of the methods used and their underlying principles. The equipment will be discussed in their specific roles in the various experiment stages, such as the range and accuracy of the equipment. The arrangement and configuration of the experimental set-up have been explained in their own chapter earlier in the report.

## G.1 Sartorius Entris 2202-1S Balance

The Sartorius Entris 2202-1S Balance is a balance that is used for weighing the samples when preparing them and also for the dry/wet cup method. The balance has a resolution of 0.01 g and has a maximum weight of 2200 g. In addition the balance has a stability time of 1.5 s. [60] The balance can be seen in picture G.1.



**Figure G.1** Picture of ENTRIS 2202 1S with the dimensions, D x W x H, 230 x 303 x 91 mm. [60]

When preparing the samples there has been made some observations when weighing the the samples. The Sartorius Entrince 2202-1S balance is sensitive to draught and in the laboratory a significant amount draught can be experienced. This has also an influence on the weighing, but to avoid any influence of the draught the balance is placed into a

box and a Plexiglas was taped at the top of the box. This reduced the influence of the draught significantly making the weighing easier and more accurate. However the balance may still depict some inaccuracy when placed on the side of the box. It is predicted that it will have a slight influence but only in decimals. This accuracy is not used when preparing the samples and therefore it is disregarded. On figure G.2 the setup with the box and Plexiglas can be seen.



**Figure G.2** Setup with the balance in a box with Plexiglas.

The balance is also used for weighing the CUPs in the dry/wet cup method. Another balance was considered for this part. It was the Sartorius Entris 224-1S Balance with an accuracy of 0.1 mg. This balance is very accurate thus a small change in weight can be detected when weighing the cups. However the balance has a maximum weight of 220 g and the cups weigh between 500-600 g which is over the allowed weight of the Entris 224-1S balance. Therefore the Entris 2202-1S is also chosen for this experiment. The Sartorius Entris 2202 1S Balance is placed in the laboratory 1.011 at Thomas Manns Vej 23C when preparing the sample, and is then moved to laboratory 1.401, when doing the dry/wet cup method. Here the balance is placed on a table making it more stable and therefore more accurate, see figure G.1.

**Table G.1** Summary of specifications for the Sartorius Entris 2202-1S balance.

| Model          | Brand     | Accuracy | Maximum weight |
|----------------|-----------|----------|----------------|
| Entris 2202-1S | Sartorius | 0.01 g   | 220 g          |

## G.2 Metal Cylinder

The samples are placed in metal cylinders to keep them in place, but also forcing the gas through the material and only letting it slip through the upper and lower surfaces of the sample. On figure G.3 a sketch of the cylinder and picture of the cylinder can be seen. The cylinder has an outer diameter of 53 mm and a wall thickness of 1.6 mm as well as a height of 51 mm

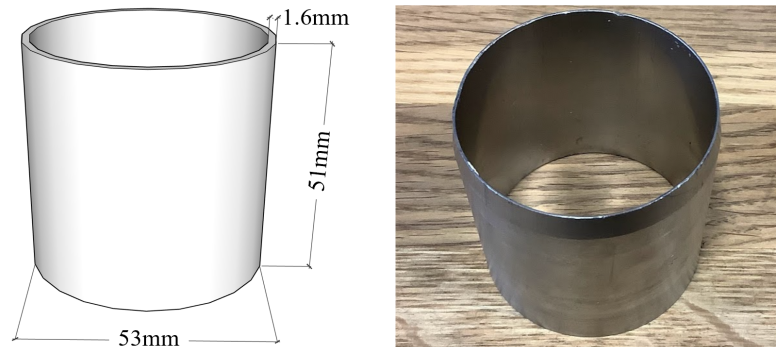


**Figure G.3** From left to right: the metal cylinder seen from above, from the side and a picture of the metal cylinder. The metal cylinder has a known height of 51.00mm, an outer diameter of 53.00mm, and an inner diameter of 49.80mm.

The metal cylinder is chosen, because the ODA20 is based on its measurement, making it the evident choice to use as container. In addition the cylinder is made of stainless steel which will not react with the water vapor in the climate chamber when doing the dry/wet cup method.

**Table G.2** Summary of specifications for the metal cylinder.

| Outer diameter | Inner diameter of 49.80mm | Height | Wall thickness |
|----------------|---------------------------|--------|----------------|
| 53 mm          | 49.8 mm                   | 51 mm  | 1.6 mm         |

## G.3 3D-Printed Pressing device

This device is used when preparing the soft materials, RWI and WFI. It is designed to avoid compressing the materials that can influence the results. The device is designed so that there is a holder and a stamper that will press down on the material. On figure G.4 the device is shown.



**Figure G.4** A device to push down the soft materials. This will ensure that the samples are not compressed. On the left; device when the stamper is down. On the right; when the stamper is up.

The pressing device is made of three 3D-printed elements and is designed to simplify the sample-making process. The pressing device is designed to hold the sample and cylinder at the same height under the hole process, which is expected to make the material more homogeneous throughout the sample by avoiding any places that can be more compressed than others. The three elements are shown in Figure G.5.

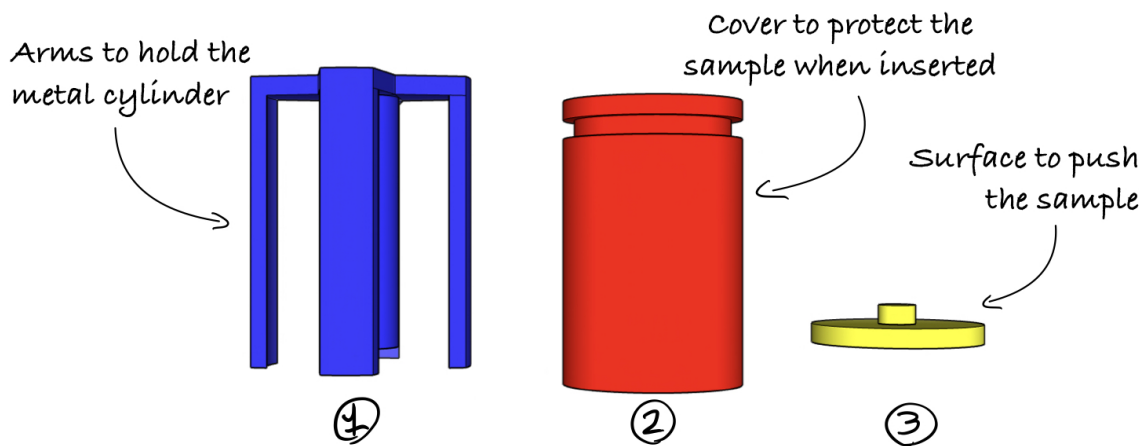


**Figure G.5** A illustration of the three 3D-printed elements used in the Pressing device.

The first element is the core of the pressing device, which has a cylinder in the middle that holds all three parts together. It has four arms designed to hold the pressing device in the same place over the metal cylinder to reduce human error. This design choice is based on investigating how the samples were to be made. Here it was found that there was a big difference in how compact the insulation materials became through the test sample. By keeping the pressing device position constant, one of the variables that can cause this error is removed.

The second element is designed to hold and protect the sample while it is inserted into the sample. It is designed to be as thin as possible to not compress the sample. The third

element is designed to be a surface attached to the first element. This surface holds the sample in cylinders while the second element is removed. Figure G.6 shows how the first and third elements move independently from the second element.

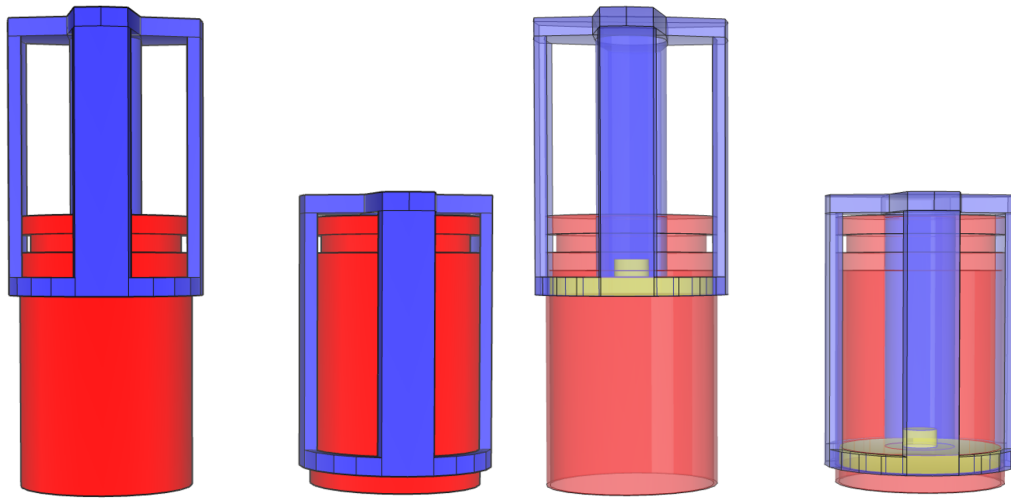


**Figure G.6** A illustration that's shown how the three elements move in relation to each other.

As shown in Figure G.6, the underside of the first and third elements will always be joined together. This means that if the pressing device is placed on top of a metal cylinder, will the sample stay in the same place inside the metal cylinder, even if the other part is removed. This process can be seen illustrated in Figure G.7.

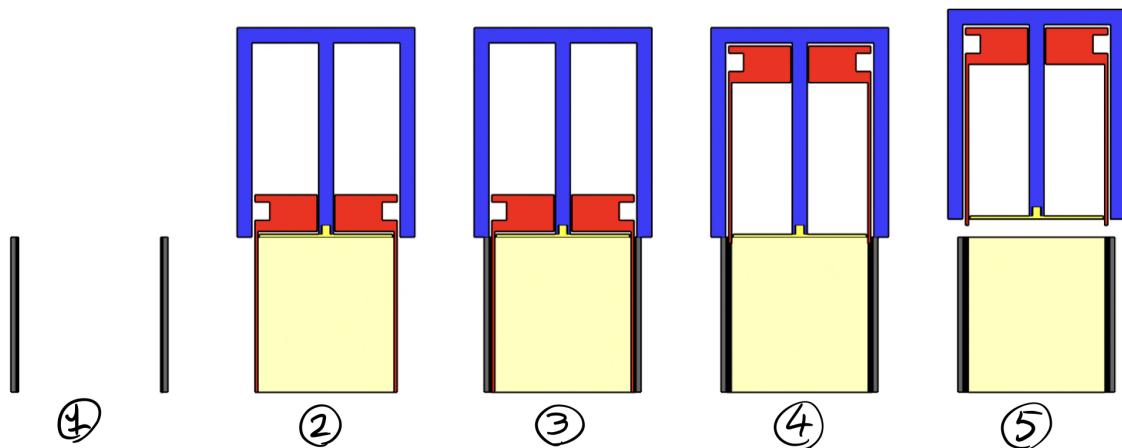


**Figure G.7** (1) is a metal cylinder, and (2) is the pressing device with a sample. First, the pressing device with a sample can be placed onto the metal cylinder (3), after which the pressing device is pushed down (4). After this, the pressing device can be removed, and the test sample is done.

## G.4 The VCL 7010 Climate Chamber

In this project, the climate chamber VCL 7010 made by Vötsch has been used. The climate chamber has primarily been used under the dry/wet cup method experiment to hold the conditions around the cup at an RH of  $50 \pm 5\%$  and a temperature of  $23 \pm 1.0^\circ\text{C}$  during the entire measurement period. The VCL 7010 is chosen as it is a 100-litre climate

chamber with a temperature range of  $-70$  to  $180\text{ }^{\circ}\text{C}$  and a humidity range of 10 to 95%. The climate chamber has been quality controlled at a temperature of  $23\text{ }^{\circ}\text{C}$  by a precision thermometer for 24 hrs and maintains the temperature throughout the period. The dry cup method experiments can be found in chapter C. The deviation over time in the climate chamber is  $\pm 0.3$  to  $\pm 0.5\text{ }^{\circ}\text{C}$  for temperature and  $\pm 1$  to  $\pm 3\%$  for humidity. [61]



**Figure G.8** Picture of the VCL 7010 climate chamber.

The VCL 7010 has a fan to mix the air to ensure uniform conditions throughout the chamber. In DS/EN ISO 12572 [1], it is recommended that the air in the chamber shall be mixed to velocities between  $0.02\text{ m/s}$  and  $0.3\text{ m/s}$  to ensure uniform conditions.

The climate chamber is also used to calibrate the IC meters used in the dry/wet cup method experiment and the calibration of the Honeywell. Here, the climate chamber was chosen because of the extensive ranges for temperature and humidity, and the calibrations can be found in Chapters M and L.

**Table G.3** Summary of specifications for the VCL 7010 climate chamber.

| Model    | Brand  | Range                                  | Deviation in time                              |
|----------|--------|--|--|
| VCL 7010 | Vötsch | $-70$ to $180\text{ }^{\circ}\text{C}$ | $\pm 1$ to $\pm 3\%$ RH                        |
|          |        | 10 to 95% RH                           | $\pm 0.3$ to $\pm 0.5\text{ }^{\circ}\text{C}$ |

## G.5 The IC-meter Mobile (GSM)

As an additional control in the climate chamber, two IC-meter will be used to monitor the temperature and the RH in the climate chamber. The IC meter is chosen because it is

easy to use and has a reliable sensor. A picture of an IC-meter can be seen in figure G.9.



**Figure G.9** The IC-meter, the backplate, the power supply, and the cable.

IC-meter is an indoor air quality sensor that measures CO<sub>2</sub> level, noise, RH, and temperature. Both sensors will be used to measure RH and temperature over the entire measuring period. Both sensors have also been calibrated, which can be seen in appendix M. The sensor the IC-meters use is the Sensirion SHT21 sensor for humidity and temperature. The sensor has a typical tolerance of  $\pm 2\%$  RH and  $\pm 0.4^\circ\text{C}$ . The IC-meters have a working range of  $-20$  to  $80^\circ\text{C}$  and an RH of 0 to 95 %.

**Table G.4** Summary of specifications for the IC-meter indoor air quality sensor.

| Model        | Brand    | Range                                       | Accuracy                                |
|--------------|----------|---|---|
| Mobile (GSM) | IC meter | $-20$ to $80^\circ\text{C}$<br>0 to 95 % RH | $\pm 0.4^\circ\text{C}$<br>$\pm 2\%$ RH |

## G.6 The Mensor 2104 Digital Pressure Gauge

A barometric pressure gauge (barometer) is needed to find the water vapor permeability of air. The Mensor 2104 digital pressure gauge will be used to measure the experiment's barometric pressure. The digital pressure gauge is chosen because it has a low uncertainty of only 0.01% and is shown in figure G.10.



**Figure G.10** The Mensor 2104 digital pressure gauge.

The barometer is also chosen as it has an outlet, meaning a tube can be pulled from the barometer into the climate chamber, and the barometer can be placed outside the chamber, thereby not occupying space in the chamber.

**Table G.5** Summary of specifications for the Mensor 2104 digital pressure gauge.

| Model | Brand  | Accuracy |
|-------|--------|----------|
| 2104  | Mensor | 0.01%    |

## G.7 The Memmert UF110 Heating Oven

An oven was used to dry the silica gel to prepare the silica gel for the experiments. The chosen oven is the Memmert UF110 heating oven using the Pt100 sensor DIN class A, temperature sensor with a temperature range of +20 to 300 °C and an accuracy of 0.1 °C for a temperature up to 99.9 °C and an accuracy of 0.5 °C starting from 100 °C. The oven is chosen as it can deliver the desired temperature for drying the silica gel and is available at Aalborg University's Department of Civil Engineering. The oven can be seen on figure G.11. [62]



**Figure G.11** The Memmert UF110 heating oven used for the silica gel. The oven has the internal dimensions of 560 x 480 x 400 mm and is sat to 105 °C.

**Table G.6** Summary of specifications for the Memmert UF110 heating oven.

| Model | Brand   | Range        | Accuracy     |
|-------|---------|--------------|--------------|
| UF110 | Memmert | 20 to 300 °C | $\pm 0.5$ °C |

## G.8 The Honeywell humidity Sensor

The Honeywell humidity sensor is a small RH sensor. The sensor is chosen for the silica gel experiments because of its size. The sensor has a length, height and width of only 4.17, 8.59, and 2.03 mm, respectively, so it can easily be placed in the conical flask. The Honeywell humidity sensor is shown in figure G.12. [63]



**Figure G.12** The Honeywell humidity sensor used for the silica gel experiments.

The sensor has an accuracy of  $\pm 3.5\%$ . [63] In order to be able to use the Honeywell

sensor, an Arduino Uno is programmed through the software Arduino IDE. Honeywell is a well-known brand in the sensor industry, and it is, therefore, easy to find code online to program the sensor quickly. The code used for this project can be seen below:

```
#define HIH4000_Pin A0 //analog pin 0

void setup() {
  Serial.begin(9600);
}

void loop() {

  //To properly caculate relative humidity, we need the temperature.
  double relativeHumidity = analogRead(HIH4000_Pin);

  double av = 0.0048875 * relativeHumidity;

  double res = (av - 0.826) / 0.031483;
  Serial.println(res);
  delay(2000); //just here to slow it down so you can read it
}
```

## G.9 The F200 Precision Thermometer

The F200 precision thermometer by ASL is designed for high-accuracy measurements, with accuracy levels within  $\pm 0.002$  °C. The F200 Precision Thermometer features a wide temperature range of  $-200$  to  $+960$  and a fast response time. The F200 is chosen as the sensor for quality control because of the sensor's reliability and accuracy, ensuring consistent and precise temperature measurements for the experiments. [64] The F200 precision thermometer is shown in figure G.13.

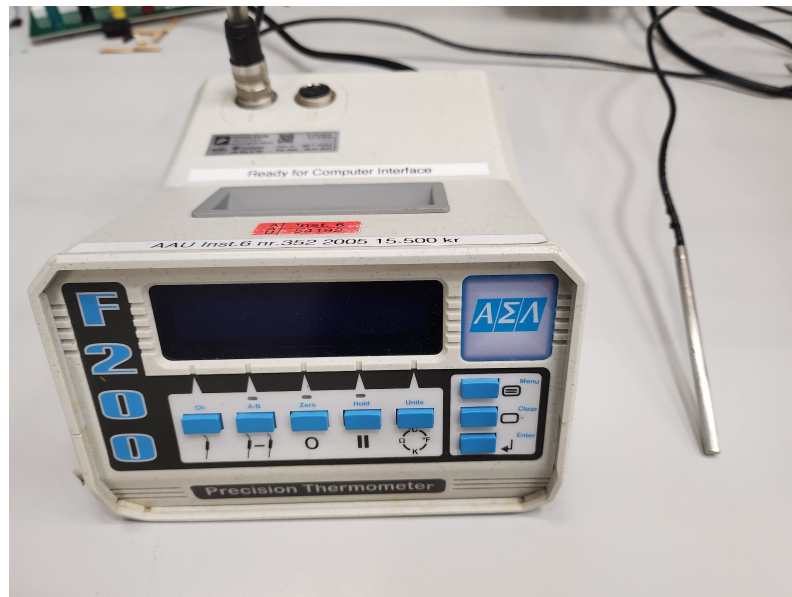


**Figure G.13** The F200 precision thermometer used for the quality control of temperature.

The sensor was only used for quality control because it was unavailable during most measurements. The control of equipment is done through random samples throughout the trial period.

**Table G.7** Summary of specifications for the F200 precision thermometer.

| Model | Brand | Range           | Accuracy   |
|-------|-------|-----------------|------------|
| F200  | ASL   | -200 to +960 °C | ± 0.002 °C |

## G.10 The Novasina Hygrodat 100 Precision Humidity Sensor

The Novasina Hygrodat 100 is a precision humidity and temperature measuring instrument. It is designed to provide accurate and reliable RH and temperature measurements. The sensor is chosen as it measures humidity with an accuracy of ± 0.5% RH and a wide measuring range of 6 to 100% RH and is easy to use. [65]



**Figure G.14** Novasina Hygrodat 100 Precision humidity Sensor used for the quality control of RH.

The sensor was only used for quality control because only one was available at Aalborg University's Department of Civil Engineering. The control of equipment is done through random samples throughout the trial period.

**Table G.8** Summary of specifications for the Novasina Hygrodat 100 precision humidity sensor.

| Model        | Brand    | Range        | Accuracy       |
|--------------|----------|--------------|----------------|
| Hygrodat 100 | Novasina | 6 to 100% RH | $\pm 0.5\%$ RH |

## G.11 The Kimo VT110 Anemometer

The Kimo VT110 Anemometer is a handheld, portable anemometer designed to measure wind speed and air temperature accurately. The Kimo VT110 has a measuring range of 0.15 to 30.00 m/s and an accuracy of  $\pm 0.05$  m/s when measuring an air velocity between 0,15 - 3 m/s. The anemometer is chosen to measure the air velocity in the climate chamber because of its accuracy, reliability, and ease of use. [66]



**Figure G.15** The Kimo VT110 Anemometer used for the air velocity in the climate chamber.

**Table G.9** Summary of specifications for the Kimo VT110 anemometer.

| Model | Brand | Range             | Accuracy       |
|-------|-------|-------------------|----------------|
| VT110 | Kimo  | 0.15 to 30.00 m/s | $\pm 0.05$ m/s |

## G.12 Oxygen Sensor

Doing the ODA20 experiments, an Oxygen sensor is needed to measure the oxygen in the chamber. The GS Oxygen Sensor KE-25F3 is chosen. The sensor is developed in Japan and is not influenced by  $\text{CO}_2$ . A picture of the oxygen sensor can be seen in figure G.16. [67]



**Figure G.16** An example of the GS Oxygen Sensor KE-25F3 by Figaro. The accuracy of this sensor is  $\pm 1\%$ .

The sensor ranges from 0-100 O<sub>2</sub>% and has an accuracy of  $\pm 1\%$ . The response time is approx. 15 seconds and the output of the sensor is in a range of 10-15.5 mV. A summary of the specifications can be seen in table G.10. [67]

**Table G.10** Summary of the specifications of the GS Oxygen Sensor KE-25F3.

| Model   | Brand  | Range                 | Accuracy  |
|---------|--------|-----------------------|-----------|
| KE-25F3 | Figaro | 0-100% O <sub>2</sub> | $\pm 1\%$ |

# The Design Process for The Test Cup H

---

A cup is needed for the dry cup method. As mentioned in C the same sample that is used in the ODA20 is also used in the dry cup method. Appendix G provides a deeper description of the test sample. The construction of the test cup will therefore be built based on the measurements of the test samples.

As described in appendix C, problems were found in a study [54] with the expected boundary conditions in the cup's air layer, as the air layer does not have an RH at 0% as expected. Therefore, it has been chosen to design the cup with a larger diameter than the test sample to create a larger surface area between the desiccant and the air layer. Here it has been chosen to give the test cup an internal diameter of 113 mm, as this gives the surface area between the desiccant and the air layer an area of 0.01 m<sup>2</sup>. The diameter has been chosen on the background of the 0.01 m<sup>2</sup> area, which makes the data easier to process. From the data shown in appendix C and appendix F, it can be seen that the amount of desiccant used can keep the RH below 5% for three weeks, which is the period that it is expected that the experiment will take. As the cup will have a slightly larger area than the conical flask used in the silica gel test, see appendix F, will it be assumed that the test cup can achieve the same RH in the air layer. It has been chosen that the layer with desiccant will be 15 mm and the air layer above it also 15 mm. The heights are chosen on the background of recommendations in DS/EN ISO 12572 [1], stating that the air layer in the test cup must have an air layer of minimum 15 mm, as this creates enough volume to mix the air layer in the cup. DS/EN ISO 12572 [1] also states that the lower layer with the desiccant also must be a minimum of 15 mm to ensure that there is enough desiccant to create the desired RH. It has been chosen to go with the minimum measurements, as this will ensure that the cup weighs as little as possible, resulting in the internal measurements shown in figure H.1.

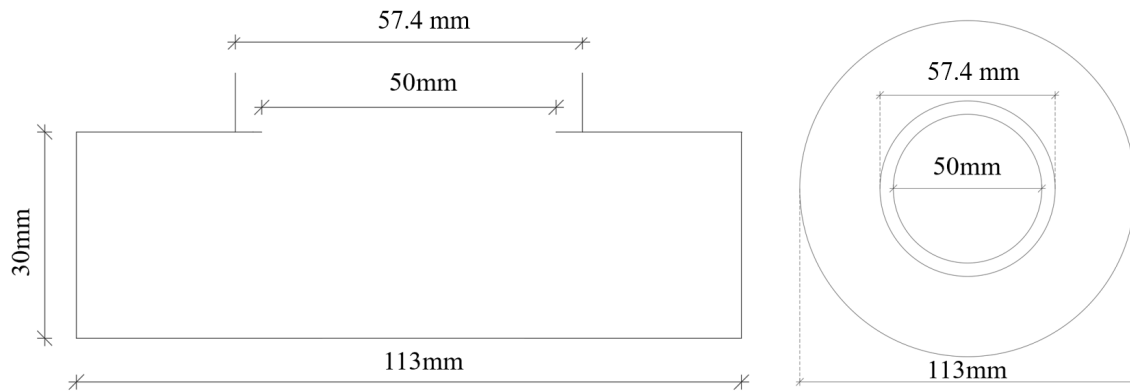


**Figure H.1** Dimensions of the test chamber seen from the top and side.

If the opening of the test cup is smaller than the sample's exposed area, the mean of the two areas needs to be calculated according to DS/EN ISO 12572 [1]. Therefore, the opening of the test cup is designed to have an opening with a diameter of 50 mm, giving it a diameter larger than the opening of the cylinder used in the test sample. This means that the area used in the calculations always will be the test sample's exposed area, simplifying the calculations based on what is described in DS/EN ISO 12572 [1]. The opening in the test cup is slightly larger than the cylinder of the test sample because minor errors during production could mean that the sample will not stand precisely on top of the opening. The larger opening allows a little room to move around without it causing the exposed area in the test sample to be blocked by the test cup.

O-rings have been chosen to seal the opening between the test sample and the test cup. An O-ring is chosen because it is relatively cheap and easy to install or remove. Here, the test cup is designed to have an internal diameter of 57.4 mm around the cylinder of the test sample, which gives a free space of 2.2 mm between the sample and the wall of the cup. The diameter is chosen so it would go well with an O-ring from RS PRO [68] with an inner diameter of 48.9 mm and a thickness of 2.62 mm. The diameter means that it will fit tightly around the 53 mm cylinder that holds the test sample. The free space of 2.2 mm between the test cup and test sample make the 2.62 mm thick O-ring so compressed that it will create an airtight seal in theory, see figure H.2.

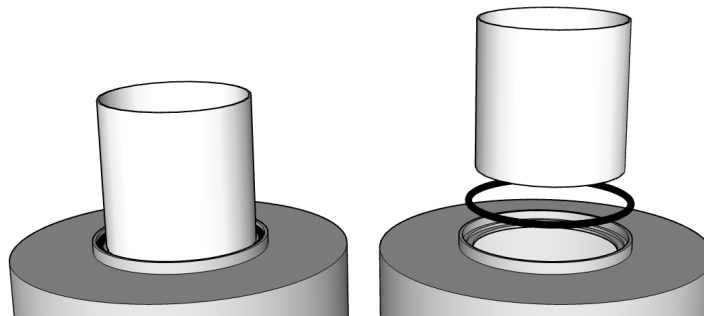


**Figure H.2** Illustration of the O-ring's location between the test cup and the test sample.

It is essential to use a non-porous material to build the test cup to ensure that moisture only passes through the sample. Non-porous materials like glass, metals and hard plastics,

meaning they will not absorb liquid or gas. [69] In DS/EN ISO 12572 [1], the test cup is recommended to be made of either glass or metals. Metal has been chosen as the material for the cup, as Aalborg University has experience working with metal and, therefore, can make test cups in-house. Different concepts for building the test cup have been investigated, resulting in different proposals.

One of the first problems to consider when using metal is how much the entire test assembly will weigh. As water vapor transmission is slow, the mass change rate over time in the cup will be low, meaning it will be essential to have a balance with a high resolution to measure the change. In DS/EN ISO 12572 [1], it is recommended to use a balance with a resolution of 0.001 g. At the location where the measurement is done, there are two types of balances available. The first is an Entris 224-1S from the brand Sartorius [70]. The balance has a wanted resolution of 0.1 mg and a max capacity of 220 g [70]. The max capacity will be a problem as the test samples can weigh up to 270 g, marking the test sample alone heavier than the max capacity of the balance.

The second balance is the Entris 2202-1S from Sartorius [70]. The balance has a lower resolution of 0.01 g but, in return, has a max capacity of 2200 g [70]. In DS/EN ISO 12572 [1], it is recommended that a scale with a resolution of 0.01 g [70] can be used for heavier test assemblies, which means that the Entris 2202-1S lives up to the recommendation. As DS/EN ISO 12572 [1] does not define the weight needed before the test assemblies fall under the definition of heavy test assembly, it will be assumed that the test assembly will be under this definition since the sample alone can weigh more than what the Entris 224-1S can weigh.

It has been chosen to look at two different types of metal to make the test cup. The first is aluminium, which has the advantage of having a low density compared to most other metals as it has a density of only  $2.710 \text{ kg/m}^3$  [71]. The other metal is stainless steel. Stainless steel has a very high density at  $7,500 - 8.000 \text{ kg/m}^3$  [72] compared to aluminium, which means the test cup will weigh more. However, due to the strength of stainless steel, it is expected that the cup can be made with thinner walls, potentially making it as light as a cup made of aluminium. [73]

The first version of the test cup was designed to be very simple by being made of two cylinders as the walls and two plates as the top and base, see figure H.3. The four parts were expected to be welded together, forming the test cup. Here a hole had to be made in the top lid, acting as an opening between the test sample and the test cup. The top cylinder guides the sample, in which an O-ring will be placed to seal it tightly and hold it precisely above the opening.

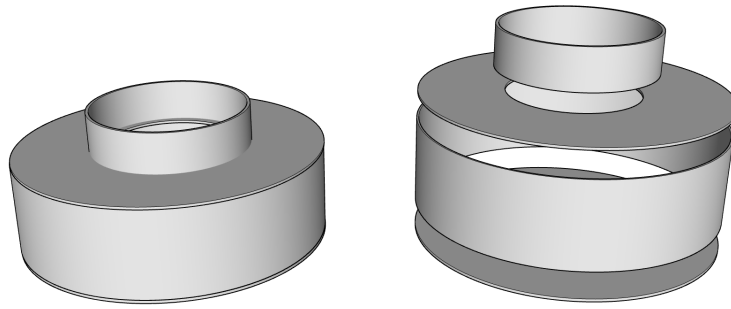


**Figure H.3** Illustration of the first version of the test cup construction.

The first problem with this construction of the cup is that it will require thick metal elements before it is possible to weld the four parts together. The technicians at Aalborg University recommended using thick metal elements if they had to be welded together, as thin elements were sensitive to error, which would create leaks in the cup. Errors will occur because the welding will be done by hand, and it will be challenging to make a consistent result without errors. Because it will be necessary to use thick elements to make the cup using this method, it has been chosen to look at other solutions to assemble the cup.

In order to make it possible to make the elements thinner, it has been decided to try to put them together using O-rings. The O-ring will be held in place by a notch in the two plates used as the cup's top and base. The notch is used to hold the O-ring in place and under pressure, which will cause it to be airtight between the two elements. The notch used in the cup can be seen in figure H.4.

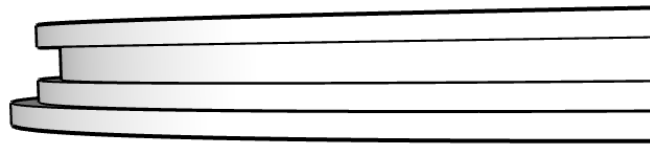


**Figure H.4** Illustration of how the base will look, where the notch that will hold the O-ring can be seen.

The cylinder between the two plates can then be made relatively thin because it only holds the base and top of the cup that holds the O-rings. This proposal can be seen in figure H.5, and due to the thinner cylinder, the entire cup will therefore weigh less than the proposal shown in figure H.4.

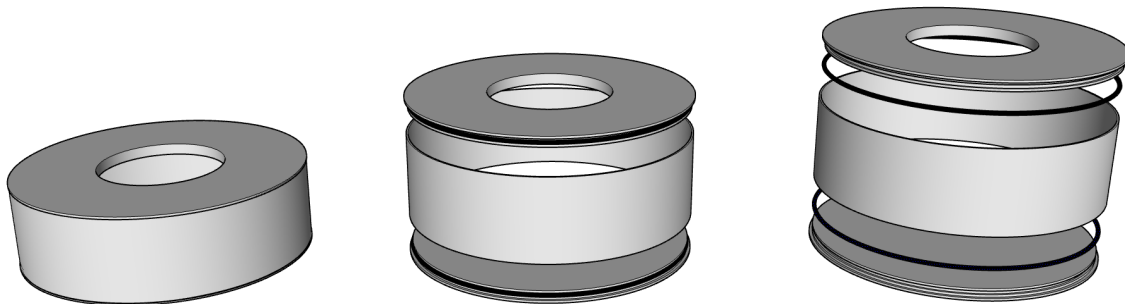


**Figure H.5** Illustration of the second version of the test cup construction.

In figure H.5, it can be seen that the top cylinder is missing. It is due to fact, that the simplest way to join the cylinder with the rest of the cup is still to weld the cylinder to the cup like in figure H.3. The welding will still mean that it will be necessary for the cylinder to be relatively thick enough to be welded together with the top plate. In addition, for the plates to hold the O-rings, the plates must have a thickness that is thicker than the diameter of the O-ring.

In order to optimize the cup's weight, new manufacturing techniques available at Aalborg University have been looked at. One of the newer techniques available is Selective Laser Sintering (SLS) printing, also known as metal 3D-printing. SLS printing involves a high-power laser melting small metal particles in powder form into a product based on a 3D model. Its high resolution makes SLS technology ideal for thin and complex geometries. [74] This method makes it possible to make the cup using only two elements. The cup will be made up of two elements because it will be necessary to make support inside the sample if it was made as a single element. Since the support will be made of metal, removing it will be difficult. The problem is solved by making the cup in two elements, which means that the support is only fixed at one end and can therefore be snapped off. The two elements can be seen in figure H.6.

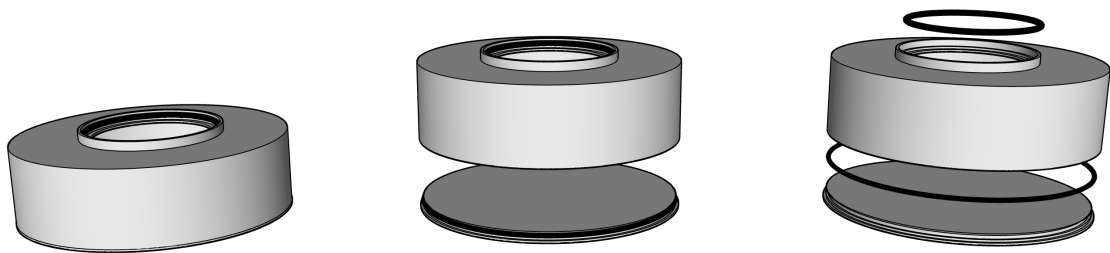


**Figure H.6** Illustration of the final version of the test cup construction.

An advantage of SLS printing is that the cup can be made from either aluminium or stainless steel. Here it has been chosen to go with aluminium, as SLS can print both metals very thinly, which makes aluminium the better choice due to its density. It has been chosen to print the cup with a thickness of 0.75 mm, as this is still thick enough that the cup will be durable and withstand being dropped.

However, SLS printing has the disadvantage that it is relatively expensive to use. Therefore, to optimize the price of the test cup, it has been chosen to make the base in the same way as in the previous proposal and then put the two elements together with an O-ring. The base is designed to be made from a sheet of aluminium, from which a notch will be made using a lathe to hold the O-ring. A O-ring of only 1.5 mm from RS Pro [75] has been chosen to make the base thin as possible. The final cup can be seen in figure H.6.

Since SLS printing is an expensive process, it has been chosen to test all proposals through a plastic 3D printer, as this will mean that most errors could be found before the first cup was printed using SLS printing. It was chosen first to make the test fits by printing rings of the joint between the cup and the base and the top ring that holds the test. It was started by only printing rings because it took less time and was cheaper, which time-optimized





**Figure H.9** A picture of the final SLS printed test cup with a test sample installed.

Options for optimizing the test cup base have also been examined. Here, it has been looked at hollowing out the base to optimize its weight. An illustration of this can be seen in figure H.10. Two different methods of hollowing out the base have been investigated: making it using a lathe or an SLS printer.



**Figure H.10** A sketch of a hollowed-out base. Here it can be seen that it has been hollowed out from the bottom, meaning that the cup retains the internal measurements.

Here it was concluded by the technicians at Aalborg University that aluminium would be too soft to work with in a lathe when it is so thin and would not work in practice. The option for SLS printing would work well here in practice, but due to the high price for this, it is considered that it would be more advantageous to spend the available money on more cups to investigate more materials rather than the slight weight change.

# Sample Validation for Wet/Dry Cup Method



Ten samples for each material have been investigated and their  $D_p$ -value determined. For these value the mean is taken to find the sample that is closest to the mean, and can be further used for the wet/dry cup method.

In the following the different materials and the  $D_p$ -value is described. The mean  $D_p$  has been calculated and the figures I.1-I.6 show the variation between the mean and the measured values of the samples.

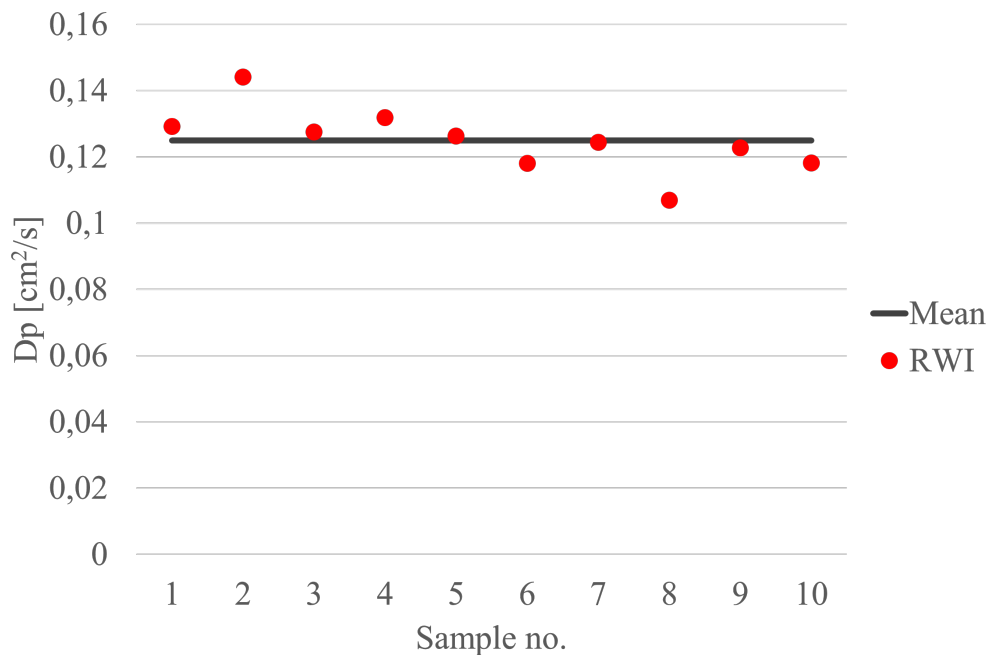


**Figure I.1** The diffusion coefficient of each RWI sample (red dots), compared to the mean value which is the black line.

Figure I.1 shows the  $D_p$ -value of the RWI samples. The diffusion coefficient of the samples are similar to each other making the relative error between -5% and 5% for most of the samples. This is expected as RWI has the same structure as this is not an organic material. Sample 2 and 8 do have a slightly higher relative error which can be caused by errors in prepping the sample. The closest to the mean is sample 7 with a deviation of 0.4 %

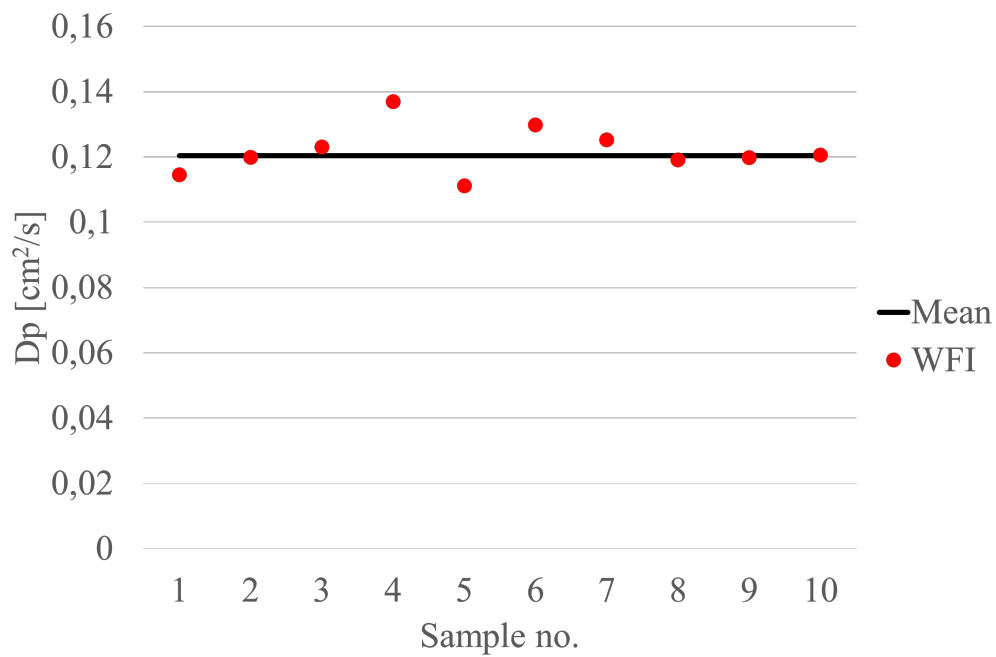


**Figure I.2** The diffusion coefficient of each WFI sample (red dots), compared to the mean value which is the black line.

WFI is similar to RWI as it also has a sample with a slightly higher value than the rest, see figure I.2. This sample has a relative error of 14% and when calculating the mean, this sample is not taken into account. The error could be due to errors in preparing the sample. The variation of the other samples in relative error is ranging between  $-8\%$  and  $8\%$ .

However when looking at organic materials such as wood, the results are different. Figure I.3 shows the  $D_p$ -value for wood.

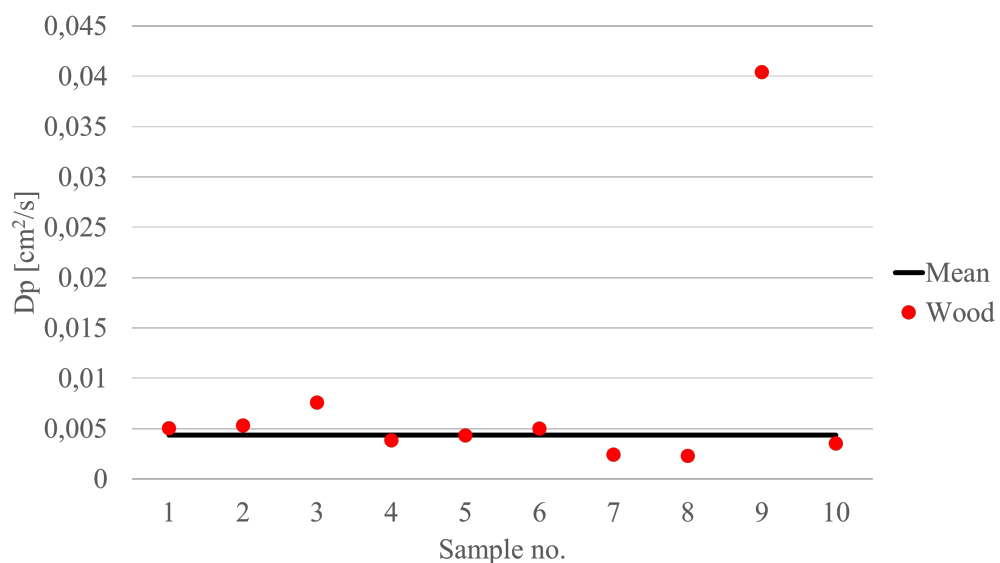


**Figure I.3** The diffusion coefficient of each Wood sample, (red dots), compared to the mean value which is the black line.

The results show that the wood samples are not similar to each other and have relative errors ranging between -50 and 73%. Sample 9 however has an error of 830% which is significantly higher than the rest. This indicates in an error made when preparing the samples, and will therefore not be included in further calculations. On the other hand the variation of the other samples is also larger, compared to RWI and WFI, which is expected as wood is an organic material and as described earlier in the project, the cell structure is not homogeneous but different in every sample. This also means that the pore structure and size can differ from sample to sample, leading to these different results.

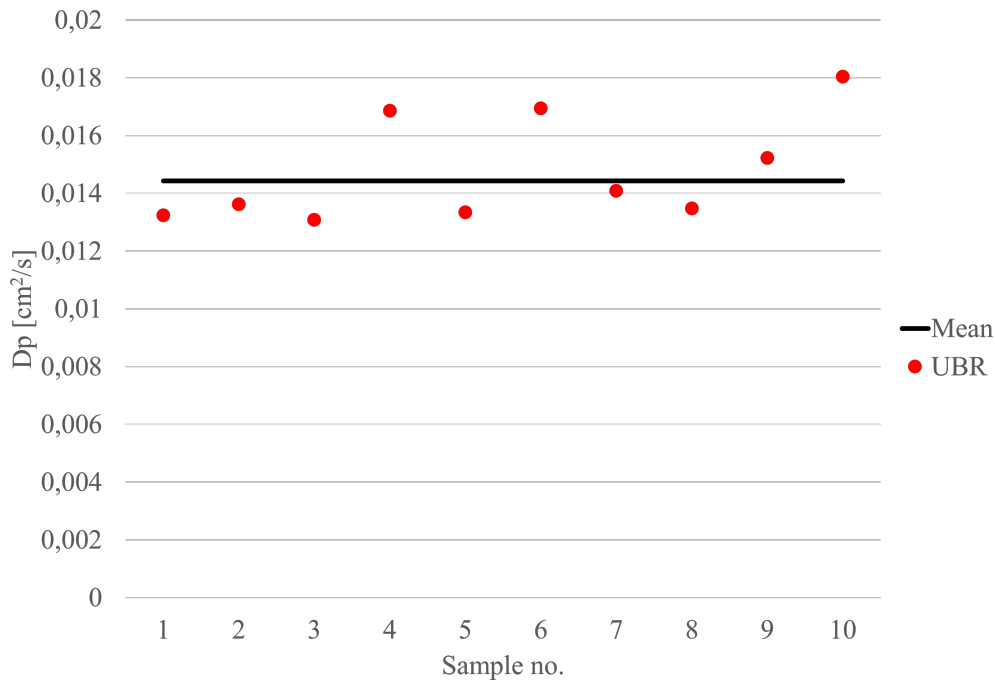


**Figure I.4** The diffusion coefficient of each UBR sample (red dots), compared to the mean value which is the black line.

UBR does just like the previous materials have a sample that has a slightly higher  $D_p$ -value of 25%, which is sample 10. However sample 4 and 6 do also stand out, having a relative error of 17% and 17.5% respectively. These are higher than the rest that range between -8 and 6%, which is similar to RWI's range. The reason for these slightly higher values could again be errors in preparing the sample. The closest to the mean diffusion coefficient is the sample no. 7.

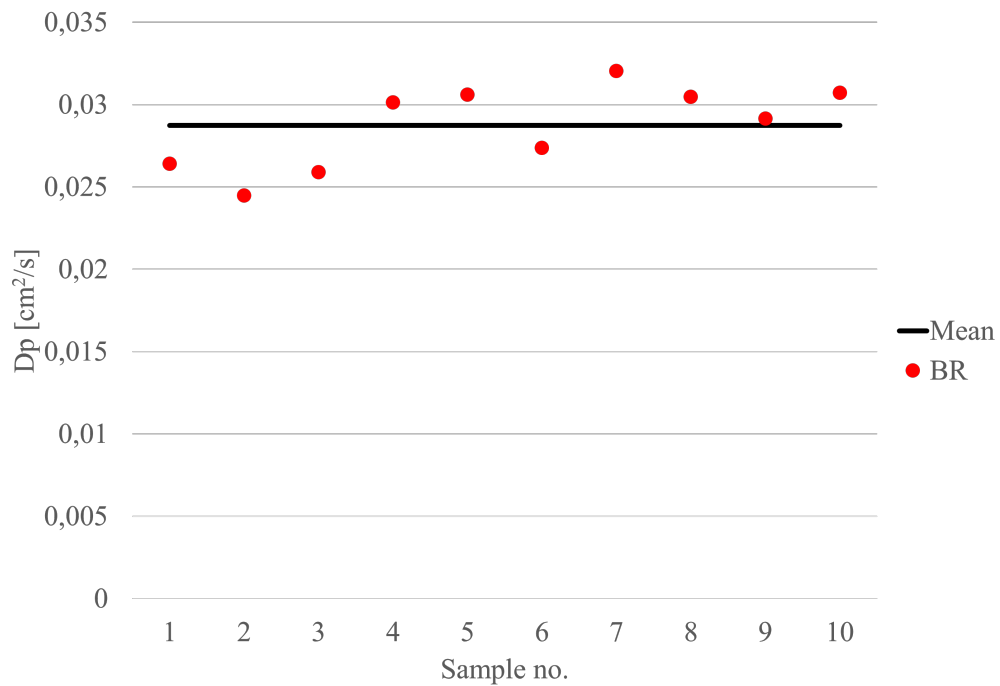


**Figure I.5** The diffusion coefficient of each BR sample (red dots), compared to the mean value which is the black line.

Figure shows the  $D_p$ -value of BR compared to the mean. It can be seen that BR also has some variation with the relative error ranging from -14 to 11 %. BR has no values that are significant to the mean, and therefore all 10 samples are considered when calculating the mean. The closest sample to the mean  $D_p$ -value is sample no. 9.

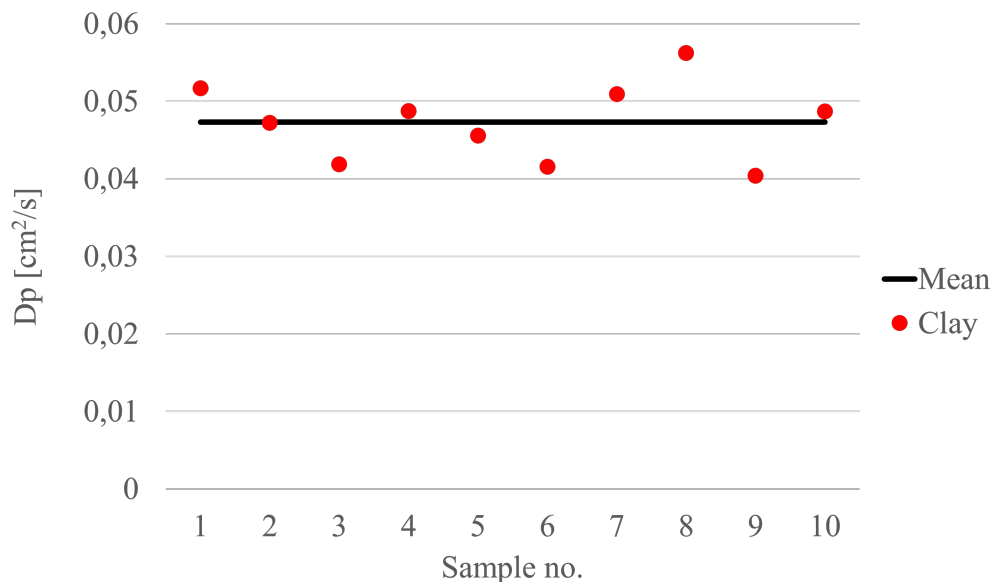


**Figure I.6** The diffusion coefficient of each clay sample (red dots), compared to the mean value which is the black line.

Clay also shows signs of errors in preparing the samples. In figure I.6 the  $D_p$ -value can be

seen. Sample 8 is higher than the others. However the relative error of the other samples ranges between -15 and 9%, with sample 8 not being far from. This makes sample 8 not significant and therefore not be excluded from further calculations. The mean diffusion coefficient has been calculated to  $0.047 \text{ m}^3 \text{ clay/m} \cdot \text{s}$  for clay with 3% water content, and the closest to the mean diffusion coefficient is the sample no. 2.

# Projection of the Test Samples Stable Permeability J

This appendix aims to show all the trend lines used in projection method 2 (PM2) described in section C.3. The projection is made by finding the trend between the mass change rate and the weight gain. Graphs will only be shown for Clay, BR, UBR and Wood, respectively, as these are the four materials that have not been able to become stable according to the recommended criteria in DS/EN ISO 12572 [1]. The function which will be used to predict the mass change rate when the test assembly gain 9g is shown in the northwest corner of all graphs.

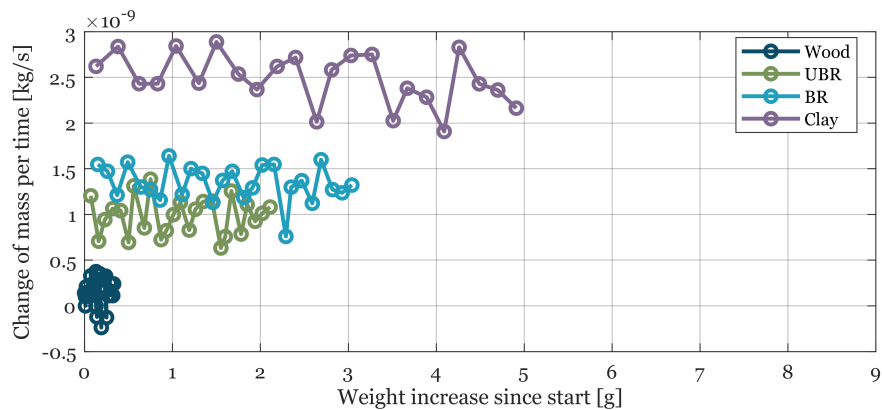


**Figure J.1** The relationship between the mass change rate and the weight gain for all four unstable test assemblies in the dry cup method.

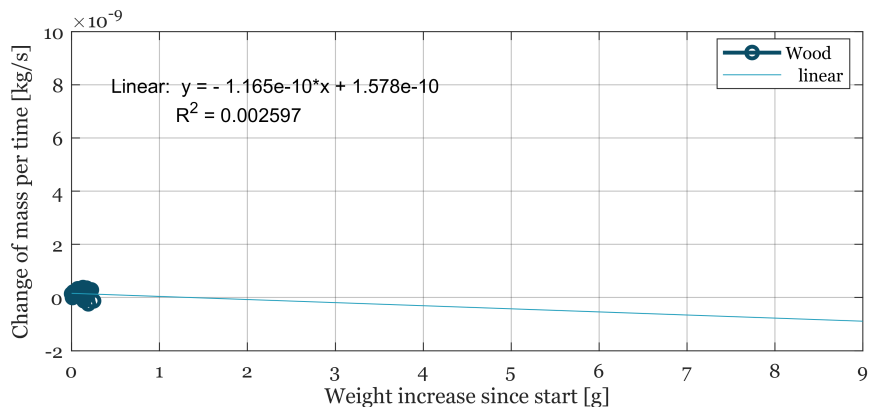


**Figure J.2** The relationship between the mass change rate and the weight gain for Wood

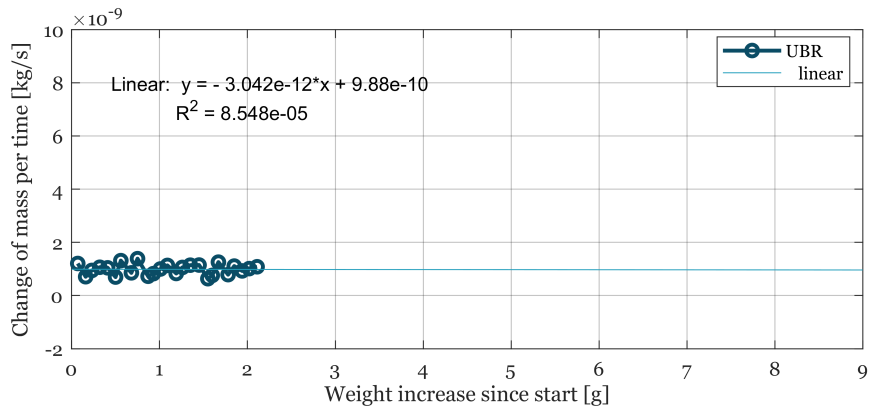


**Figure J.3** The relationship between the mass change rate and the weight gain for UBR

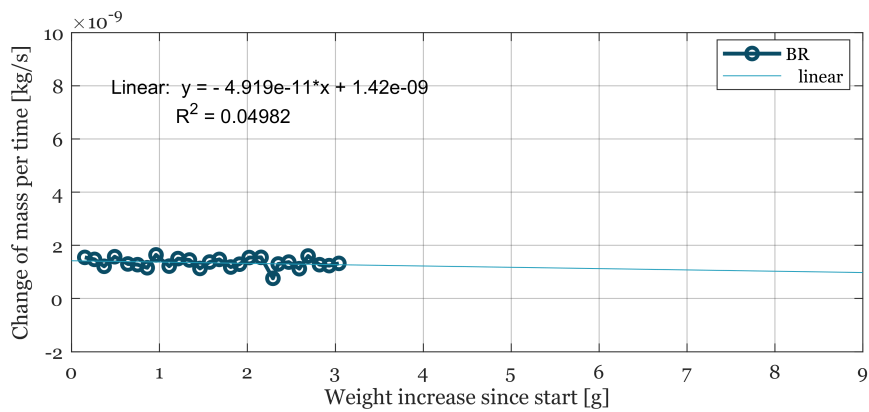


**Figure J.4** The relationship between the mass change rate and the weight gain for BR

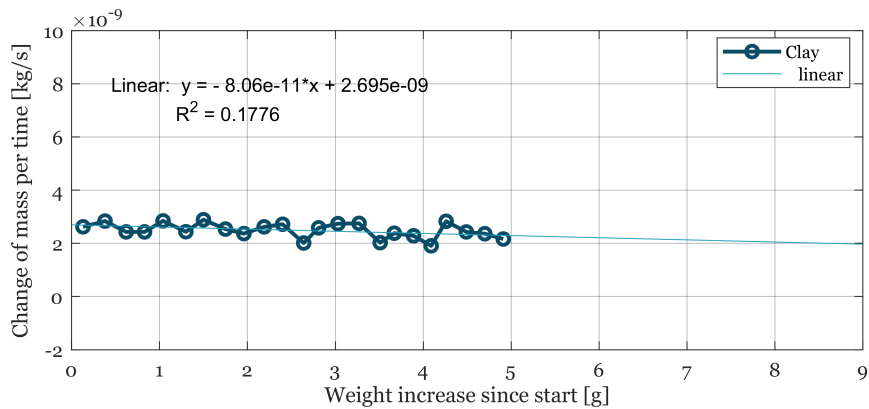


**Figure J.5** The relationship between the mass change rate and the weight gain for Clay

# Graphs for Comparison of Pure Diffusion Coefficient and Water Vapor Permeability



In the appendix, four graphs will be shown, all showing a relationship between pure diffusion coefficient and water vapor permeability. The purpose is to compare the two projection methods found in section C.3 to the final data found through the dry cup method. The first graph compares the measured pure diffusion and the measured water vapor permeability, as shown in figure K.1. In figure K.2 is the function found in figure K.1 compared to all measured pure diffusion coefficients measured in ODA20, while figures K.3 and K.4 show the same relationship, but for the predicted water vapor permeability through PM1 and PM2.

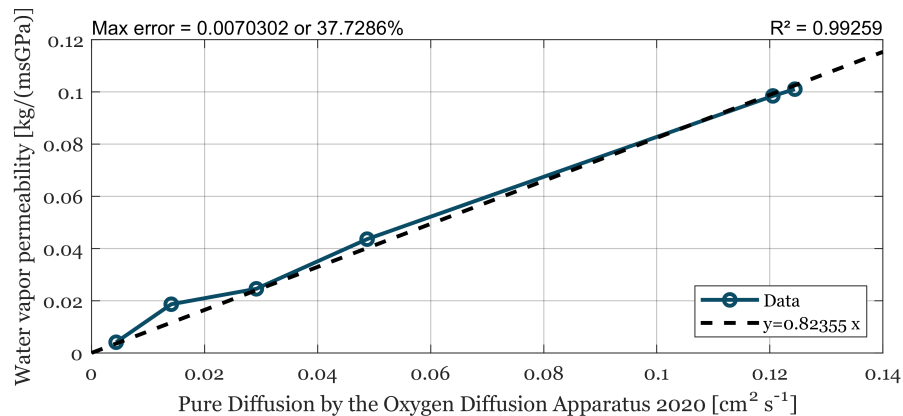


**Figure K.1** The relationship between the measured pure diffusion coefficient and the measured water vapor permeability for all six test samples used in the dry cup method.

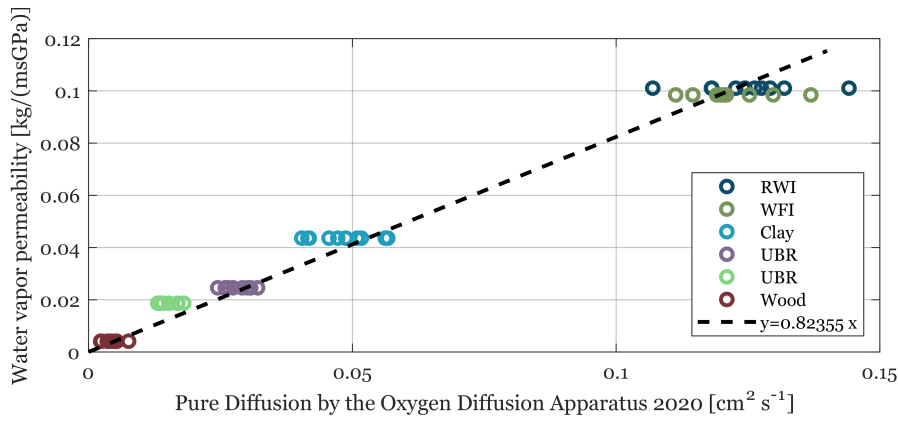


**Figure K.2** The relationship between the measured pure diffusion coefficient for all test samples in the ODA20 and the measured water vapor permeability for all six test samples used in the dry cup method.

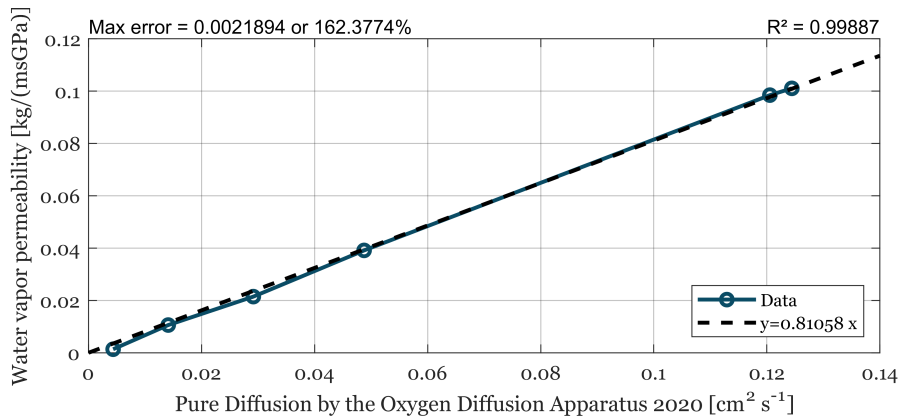


**Figure K.3** The relationship between the measured pure diffusion coefficient and the predicted water vapor permeability for all six test samples using the PM1.

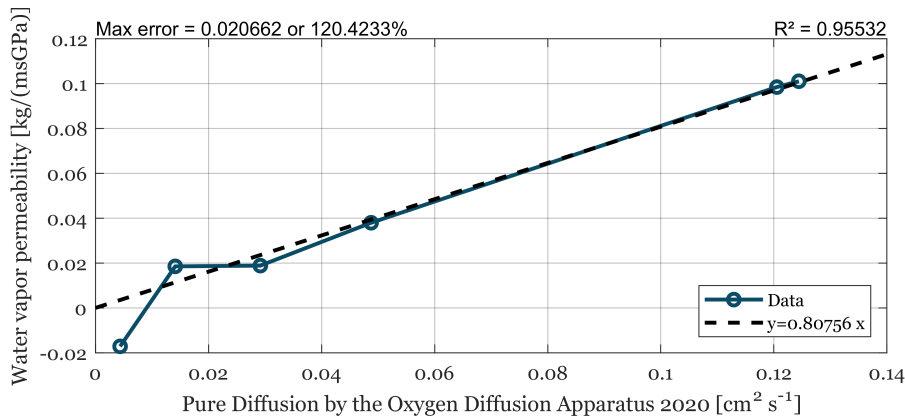


**Figure K.4** The relationship between the measured pure diffusion coefficient and the predicted water vapor permeability for all six test samples using the PM2.

# Calibration of RH sensors



This appendix describes the calibration of the Honeywell sensors that will be used to test the silica gel stability. The calibration will ensure that the Honeywell sensors provide accurate and reliable measurements during the experiment. The equipment that will be used is the Honeywell sensors that will be calibrated and a climate chamber with controlled RH and temperature levels. The climate chamber that will be used is the VCL 7010, and details about the climate chamber can be found in chapter G.

Before the Honeywell sensors were placed in the climate chamber, the chamber was controlled to be clean and dry. Four calibration points have been selected for the calibrations. The points have been picked based on the climate chamber range.

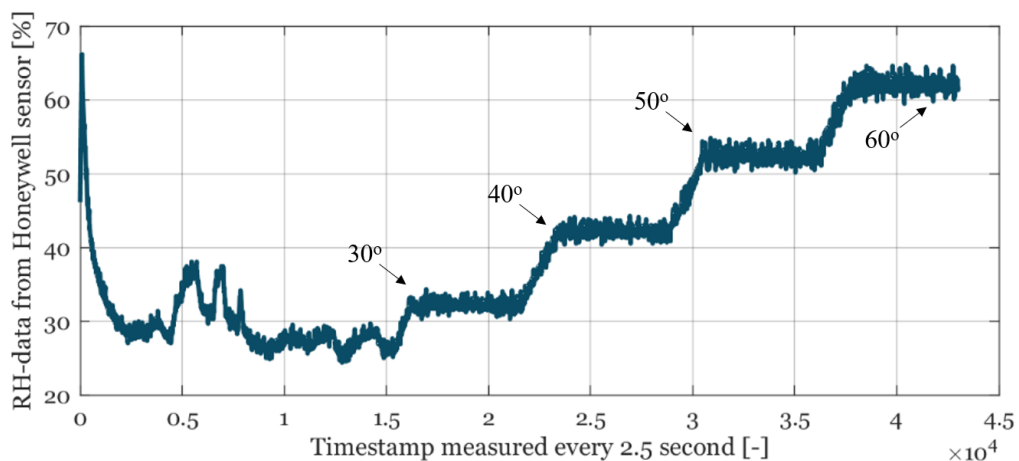


**Figure L.1** The raw data measured by the Honeywell sensor in the climate chamber. The measurement points were 30, 40, 50 and 60 % RH.

As shown in figure L.1, the four measurement points were 30, 40, 50, and 60% RH, respectively. It can also be seen that attempts were made at an RH of 20%, but the climate chamber could not keep this stable, and the data was not used for the calibration.

The Honeywell sensor will be calibrated by making a calibration graph comparing the data from the Honeywell sensors with data from the VCL 7010. It has been chosen to use the data from the VCL 7010, as its precision is controlled and gives reliable results. Because the climate chamber has not been calibrated, a quality control of its accuracy has been carried out. The quality control is done using the Novasina Hygrodat 100 Precision RH Sensor. The VCL 7010 is checked at the four previously described measuring points by comparing the data for the Novasina Hygrodat 100. Since both sensors measured the same with a difference of max 0.1 % RH, it has been chosen to use the four points to calibrate

the sensor. Details about the Novasina Hygrodat 100 Precision RH Sensor can be found in chapter G, and an example of a calibration graph can be found in Figure L.2.

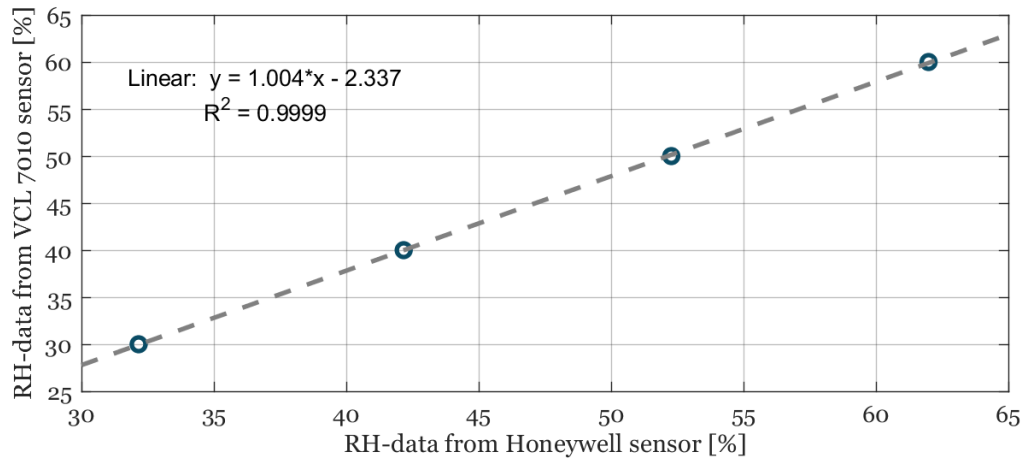


**Figure L.2** The calibration graph for the Honeywell sensors.

## L.1 The Matlab Code used to process the data

The software program Matlab from Mathworks has been used to process the data from the Honeywell sensors. The code used can be seen below.

```

clc
clear all
close all

%% The part below import the data from the first sensor into matlab
opts = delimitedTextImportOptions("NumVariables", 1);

% Specify range and delimiter
opts.DataLines = [1, Inf];
opts.Delimiter = ",";

% Specify column names and types
opts.VariableNames = "VarName1";
opts.VariableTypes = "double";

% Specify file level properties
opts.ExtraColumnsRule = "ignore";
opts.EmptyLineRule = "read";

% Import the data
HoneywellDataCOM3cal = readtable("E:\LUC_PAC\HoneywellData_COM3_cal
.txt", opts);

%% This part allows matlab to read the imported data

```

```

Com3 = HoneywellDataCOM3cal.VarName1; % This tells matlab what data to read
Com3 = Com3(~isnan(Com3)); % This removes NaN from the data

%% This part plots the data from the sensor into a 2d graph
plot(Com3) % Plot of the data from the first sensor
ylabel("RH-data from Honeywell sensor [%]") % The label on the y-axis
xlabel("Time measured every 2.5 second") % The label on the x-axis
exportgraphics(gcf,'C:\Uni\Marster\salt solution\CAL_1_salt_solution_COM3
    .png','Resolution',95) % This exports the 2d graph as a png photo

%% This part makes the calibration graph
x = 7000; % 7000 is the time between the different measuring points
    [Measured every 2.5 seconds]
Maalt_Com3 = [mean(Com3(17500:21500)), mean(Com3(17500+x:21500+x)),
    mean(Com3(17500+x*2:21500+x*2)), mean(Com3(17500+x*3:21500+x*3))],
    % The mean temperature measured by the Honeywell sensor over a fixed
    period
True_Com3 = [30, 40, 50, 60], % The RH measures by the VCL 7010 in the
    fixed period

plot(Maalt_Com3,True_Com3,'o') % This plots the calibration graph
xlabel("RH-data from Honeywell sensor [%]") % The label on the x-axis
ylabel("RH-data from VCL 7010 sensor [%]") % The label on the y-axis
exportgraphics(gcf,'C:\Uni\Marster\salt solution\CAL_2_salt_solution_COM3
    .png','Resolution',95) % This exports the calibration graph as a png photo

%% The part below imports the data from the first second into matlab
opts = delimitedTextImportOptions("NumVariables", 1);

% Specify range and delimiter
opts.DataLines = [1, Inf];
opts.Delimiter = ",";

% Specify column names and types
opts.VariableNames = "VarName1";
opts.VariableTypes = "double";

% Specify file level properties
opts.ExtraColumnsRule = "ignore";
opts.EmptyLineRule = "read";

% Import the data
HoneywellDataCOM4cal = readtable("E:\LUC_PAC\HoneywellData_COM4_cal.txt", opts);

```

# Calibration of IC meter



This appendix describes the calibration of the IC meter indoor air quality sensor used to monitor the temperature and the RH in the climate chamber. The calibration will ensure the IC meters provide accurate and reliable measurements during the dry cup method experiment. The equipment that will be used is the Honeywell sensors that will be calibrated and a climate chamber with controlled RH and temperature levels. The climate chamber that will be used is the VCL 7010, and details about the climate chamber can be found in chapter G.

As in chapter L, the chamber was controlled to be clean and dry before the IC meters were placed in the climate chamber. As the IC meter is an indoor air quality sensor, it can measure both RH and temperature, and it is necessary to calibrate it for both parts.

## M.1 Calibration of the RH sensor in the IC meter

Five calibration points have been selected for calibrating the RH sensor in the IC meter. The points have been picked based on the range expected during the dry cup method experiments. A quality control has been done at the five setpoints using a precision sensor to make sure the VCL 7010 give reliable results.

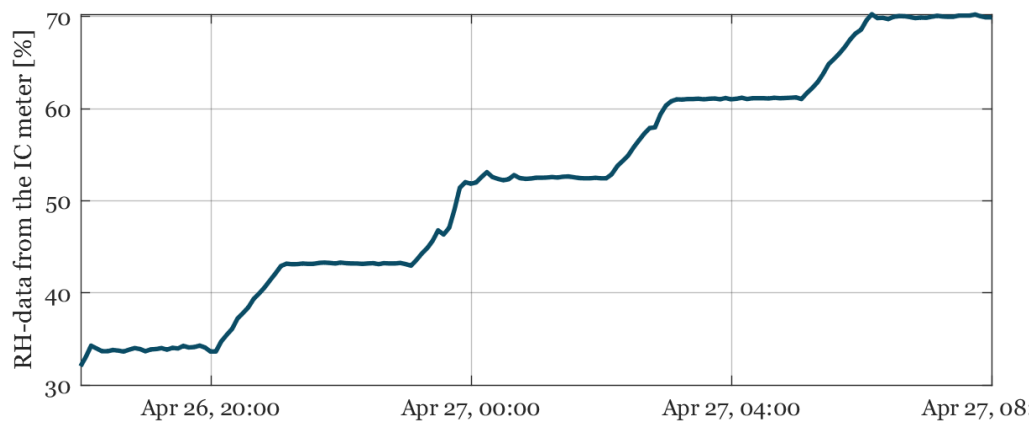


**Figure M.1** The raw data measured by the IC meter in the climate chamber.

Figure M.2 shows that the five measurement points were 30, 40, 50, 60 and 70% RH, respectively. As described in appendix L, attempts were made at an RH of 20%, but the climate chamber could not keep this stable, and the data was not used for the calibration and is therefore not shown in Figure M.2. To be sure that the climate chamber has reached the desired measurement point, the chamber is programmed to have the desired humidity for three hours, where only data from the last hour and a quarter will be used for the

calibration. It has been chosen to use the first hour to stabilize the climate chamber, as it has been found from trial and error that this is how long the climate chamber needs.

The IC meter will be calibrated by making a graph comparing the data from the RH measured by the IC meter with data from the VCL 7010. It has been chosen to use the data from the VCL 7010, as its precision is controlled and gives reliable results. Because the climate chamber has not been calibrated, a quality control of its accuracy has been carried out. The quality control is done using the Novasina Hygrodat 100 Precision RH Sensor. The VCL 7010 is checked at the five previously described measuring points by comparing the data for the Novasina Hygrodat 100. Since both sensors measured the same with a difference of max 0.1 % RH, it has been chosen to use the five points to calibrate the sensor. Details about the Novasina Hygrodat 100 Precision RH Sensor can be found in chapter G, and an example of a calibration graph can be found in Figure M.2.

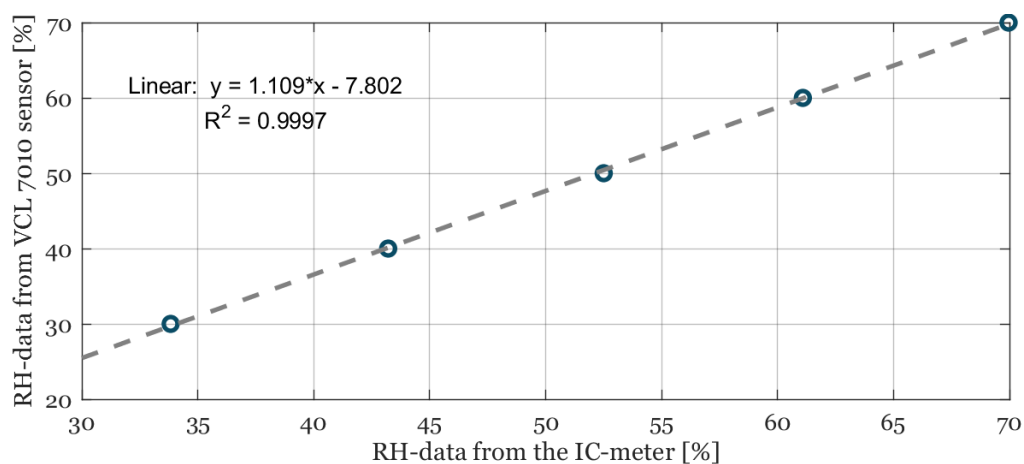


**Figure M.2** The calibration graph for the IC meter.

## M.2 Calibration of the temperature sensor in the IC meter

Eight calibration points have been selected for calibrating the temperature sensor in the IC meter. The points have been picked based on the range expected during the dry cup method experiments. A quality control has been done at the eight setpoints using a precision sensor to make sure the VCL 7010 give reliable results.

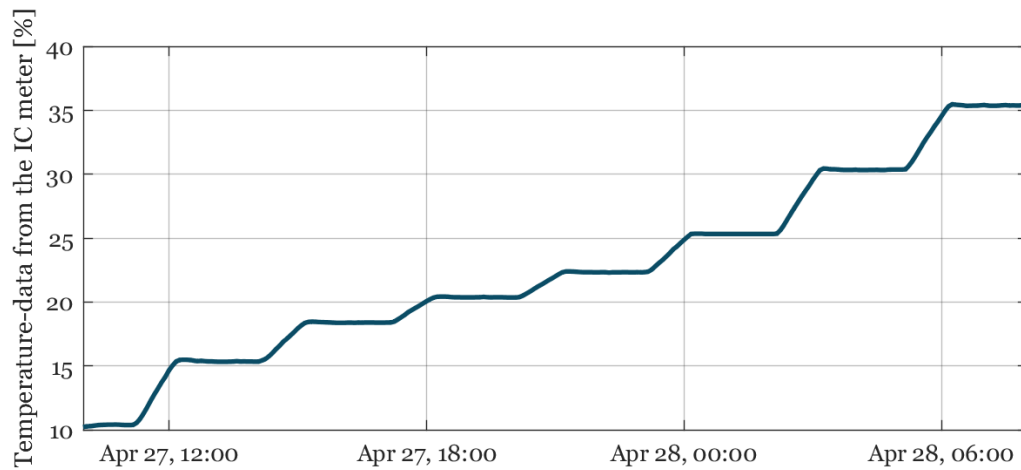


**Figure M.3** The raw data measured by the IC meter in the climate chamber.

Figure M.3 shows that the eight measurement points were 10, 15, 18, 20, 22, 25, 30, and 35 °C, respectively. To be sure that the climate chamber has reached the desired measurement point, the chamber is programmed the same way as in the RH calibration, meaning it is programmed to have the desired temperature for three hours, where only data from the last hour and a quarter will be used for the calibration.

The IC meter will be calibrated by making a graph comparing the data from the temperature measured by the IC meter with data from the VCL 7010. It has been chosen to use the data from the VCL 7010, as its precision is controlled and gives reliable results. Because the climate chamber has not been calibrated, a quality control of its precision has been carried out. The quality control is done using the F200 precision thermometer. The VCL 7010 is checked at the eight previously described measuring points by comparing the data for the F200. Since both sensors measured the same with a difference of max 0.1 °C, using the eight points to calibrate the sensor has been chosen. Details about the F200 precision thermometer can be found in chapter G, and an example of a calibration graph can be found in Figure M.1.

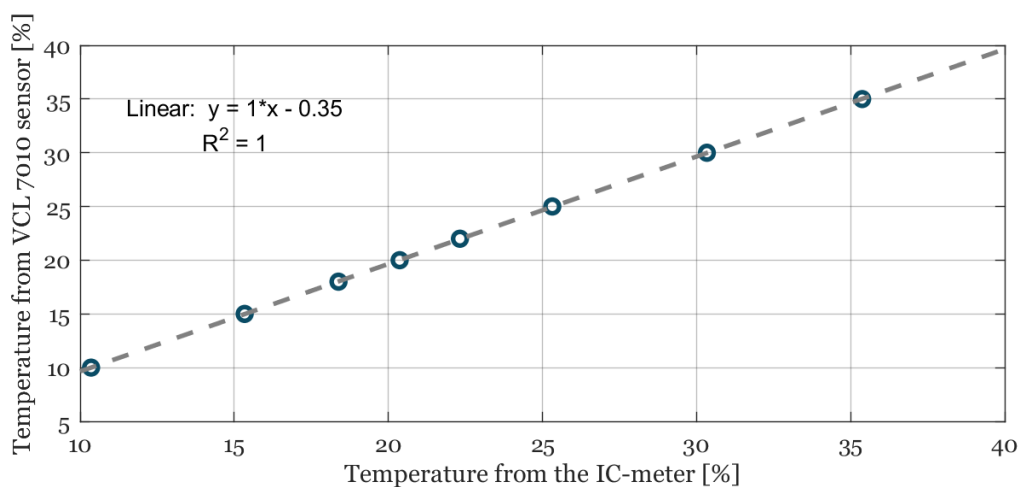


**Figure M.4** The calibration graph for the IC meter.

## M.3 The Matlab Code used to process the data

The software program Matlab from Mathworks has been used to process the data from the IC meters. The code used can be seen below.

```

clc
clear all
close all

%% The part below import the data from the first sensor into matlab
opts = delimitedTextImportOptions("NumVariables", 9);

% Specify range and delimiter
opts.DataLines = [3, Inf];
opts.Delimiter = ";";

% Specify column names and types
opts.VariableNames = ["Time", "DATEEUROPECOPENHAGEN", "TIMEEUROPECOPENHAGEN"
    , "TEMPERATUREC", "HUMIDITY", "CO2PPM", "NOISEAVGDBA", "NOISEPEAKDBA",
    "LIGHTLUX"];
opts.VariableTypes = ["datetime", "datetime", "datetime", "double", "double"
    , "double", "double", "double", "string"];

% Specify file level properties
opts.ExtraColumnsRule = "ignore";
opts.EmptyLineRule = "read";

% Specify variable properties
opts = setvaropts(opts, "LIGHTLUX", "WhitespaceRule", "preserve");
opts = setvaropts(opts, "LIGHTLUX", "EmptyFieldRule", "auto");
opts = setvaropts(opts, "Time", "InputFormat", "yyyy-MM-dd HH:mm:ss");
opts = setvaropts(opts, "DATEEUROPECOPENHAGEN", "InputFormat", "yyyy-MM-dd");
opts = setvaropts(opts, "TIMEEUROPECOPENHAGEN", "InputFormat", "HH:mm:ss");
opts = setvaropts(opts, ["TEMPERATUREC", "HUMIDITY", "CO2PPM", "NOISEAVGDBA"
    , "NOISEPEAKDBA"], "DecimalSeparator", ",");
opts = setvaropts(opts, ["TEMPERATUREC", "HUMIDITY", "CO2PPM", "NOISEAVGDBA"
    , "NOISEPEAKDBA"], "ThousandsSeparator", ".");

% Import the data
ICmeter = readtable("C:\Users\patri\Downloads\IC-Meter-17.csv", opts);

%% This part allows matlab to read the imported data
xxx = 5; % This part removes the first five points, as these points are
    affected by the setup of the sensor
ICmeter_Time = ICmeter.Time(xxx:end,1); % This tells matlab what data to
    read as the time

```

```

ICmeter_Temp = ICmeter.TEMPERATUREC(xxx:end,1); % This tells matlab what
    data to reed as the tempeture
ICmeter_Humi = ICmeter.HUMIDITY(yyy:end,1); % This tells matlab what
    data to reed as the humidity
ICmeter_Time=datettime(ICmeter_Time,'InputFormat','dd-mmm-yyyy HH:mm');
    % This tells matlab to reed the time data as time

%% This part plots the temperature data from the sensor into a 2d graph
plot(ICmeter_Time,ICmeter_Temp) % Plot of hte data som the first
    temperature sensor
tstart = datettime('27-04-2023 10:00:00'); % This is the start time
tend = datettime('28-04-2023 08:00:00'); % This is the end time
xlim([tstart tend]); % This is the start and end time from above
ylabel("Temperature-data from the IC meter [%]") % The label on the
    y-aksel
xlabel("Time") % The label on the x-aksel
exportgraphics(gcf,'C:\Uni\Marster\salt solution\CAL_IC17_temp.png',
    'Resolution',180) % This eksports the 2d graph as a png photo

%% This part plots the humidity data from the sensor into a 2d graph
plot(ICmeter_Time,ICmeter_Humi) % Plot of hte data som the first
    temperature sensor
tstart = datettime('26-04-2023 18:00:00'); % This is the start time
tend = datettime('27-04-2023 08:00:00'); % This is the end time
xlim([tstart tend]); % This is the start and end time from above
ylabel("RH-data from the IC meter [%]") % The label on the y-aksel
xlabel("Time") % The label on the x-aksel
exportgraphics(gcf,'C:\Uni\Marster\salt solution\CAL_IC17_RH.png',
    'Resolution',180) % This eksports the 2d graph as a png photo

%% This part make the calibration graph
Temp_10 = mean(ICmeter_Temp(240:254)); % Takes the mean of the data
Temp_15 = mean(ICmeter_Temp(275:289)); % Takes the mean of the data
Temp_18 = mean(ICmeter_Temp(312:326)); % Takes the mean of the data
Temp_20 = mean(ICmeter_Temp(344:358)); % Takes the mean of the data
Temp_22 = mean(ICmeter_Temp(380:394)); % Takes the mean of the data
Temp_25 = mean(ICmeter_Temp(416:430)); % Takes the mean of the data
Temp_30 = mean(ICmeter_Temp(454:468)); % Takes the mean of the data
Temp_35 = mean(ICmeter_Temp(489:503)); % Takes the mean of the data

Humi_30 = mean(ICmeter_Humi(51:65)); % Takes the mean of the data
Humi_40 = mean(ICmeter_Humi(92:106)); % Takes the mean of the data
Humi_50 = mean(ICmeter_Humi(131:145)); % Takes the mean of the data
Humi_60 = mean(ICmeter_Humi(160:174)); % Takes the mean of the data
Humi_70 = mean(ICmeter_Humi(196:210)); % Takes the mean of the data

```

```
Temp = [Temp_10 Temp_15 Temp_18 Temp_20 Temp_22 Temp_25 Temp_30 Temp_35]';
    % Makes a matrix om the measured points
Humi = [Humi_30 Humi_40 Humi_50 Humi_60 Humi_70]';
    % Makes a matrix om the measured points

Temp_true = [10 15 18 20 22 25 30 35]'; % Makes a matrix om the true points
Humi_true = [30 40 50 60 70]'; % Makes a matrix om the true points

plot(Temp,Temp_true,'o') % This plots the calibration graph for the
    temperature
xlabel("Temperature from the IC-meter [%]") % The label on the x-aksel
ylabel("Temperature from VCL 7010 sensor [%]") % The label on the y-aksel

plot(Humi,Humi_true,'o') % This plots the calibration graph for the humidity
xlabel("RH-data from the IC-meter [%]") % The label on the x-aksel
ylabel("RH-data from VCL 7010 sensor [%]") % The label on the y-aksel
```

# Calibration of ODA20

# N

To get precise data, the ODA20 has to be calibrated. This will be done by using test dummies as samples. These test dummies are plastic cylinders with different amounts of holes. The setup and procedure are described in section D.3. The data is then used to find a calibration graph determining the diffusion coefficient of the given test dummy.

## N.1 Equipment

Additional equipment is used when calibrating the ODA20. The equipment used in this section is similar to what is used in appendix D. In addition, the equipment in table N.1 will also be used.

**Table N.1** List of equipment.

| Brand | Model                   | Description       | Serial Number |
|-------|-------------------------|-------------------|---------------|
| -     | Ø51mm with 40x3mm holes | Calibration dummy | -             |
| -     | Ø51mm with 30x3mm holes | Calibration dummy | -             |
| -     | Ø51mm with 21x3mm holes | Calibration dummy | -             |
| -     | Ø51mm with 16x3mm holes | Calibration dummy | -             |
| -     | Ø51mm with 4x3mm holes  | Calibration dummy | -             |
| -     | Ø51mm closed            | Calibration dummy | -             |

## N.2 How the ODA is Calibrated

For the calibration of the ODA20, plastic cylinders, also called test dummies, are used. These have different amounts of holes that demonstrates types of materials with varying sizes of pores and pore amounts. The different test dummies can be seen in figure N.1. The procedure for using the ODA20 is described in D.3.1 and will not be described any further.



**Figure N.1** Different test dummies from left to right: 1) 40x3mm, 2) 30x3mm, 3) 21x3mm, 4) 16x3mm 5) 4x3mm 6) closed.

The data from the test dummies are used to find the slope constant  $K_c$  which will correct the measured  $D_p$ -value of the samples. For this the  $K_c$ -value that fits the dummies best needs to be calculated. In order to find the  $K_c$ -value, the theoretical  $D_p$ -value is calculated with the equation N.1

$$D_{ptheory} = ratio_{dummy} \cdot 0.205 \quad (N.1)$$

The ratio of the dummy can be find with the equation N.2

$$ratio_{dummy} = A_{holes}/A_{dummy} \quad (N.2)$$

Where  $A_{holes}$  is the area of the holes in the dummy and  $A_{dummy}$  is the area of the hole dummy. Often the  $K_c$ -value from the test dummy that is closed fits the best. Therefore the  $K_c$ -value from the closed dummy will be taken.

### N.3 Results

The measured  $D_p$ -value is shown graphically with the theoretical  $D_p$  along the x-axis and the measured on the y-axis. The diffusion coefficient of the test dummies is found as described in D.1. The linear function is determined after the lowest  $D_p$ -value, which is the closed dummy in most cases. The slope constant  $K_c$ , from the closed dummy, is therefore chosen for the testcells and the slope constant for all the testcells can be seen in table N.2. Figure N.2 shows an example of the calibration graph. Here the cross is the measured value, and the dot is the measured value, corrected with the  $K_c$ -value.

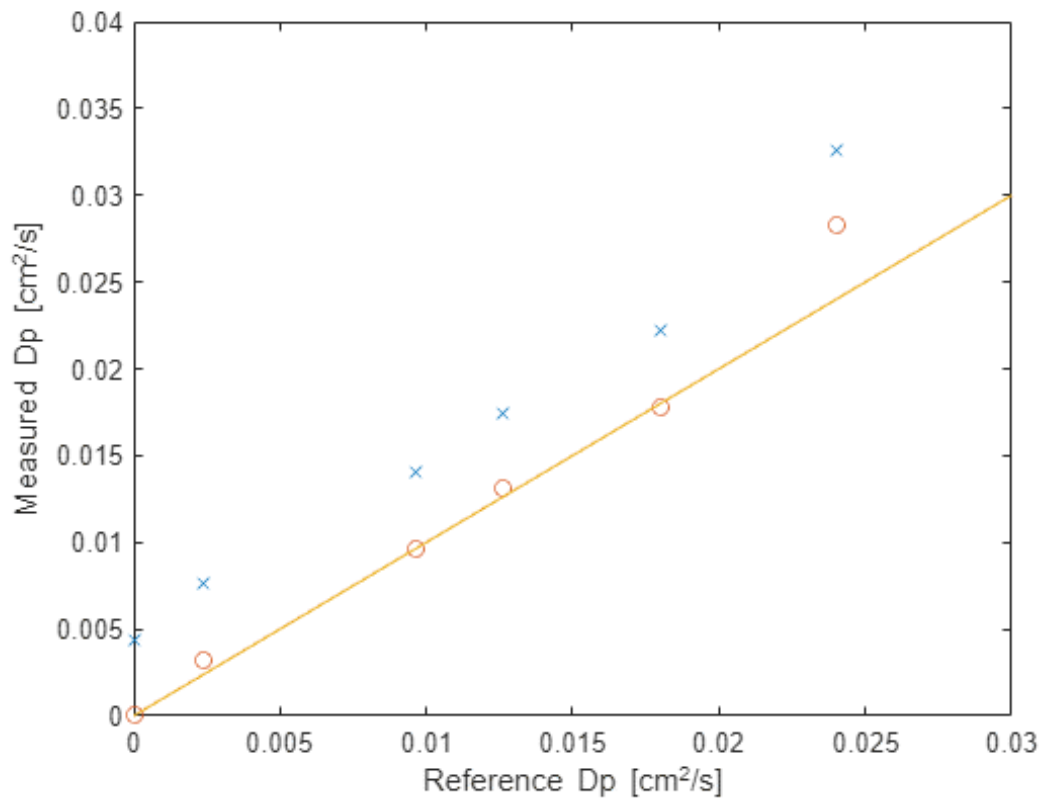


**Figure N.2** An example of a calibration graph. The cross marks the measured  $D_p$ -value and the dot marks the measured  $D_p$ -value corrected with the  $K_c$ -value. This calibration graph is from Testcell 2. The dots and crosses mark one test dummy, starting from the lowest one: closed, 4x3mm, 16x3mm, 21x3mm, 30x3mm, 40x3mm.

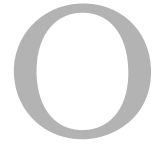
The calibration graphs for each ODA20 can be seen in appendix O.

These slope constants will be used later on when data processing the samples and also when doing the study of casting technique which is described in appendix E.

**Table N.2** Slope constant of the ODA20 2-6 and 8-9.

| ODA20 Testcell | Slope constant $K_c$ [-] |
|----------------|--------------------------|
| 2              | 3.7685e-05               |
| 3              | 2.4271e-05               |
| 4              | 6.9372e-05               |
| 5              | 5.5004e-05               |
| 6              | 3.5423e-05               |
| 8              | 2.5231e-05               |
| 9              | 3.6153e-05               |

# Calibration graphs of the ODA20



In this chapter the calibration graphs of the ODA20 are shown. As more than one apparatus are used in this project, the graph for every apparatus are shown. The ODA20 needs to be calibrated every three weeks, therefore multiple graphs for the same apparatus can be seen. Test samples have been tested in week 14 and 18 in 2023 and these graphs are shown in the next two sections. The method of calibrating the ODA20 can be seen in appendix N.

## O.1 Week 14

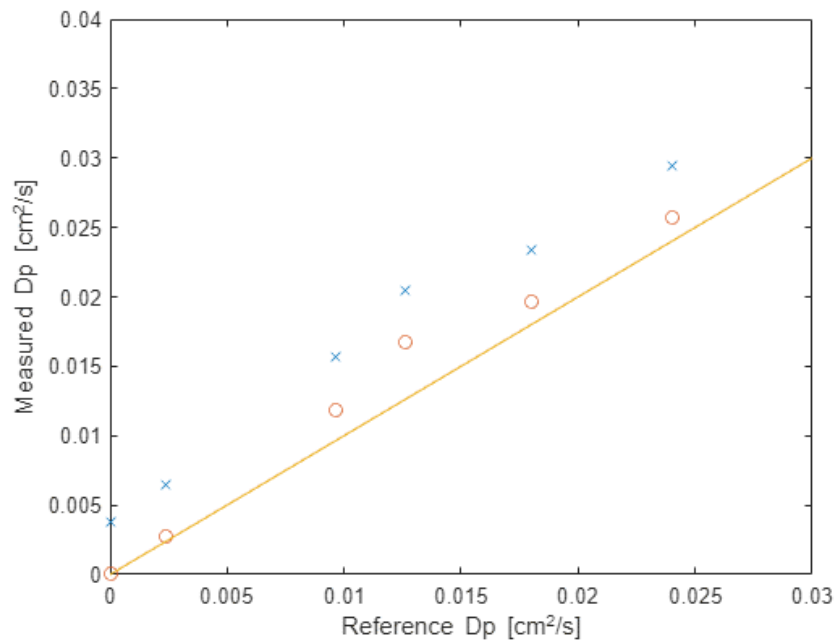


**Figure O.1** Calibration graph of Testcell 2. The cross marks the measured  $D_p$ -value and the dot marks the  $D_p$ -value after the calibration. The dots and crosses mark one test dummy, starting from the lowest one: closed, 4x3mm, 16x3mm, 21x3mm, 30x3mm, 40x3mm.

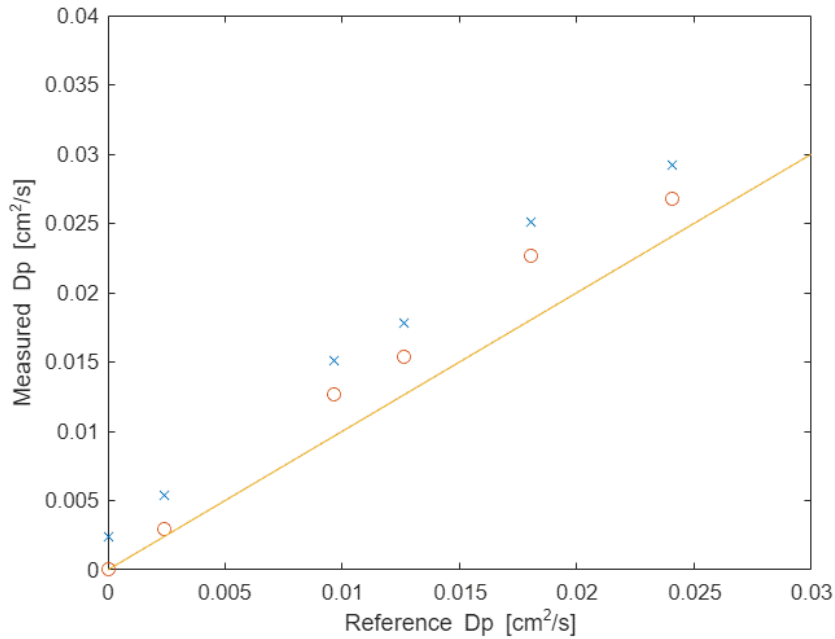


**Figure O.2** Calibration graph of Testcell 3. The cross marks the measured  $D_p$ -value and the dot marks the  $D_p$ -value after the calibration. The dots and crosses mark one test dummy, starting from the lowest one: closed, 4x3mm, 16x3mm, 21x3mm, 30x3mm, 40x3mm.

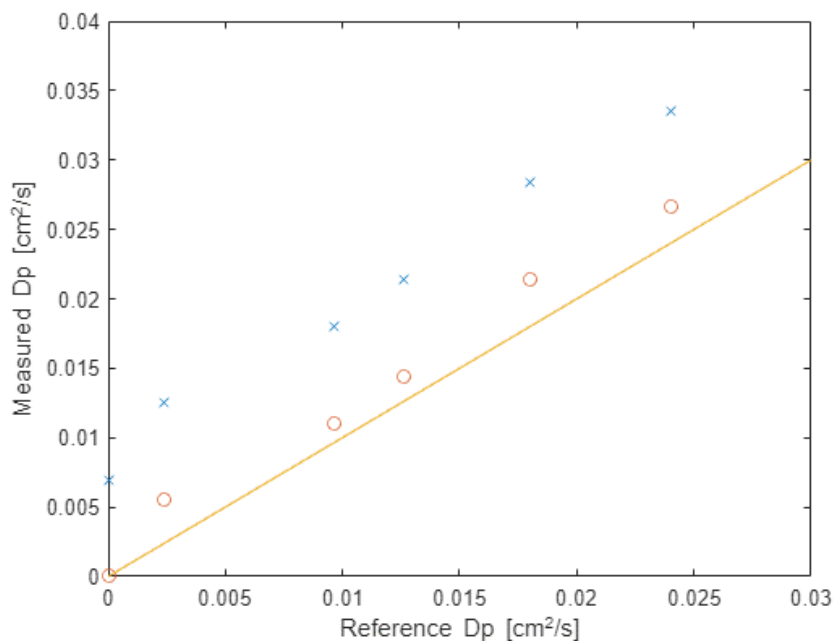


**Figure O.3** Calibration graph of Testcell 4. The cross marks the measured  $D_p$ -value and the dot marks the  $D_p$ -value after the calibration. The dots and crosses mark one test dummy, starting from the lowest one: closed, 4x3mm, 16x3mm, 21x3mm, 30x3mm, 40x3mm.

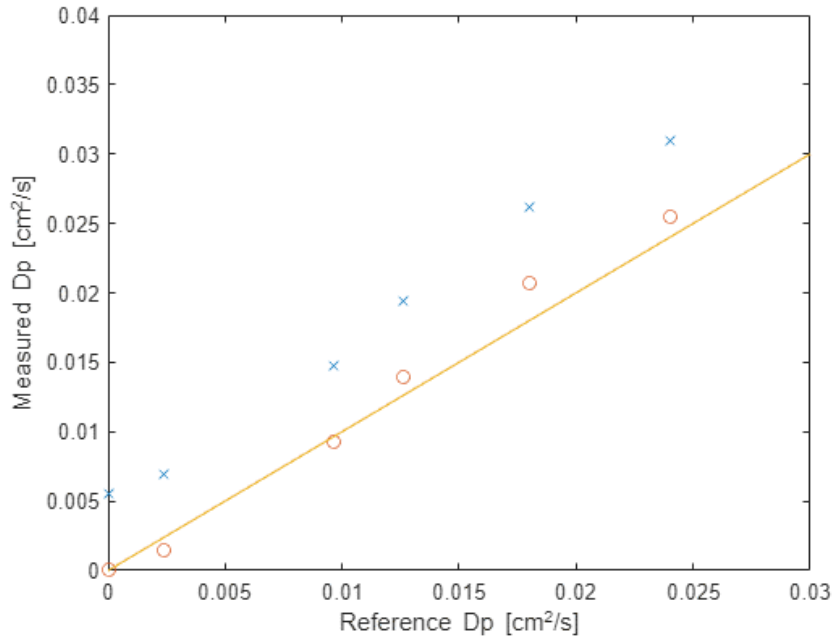


**Figure O.4** Calibration graph of Testcell 5. The cross marks the measured  $D_p$ -value and the dot marks the  $D_p$ -value after the calibration. The dots and crosses mark one test dummy, starting from the lowest one: closed, 4x3mm, 16x3mm, 21x3mm, 30x3mm, 40x3mm.

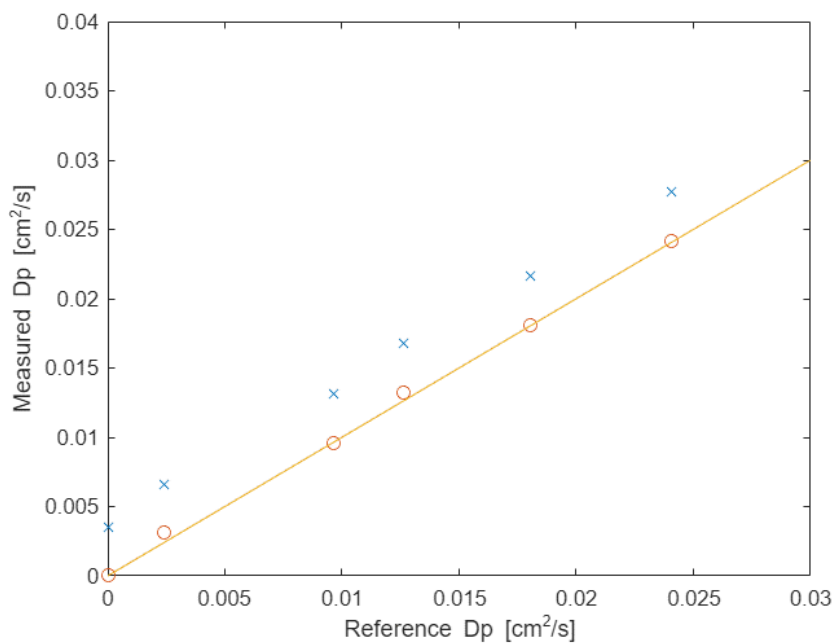


**Figure O.5** Calibration graph of Testcell 6. The cross marks the measured  $D_p$ -value and the dot marks the  $D_p$ -value after the calibration. The dots and crosses mark one test dummy, starting from the lowest one: closed, 4x3mm, 16x3mm, 21x3mm, 30x3mm, 40x3mm.

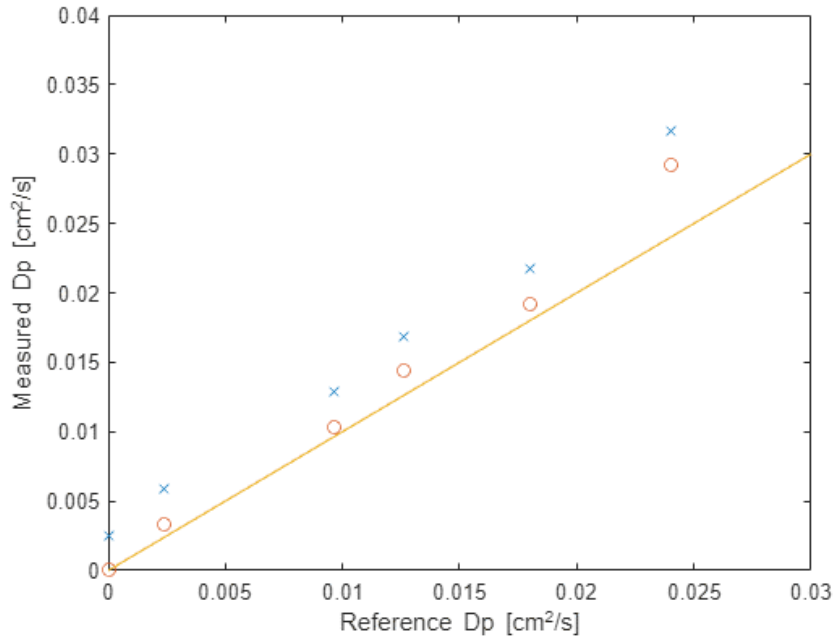


**Figure O.6** Calibration graph of Testcell 8. The cross marks the measured  $D_p$ -value and the dot marks the  $D_p$ -value after the calibration. The dots and crosses mark one test dummy, starting from the lowest one: closed, 4x3mm, 16x3mm, 21x3mm, 30x3mm, 40x3mm.

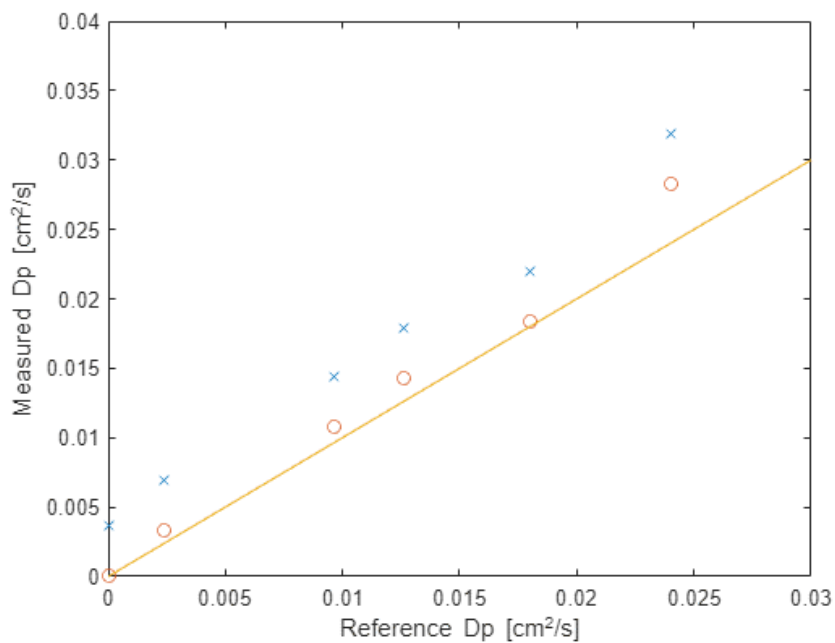


**Figure O.7** Calibration graph of Testcell 9. The cross marks the measured  $D_p$ -value and the dot marks the  $D_p$ -value after the calibration. The dots and crosses mark one test dummy, starting from the lowest one: closed, 4x3mm, 16x3mm, 21x3mm, 30x3mm, 40x3mm.

## O.2 Week 18

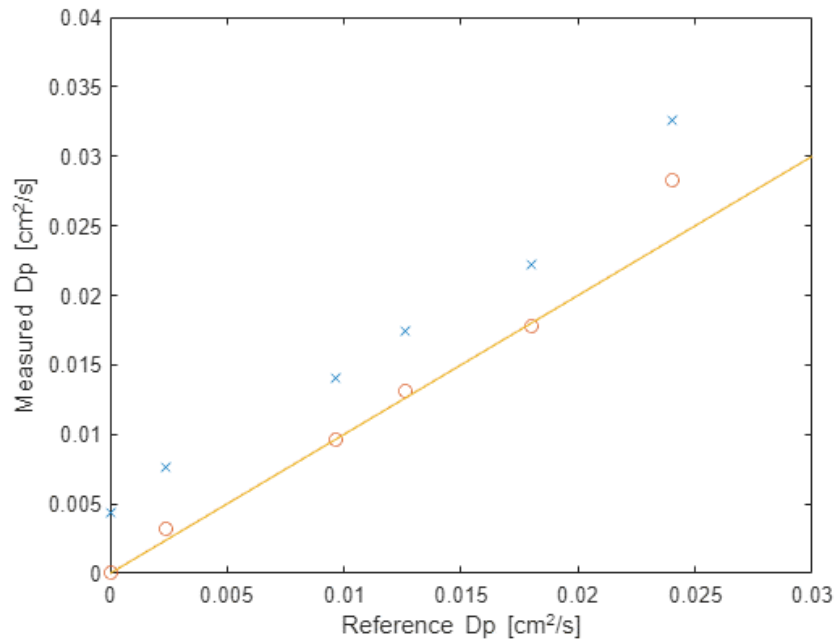


**Figure O.8** Calibration graph of Testcell 2. The cross marks the measured  $D_p$ -value and the dot marks the  $D_p$ -value after the calibration. The dots and crosses mark one test dummy, starting from the lowest one: closed, 4x3mm, 16x3mm, 21x3mm, 30x3mm, 40x3mm.

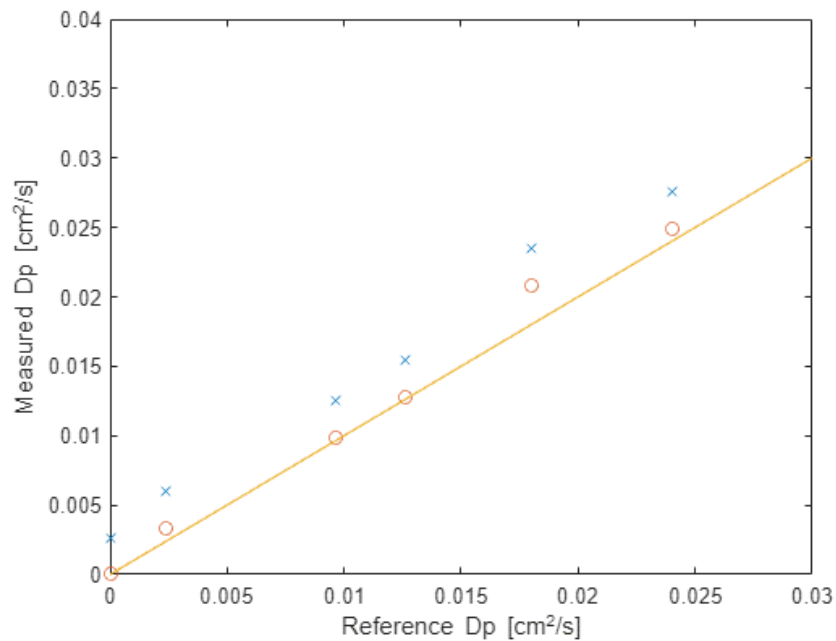


**Figure O.9** Calibration graph of Testcell 3. The cross marks the measured  $D_p$ -value and the dot marks the  $D_p$ -value after the calibration. The dots and crosses mark one test dummy, starting from the lowest one: closed, 4x3mm, 16x3mm, 21x3mm, 30x3mm, 40x3mm.

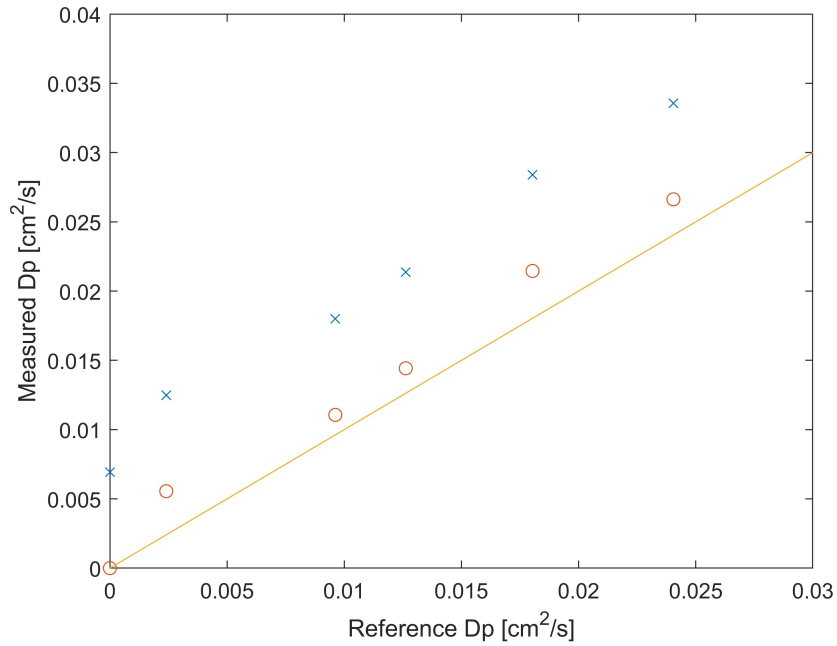


**Figure O.10** Calibration graph of Testcell 4. The cross marks the measured  $D_p$ -value and the dot marks the  $D_p$ -value after the calibration. The dots and crosses mark one test dummy, starting from the lowest one: closed, 4x3mm, 16x3mm, 21x3mm, 30x3mm, 40x3mm.

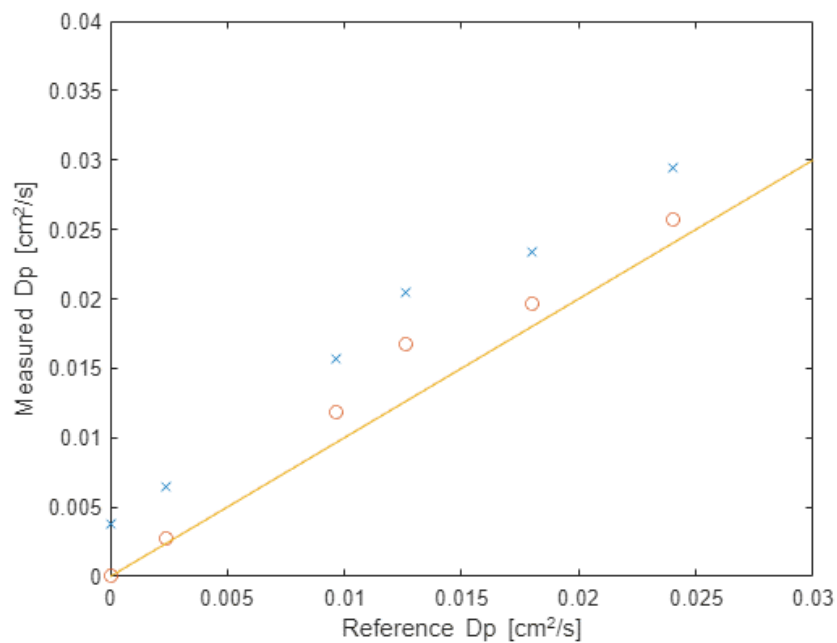


**Figure O.11** Calibration graph of Testcell 5. The cross marks the measured  $D_p$ -value and the dot marks the  $D_p$ -value after the calibration. The dots and crosses mark one test dummy, starting from the lowest one: closed, 4x3mm, 16x3mm, 21x3mm, 30x3mm, 40x3mm.

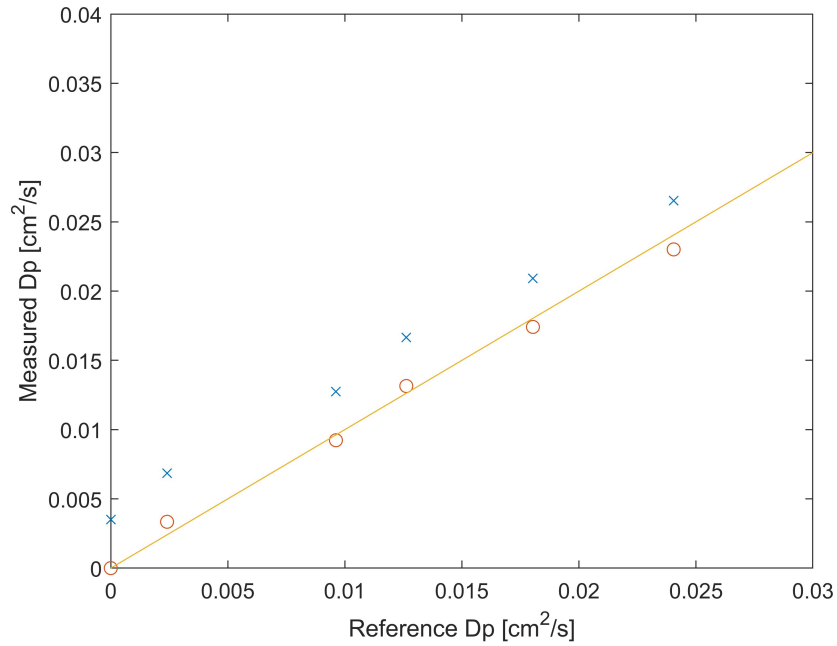


**Figure O.12** Calibration graph of Testcell 6. The cross marks the measured  $D_p$ -value and the dot marks the  $D_p$ -value after the calibration. The dots and crosses mark one test dummy, starting from the lowest one: closed, 4x3mm, 16x3mm, 21x3mm, 30x3mm, 40x3mm.

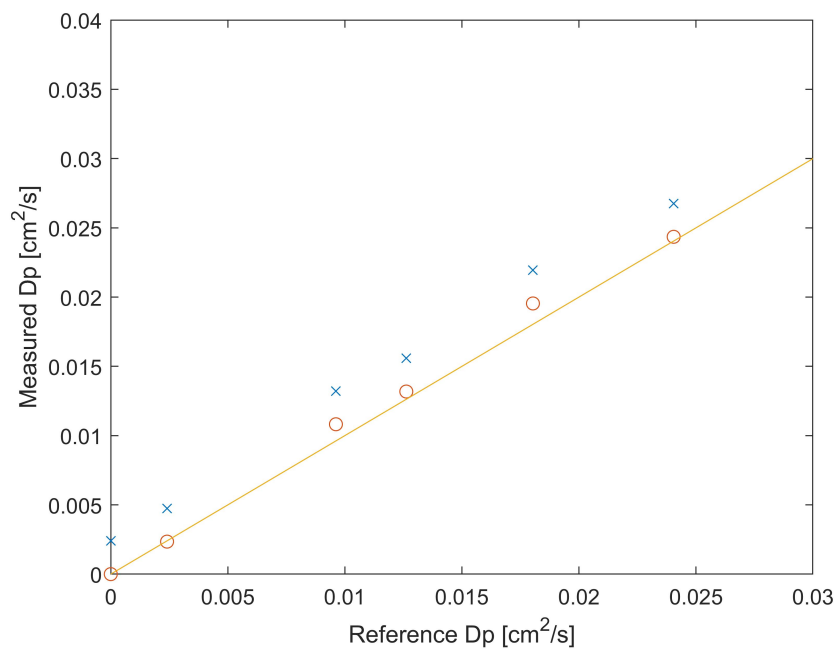


**Figure O.13** Calibration graph of Testcell 8. The cross marks the measured  $D_p$ -value and the dot marks the  $D_p$ -value after the calibration. The dots and crosses mark one test dummy, starting from the lowest one: closed, 4x3mm, 16x3mm, 21x3mm, 30x3mm, 40x3mm.

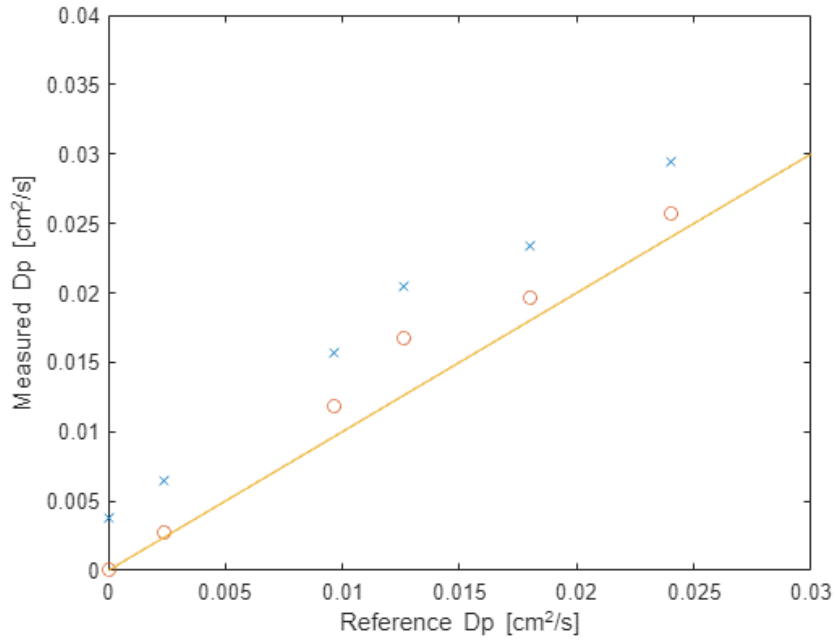


**Figure O.14** Calibration graph of Testcell 9. The cross marks the measured  $D_p$ -value and the dot marks the  $D_p$ -value after the calibration. The dots and crosses mark one test dummy, starting from the lowest one: closed, 4x3mm, 16x3mm, 21x3mm, 30x3mm, 40x3mm.

# Example data of each Material P

---

The graphs in this chapter, show an example of the raw data and the slope constant, that is used to find the  $D_p$ -value of the material. The method on finding the  $D_p$ -value can be seen in appendix D.

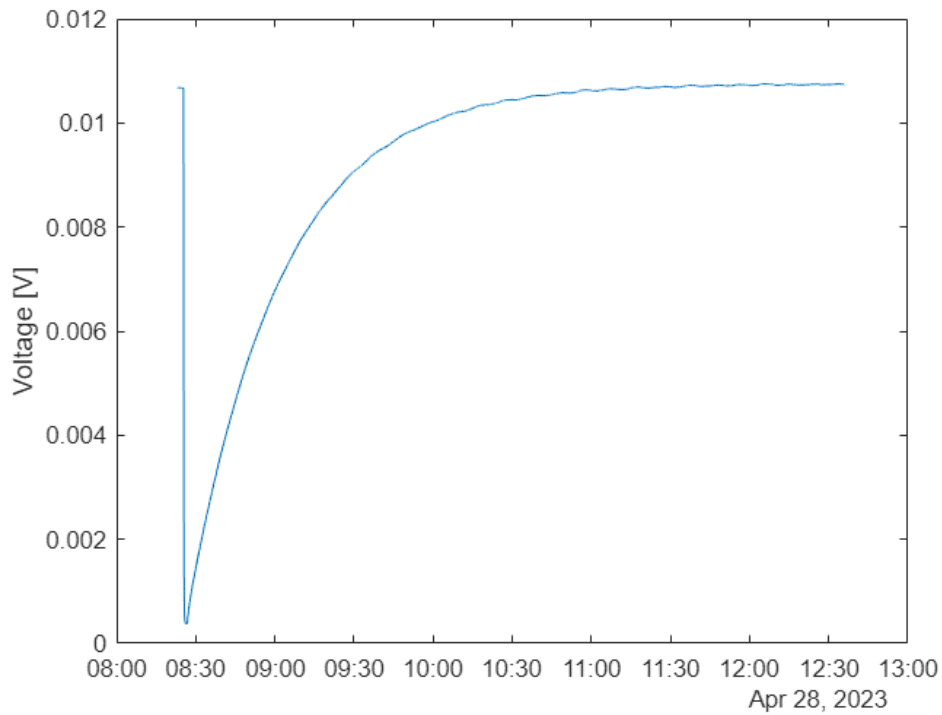


**Figure P.1** Example of raw data of a brick sample.

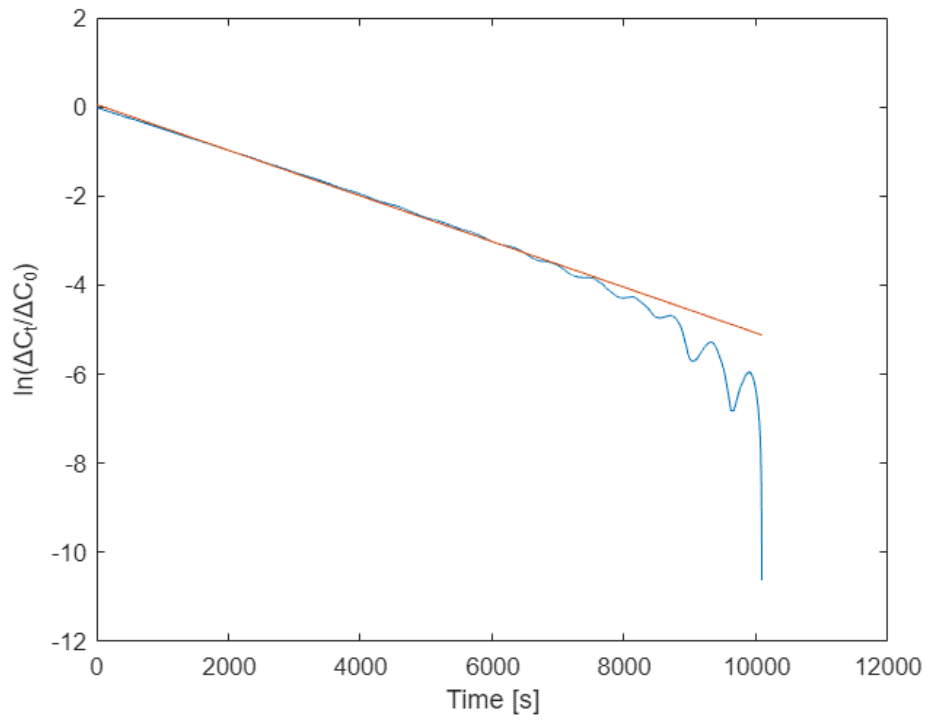


**Figure P.2** Example of determination of the  $D_p$ - coefficient.

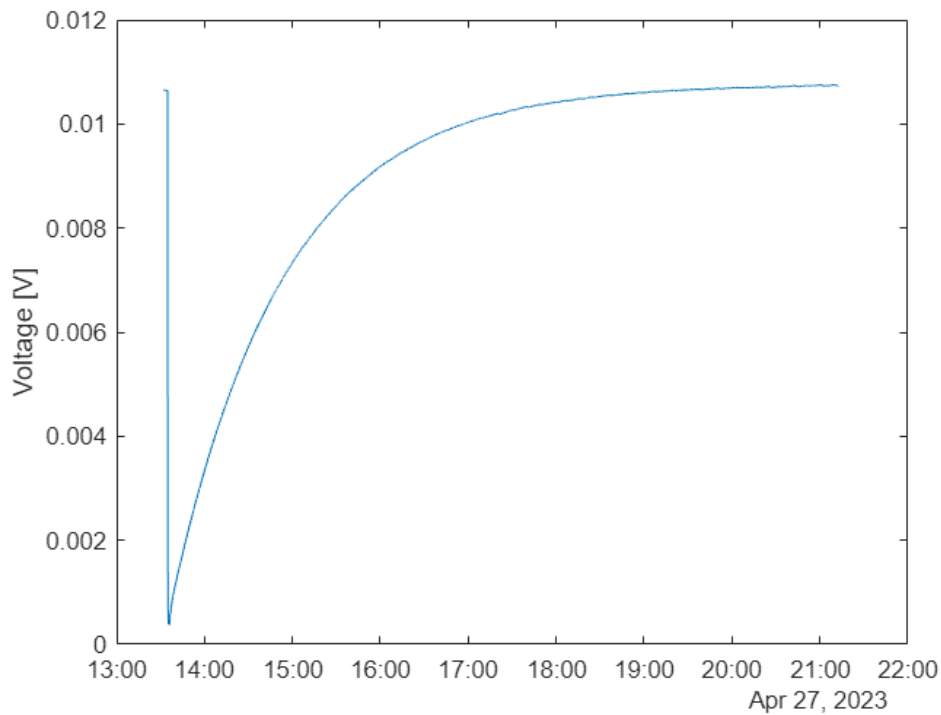


**Figure P.3** Example of raw data of an unfired brick sample.

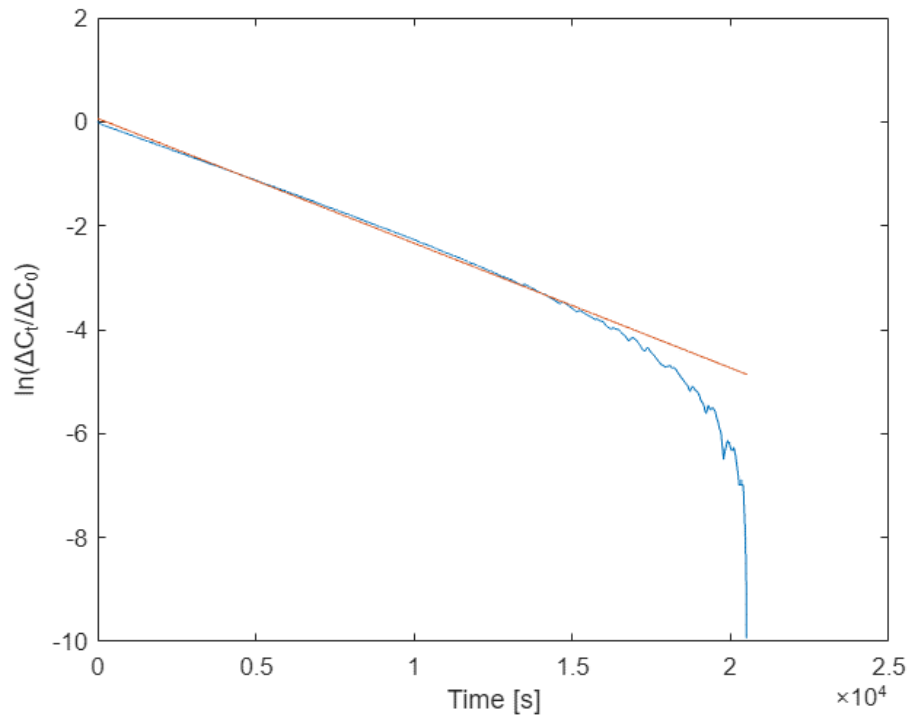


**Figure P.4** Example of determination of the  $D_p$ - coefficient for unfired brick.

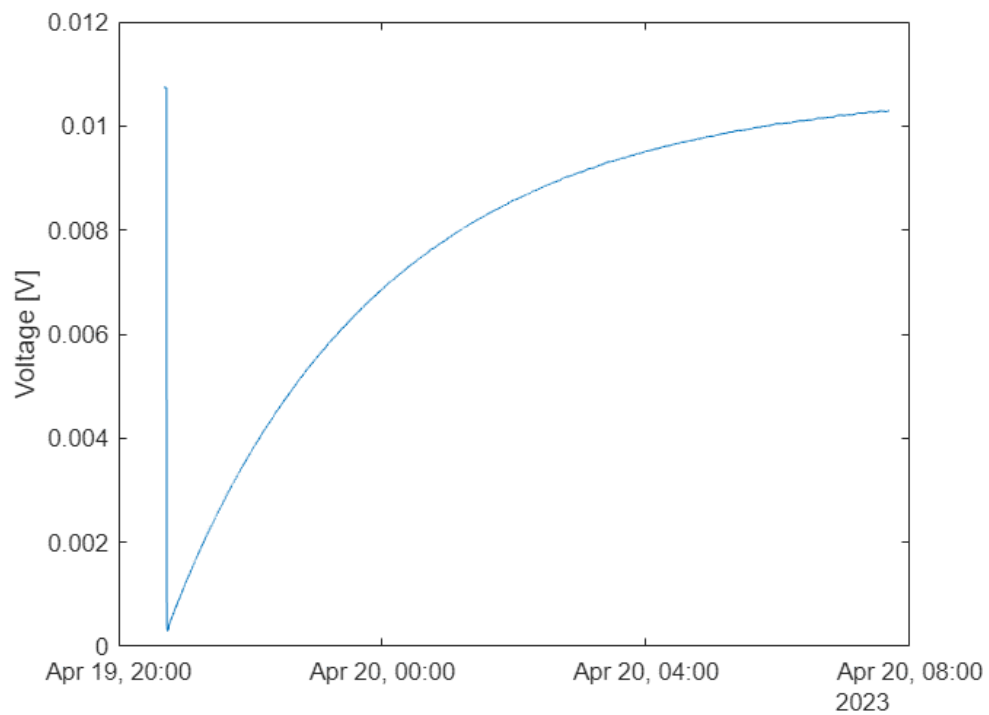


**Figure P.5** Example of raw data of a wood sample.

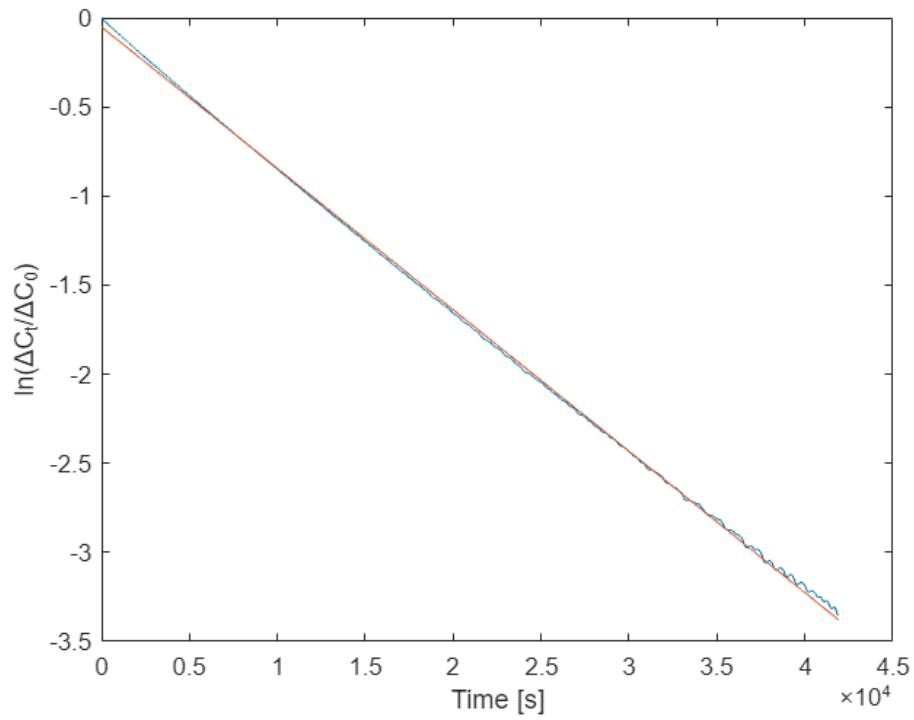


**Figure P.6** Example of determination of the  $D_p$ - coefficient for wood.

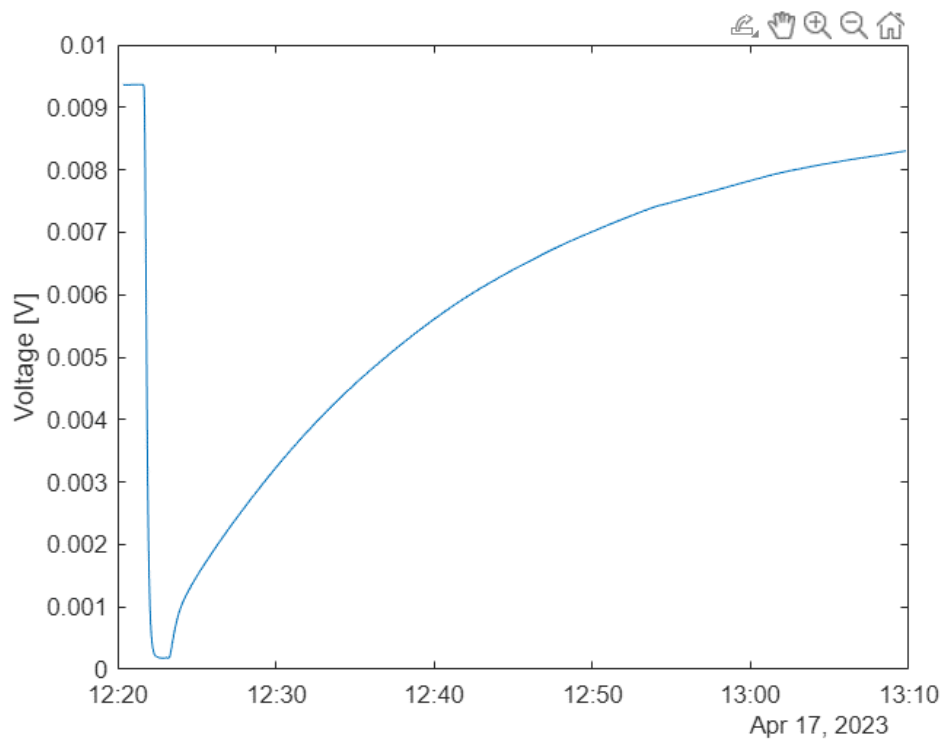


**Figure P.7** Example of raw data of a clay sample with 3% water content.

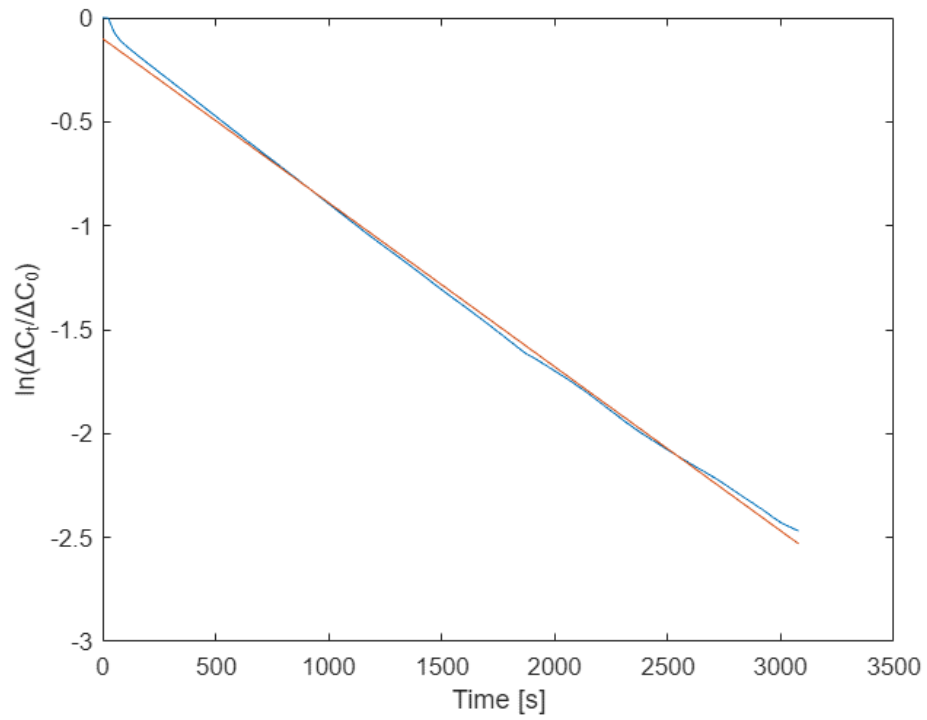


**Figure P.8** Example of determination of the  $D_p$ - coefficient for clay with 3% water content.

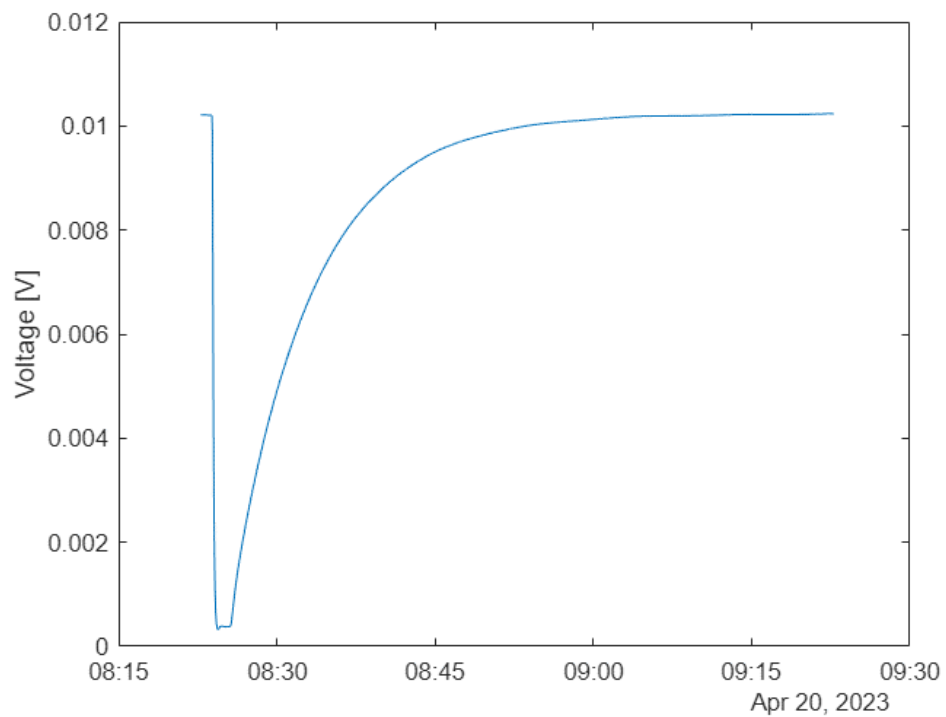


**Figure P.9** Example of raw data of a wood fiber insulation sample.

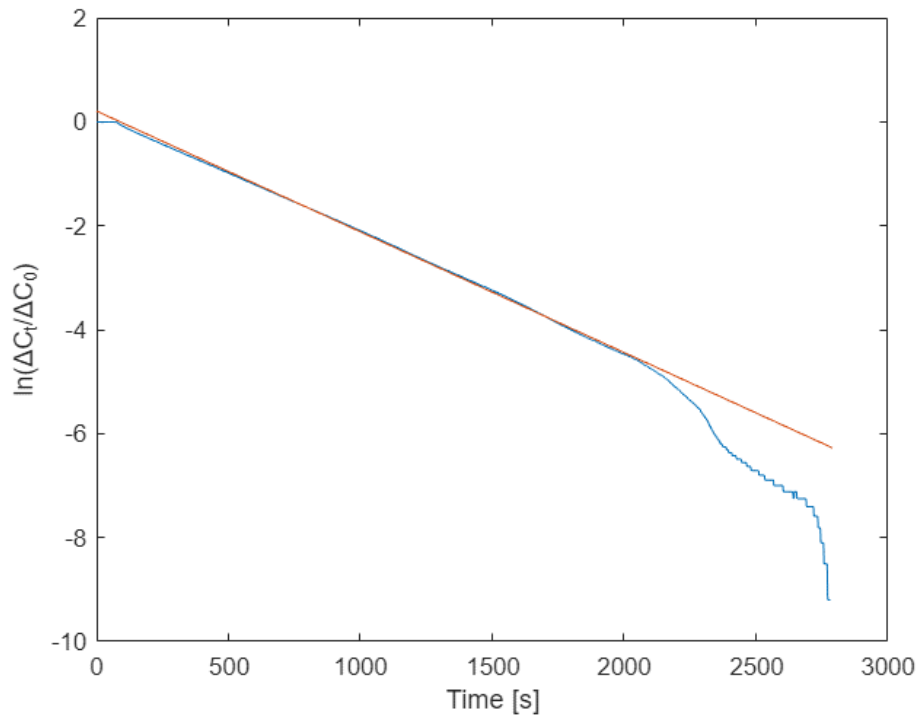


**Figure P.10** Example of determination of the  $D_p$ - coefficient for wood fiber insulation.

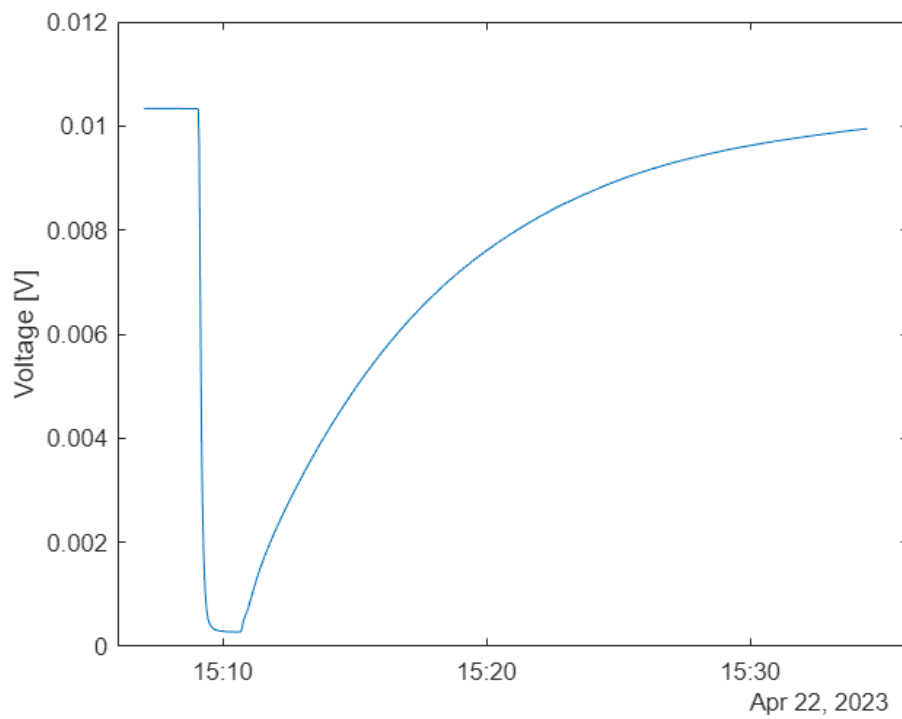


**Figure P.11** Example of raw data of a Rockwool sample.

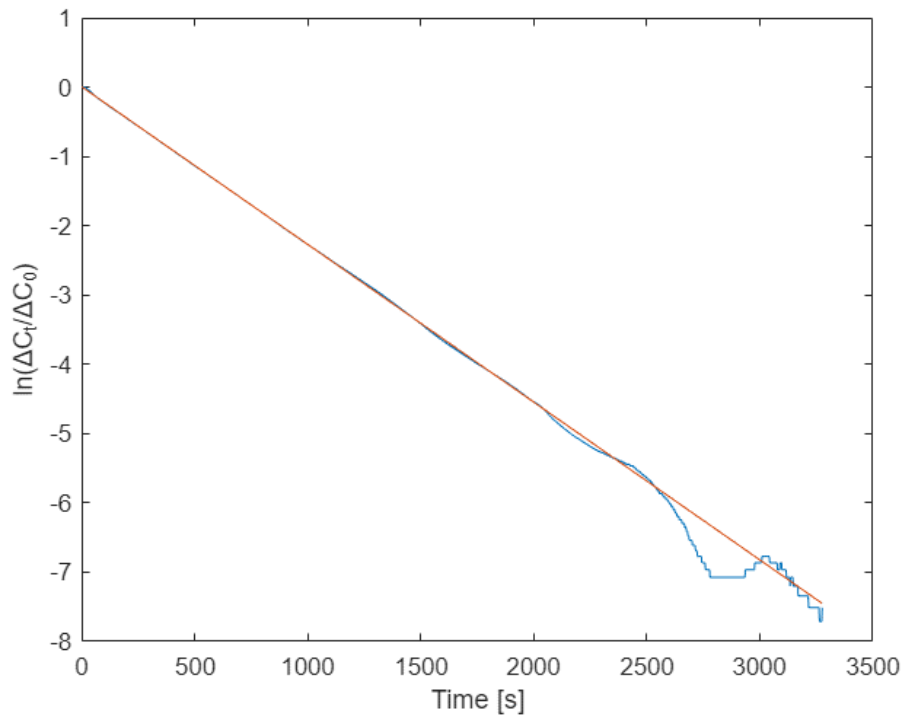


**Figure P.12** Example of determination of the  $D_p$ - coefficient for a Rockwool sample.